A Study on Dynamic Path Provisioning for Space Division Multiplexed Optical Networks

Submitted to Graduate School
of Information Science and Technology
Osaka University

July 2017

Shohei FUJII

List of Publications by the Author

I. Journals

[1] S. Fujii, Y. Hirota, H. Tode, and T. Watanabe, "On-Demand Routing and Spectrum Allocation for Energy-Efficient AoD Nodes in SDM-EONs," IEEE/OSA Journal of Optical Communications and Networking (conditional acceptance).

[2] S. Sugihara, Y. Hirota, S. Fujii, H. Tode, and T. Watanabe "Dynamic Resource Allocation for Immediate Reservation and Advance Reservation in Space Division Multiplexing-based Elastic Optical Networks," IEEE/OSA Journal of Optical Communications and Networking, vol. 9, no. 3, pp. 183–197, Apr. 2017.

[3] S. Fujii, Y. Hirota, H. Tode, and K. Murakami, "On-Demand Spectrum and Core Allocation Reducing Crosstalk of Multi-Core Fibers in Elastic Optical Networks," IEEE/OSA Journal of Optical Communications and Networking, vol. 6, no. 12, pp. 1059–1071, Dec. 2014.

II. International Conferences

[1] S. Fujii, Y. Hirota, H. Tode, and T. Watanabe, "Effective Wavelength and Core Selection for OPS Networks Reducing Inter-Core Crosstalk of Multicore Fiber," OSA Advanced Photonics Congress on Photonics in Switching (PS), July 2017.

[2] K. Nagatomi, S. Sugihara, S. Fujii, Y. Hirota, H. Tode, and T. Watanabe "A Study on Spectrum Assignment and Resource Sharing Method in Elastic Optical Packet and Circuit Integrated Networks," 21th OptoElectronics and Communications Conference (OECC) / International Conference on Photonics in Switching (PS), TuF2-4, Sep. 2016.

[3] S. Fujii, Y. Hirota, H. Tode, and T. Watanabe, "On-Demand Spectrum Allocation Considering Reliability of Backplane in AoD Nodes," HPSR Workshop in conjunction with IEEE 17th International Conference on High Performance Switching and Routing (HPSR), June 2016.

[4] S. Sugihara, Y. Hirota, S. Fujii, H. Tode, and T. Watanabe “Routing and Spectrum Allocation Method for Immediate Reservation Requests in Elastic Optical Networks,” International Conference on Photinics in Switching (PS), ThIII2.5, Sep. 2015.

[5] S. Fujii, Y. Hirota, H. Tode, and T. Watanabe, “Dynamic Spectrum and Core Allocation Reducing Costs of Architecture on Demand Nodes,” 40th European Conference on Optical Communication (ECOC), P.6.23, Sep. 2014.

[6] S. Fujii, Y. Hirota, H. Tode, and T. Watanabe, “Dynamic Spectrum and Core Allocation with Spectrum Region Reducing Costs of Building Modules in AoD Nodes,” IEEE 16th International Telecommunications Network Strategy and Planning Symposium (Networks), wed.s2.3, Sep. 2014.

[7] S. Fujii, Y. Hirota, and H. Tode, “Dynamic Resource Allocation with Virtual Grid for Space Division Multiplexed Elastic Optical Network,” 39th European Conference and Exhibition on Optical Communication (ECOC), P.5.15, Sep. 2013.

[8] S. Fujii, Y. Hirota, H. Tode, and K. Murakami, “On-Demand Spectrum and Core Allocation for Multi-Core Fibers in Elastic Optical Network,” Optical Fiber Communication Conference and Exposition (OFC) and The National Fiber Optic Engineers Conference (NFOEC), OTh4B.4, Mar. 2013.

[9] S. Fujii, Y. Hirota, H. Tode, and K. Murakami, “Path Division Method for Fairness in Dynamic Elastic Optical Path Networks,” International Conference on Photonics in Switching (PS), Th-S35-O12, Sep. 2012.

III. Domestic Conferences

[1] S. Fujii, Y. Hirota, H. Tode, and T. Watanabe, “A Study on Performance Evaluation of OPS Transmission for Reducing Inter-core Crosstalk of Multi-Core Fiber,” Technical Report of IEICE, vol. 116, no. 498, PN2016-95, pp. 67–71, Mar. 2017 (written in Japanese).

[2] S. Fujii, Y. Hirota, H. Tode, and T. Watanabe, “[Encouragement Talk] Dynamic Routing with Energy-Efficient AoD Nodes Utilizing Space Division Multiplexing Technology,”

Technical Report of IEICE, vol. 115, no. 497, PN2015-110, pp. 39–46, Mar. 2016 (written in Japanese).

[3] S. Sugihara, Y. Hirota, S. Fujii, H. Tode, and T. Watanabe, "Routing and Spectrum Assignment for Immediate and Advance Reservation Requests in Elastic Optical Networks," Technical Report of IEICE, vol. 115, no. 430, PN2015-74, pp. 241–246, Jan. 2016 (written in Japanese).

[4] S. Sugihara, Y. Hirota, S. Fujii, H. Tode, and T. Watanabe, "A Spectrum Assignment Method for Co-Existence of Immediate Allocation and Advance Allocation," in Proceedings of the 2015 IEICE General Conference, B-12-20, Mar. 2015 (written in Japanese).

[5] S. Fujii, Y. Hirota, H. Tode, and T. Watanabe, "A Study on a Routing Method for Energy Efficient AoD Nodes in Elastic Optical Networks," in Proceedings of the 2015 IEICE Society Conference, B-12-15, Aug. 2015 (written in Japanese).

[6] S. Fujii, Y. Hirota, H. Tode, and T. Watanabe, "A Spectrum Assignment for Large Scale AoD Nodes Reducing Power Consumption," Technical Report of IEICE, vol. 114, no. 518, PN2014-96, pp. 109–114, Mar. 2015 (written in Japanese).

[7] S. Fujii, Y. Hirota, H. Tode, and T. Watanabe, "On-Demand Spectrum Allocation for AoD Nodes in Elastic Optical Path Network," Technical Report of IEICE, vol. 114, no. 109, PN2014-10, pp. 53–58, June 2014 (written in Japanese).

IV. Awards

[1] Young Researchers Award of Technical Committee on Photonic Network, "A Spectrum Assignment for Large Scale AoD Nodes Reducing Power Consumption," Mar. 2016

[2] IEEE Kansai Section Student Paper Awards, "On-Demand Spectrum and Core Allocation Reducing Crosstalk of Multi-Core Fibers in Elastic Optical Networks," Feb. 2016.

[3] Student Workshop Award of Technical Committee on Photonic Network, "A Study on Dynamic Spectrum Allocation Considering Variable Required Bandwidths for Low-Power-Consumption AoD Nodes," Mar. 2015.

Abstract

This dissertation describes the research of "A study on dynamic path provisioning for space division multiplexed optical networks," which has been studied since 2012 by the author who was a bachelor student and master student and has been a Ph.D. student in the Department of Information Networking, Graduate School of Information Science and Technology, Osaka University.

In order to accommodate the future exponentially increasing Internet traffic, an extremely large capacity backbone network will be required. The elastic optical network (EON), which is a novel spectrally efficient network architecture developed from the present wavelength division multiplexing networks, is intensively researched and achieves a further expanded capacity of optical backbone networks. Moreover, space division multiplexing (SDM) technology is also expected as a solution of the capacity problem by overcoming the physical limit of existing optical fiber capacity, and a MCF is the promising candidate among future SDM-base optical fibers.

Although EONs and SDM-based optical fibers dramatically expand the capacity of optical backbone networks, they make new challenges to maximize the advantage. The most important requirement of SDM-EONs from the networking perspective is to establish appropriate resource management methods to provision optical paths. This is because SDM-EONs have the flexible, fine-grained and spatially expanded spectrum resources, that should be managed by a new method which is different from the traditional ones. There are various researches focusing on the optical path provisioning methods in SDM-EONs, however, there is a lack of two important factors: physical constraints and scalability for large scale networks. SDM-EONs have physical constraints based on the optical reach of modulation formats and the unique signal impairment in MCFs. In EONs, spectrally inefficient modulation formats are selected to long-haul optical paths owing to their low optical signal to noise ratio (OSNR). To mitigate the constraint, the arrangement of signal regeneration, which can compensate the OSNR of long-haul transmissions, is important. The regeneration placement (RP) problem should be solved to improve the spectral advantage and fairness regarding with the transmission distance. Moreover, considering spatial resources of SDM-EONs, we can efficiently accommodate the various types of services

by arranging the allocated resources in additional spatial channels with satisfying the physical constraints. Then, the unique signal impairment in MCFs means inter-core crosstalk (XT). The existing researches indicate the possibility of XT reduction from the perspective of networking, while the existing schemes of XT reduction depend on the proposals of sophisticated structures of MCFs. SDM-EONs also have the serious scalability problem because the spatial enlargement of optical networks makes optical switching requirements larger and more complex. In particular, SDM-EONs explosively increase the power consumption of optical switching nodes based on traditional architectures.

This dissertation proposes three schemes to solve the above issues. First, I propose a spectrally efficient path provisioning method considering RP problem. The proposed method divides end-to-end single optical path into multiple optical sub-paths utilizing regenerations in order to improve the spectral efficiency and fairness of SDM-EONs. Second, I proposed a path provisioning method reducing spectral fragmentation and effectively accommodating several types of services applications. I focused on a service reservation scheme that are considered to be different for each service application, and the proposed method arranges the allocated resources by constructing prioritized area in spectral and spatial domains. Third, I propose a path provisioning method reducing inter-core XT of MCFs. The proposed XT reduction is based on the prioritized core selection considering the qualitative characteristics and existing formulations of XT in MCFs. The proposed method also improves the capacity of SDM-EONs by reducing fragmentation. Finally, I propose the energy-efficient SDM-EON system which consists of switching node architecture and a path provisioning method. The proposed node architecture reduce the power consumption by simplifying the signal processing modules which is required for flexible filtering in EONs, and the proposed path provisioning method is designed to be suitable for the architecture. The proposed system also performs large network capacity considering spectral fragmentation.

The dissertation evaluates the performance of the proposed schemes through computer simulations. I confirm the effectiveness of the proposed schemes from the evaluation. The contributions of these proposals will help to expand the capacity of the future backbone networks.

Acknowledgments

First at all, I would like to express my deep and sincere gratitude to my advisor, Professor Takashi Watanabe of the Department of Information Networking in Graduate School of Information Science and Technology, Osaka University, for his supervision, continuing encouragement, valuable discussions, academic advice, and various supports throughout my studies and the preparation of this dissertation as a chief adviser.

I also would like to express my heartfelt appreciation to Emeritus Professor Koso Murakami of the Department of Information Networking in Graduate School of Information Science and Technology, Osaka University for his supervision, helpful comments, constructive advice, wide-ranging discussion, and various supports.

I would like to express my deep gratitude to Professor Masayuki Murata, Professor Toru Hasegawa, Professor Teruo Higashino and Professor Morito Matsuoka of the Department of Information Networking in Graduate School of Information Science and Technology, Osaka University for serving as members on my dissertation committee.

I would like to express my sincere appreciation to Professor Hideki Tode of the Department of Computer Science and Intelligent Systems in Graduate School of Engineering, Osaka Prefecture University for his supervision, helpful comments, valuable discussions, and various supports.

I owe a deep debt of gratitude to Dr. Yusuke Hirota of the National Institute of Information and Communications Technology for his helpful comments, various impressive advices, valuable discussions, and various supports.

My sincere thanks also go to Associate Professor Shunsuke Saruwatari of the Department of Information Networking in Graduate School of Information Science and Technology, Osaka University, all of whom provided valuable advices. The conversations and discussions with him inspire me greatly.

I would like to express my gratitude to Professor Kazuhiko Kinoshita of Institute of Technology and Science, the University of Tokushima for his many academic advices and comments for my study.

I would like to thank Ms. Mariko Tsukuda, Ms. Ami Takahashi, Ms. Satoko Tsuda and

Ms. Yukiko Nakano, secretaries of the Department of Information Networking in Graduate School of Information Science and Technology, Osaka University for their help and support.

I would also thank my closest collaborators who belong or belonged to Watanabe Laboratory: Mr. Naohiro Wakabayashi, Mr. Yoshihiko Hatada, Mr. Seitaro Sugihara and Mr. Ken Nagatomi.

I also thank other colleagues who belong or belonged to Watanabe Laboratory or Murakami Laboratory for their contributions on my research. I could have never achieved this goal without their contributions. The list is so long that I cannot write down all their names.

Last but not least, I am particularly grateful to my parents and sister for their understanding, encouragement, perpetual support and the unconditional love over the years.

Contents

List of Figures

Chapter 1

Introduction

As a growth of the Internet, the network traffic has been increasing explosively. Furthermore, the network traffic has diversified into various types; not only plain text data such as World Wide Web or e-mail, but also multimedia data such as video streaming or voice over IP. Mobile phones and other wireless devices widely spread, and people can easily access the Internet without desktop computers. Ministry of Internal Affairs and Communications shows that the Internet traffic volume is increasing exponentially in Japan [3], and Cisco Visual Networking Index estimates the volume of global IP traffic in 2020 to be 194,374 PB per Month [4]. To accommodate the increasing traffic, there is a requirement to expand the transmission capacity of core optical networks. For realizing the large capacity optical network, wavelength division multiplexing (WDM) technology has been developed [5, 6]. It enables to multiply its capacity by multiplexing many wavelength channels into a single optical fiber.

However, the capacity expansion of the WDM technology is not enough, and we need further enlargement of transmission capacity in order to accommodate future increasing traffic request. Elastic optical network (EON) is a promising technology for future core/metro optical networks which achieve the larger transmission capacity than that of traditional WDM networks [7, 8, 9, 10]. In the traditional WDM networks, allocated wavelengths are arranged with fixed spacing, and the modulation format and other key parameters are designed to cope with the worst case physical impairments for all network infrastructures. Therefore, the traditional WDM networks waste their spectrum resources when bandwidth required for an optical path is not sufficient to fill the entire capacity of wavelength. In contrast to the traditional WDM networks, EONs can flexibly allocate minimum necessary spectrum resources to optical paths

according to required bandwidth. The basic concept underlying EONs is presented in [7]. In EONs, a unit of assigned spectrum resources is smaller than that of WDM networks; the unit is known as a frequency slot (FS). EONs can flexibly select the appropriate number of FSs and modulation format allocated to an optical path, depending on the required transmission rate and optical reach [11, 2]. Figure 1.1 summarizes the unique features of EONs with regard to their spectrum utilization. EONs flexibly supplies the cost-effective segmented optical paths, optical paths with minimum necessary bandwidth, and spectrally effective aggregated optical paths.

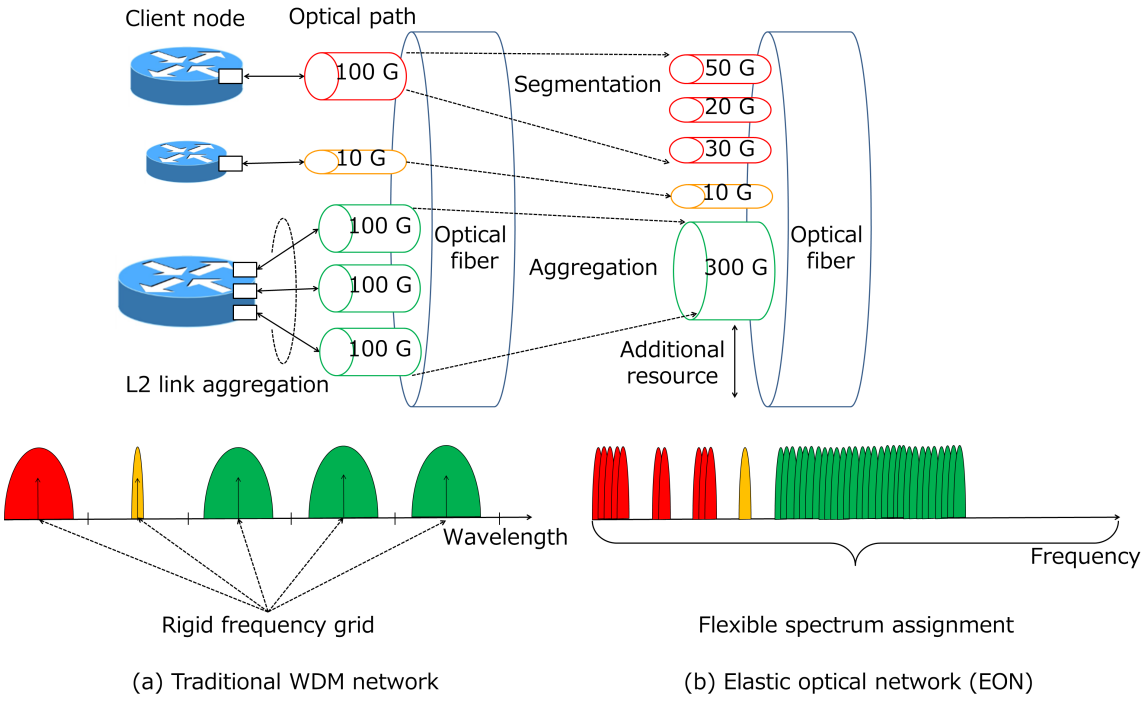

Figure 1.1: Architecture of EON.

From the networking perspective, it is important to solve the routing and spectrum allocation (RSA) problem, which is equivalent to the routing and wavelength assignment (RWA) problem in WDM networks, in order to enhance the advantages in a transmission capacity of EONs by effective resource management [12, 13]. In traditional WDM networks, the RWA problem has one important constraint, which forces each optical path to be assigned the same wavelength at all links for a high-speed and energy-efficient end-to-end all-optical transmission [14, 15, 16]. This constraint is known as wavelength continuity constraint, and it is transformed to a spectrum continuity constraint in the RSA problem. In EONs, the RSA problem also has additional

constraint, which forces each optical path to be assigned contiguous FSs at all links. This is because EONs utilize orthogonal frequency-division multiplexing (OFDM) modulation technique [17, 18], and contiguous FSs are necessary to obtain the spectral advantages relating to an overlap of OFDM subcarriers [8]. While EONs can flexibly establish optical paths with different minimum necessary FSs, this heterogeneous bandwidth allocation makes new challenge. In scenarios of heterogeneous bandwidth allocation, spectrum resources of EONs are fragmented by repeating the establishment and release of optical paths. To improve the spectral efficiency of EONs, it is important to take this spectrum fragmentation problem into account [19, 20, 21].

Various studies have explored the RSA problem, and many RSA algorithms have been proposed to establish appropriate optical paths in EONs. There are mainly two different approaches to solve the RSA problem. The one is static RSA [22,23,24], and the other is dynamic RSA [25,26,27]. The static RSA deals with the routing and FSs assignment during the network planning stage. In the static RSA, traffic matrix is given in advance, and process of the routing and spectrum allocation are performed off-line. In contrast to such a static traffic scenario, the realistic network traffic changes from hour to hour and the timing of generating optical path requests is unknown. Therefore, the dynamic RSA is more practical approach to solve the RSA problem.

Additionally, the trade-off between the spectral efficiency and maximum transmission distance of modulation formats is the important factor to solve the RSA problem [11, 2]. EONs can flexibly select not only the number of FSs but also the modulation formats according to the optical signal-to-noise ratio (OSNR) of required optical path. When a short optical path is required, EONs can select spectrally efficient modulation formats such as 16-QAM (quadrature amplitude modulation) and 64-QAM because an OSNR of short optical paths tend to be higher. On the other hand, when a long optical path is required, EONs have to select spectrally inefficient modulation formats such as quadrature phase-shift keying (QPSK) because an OSNR of long optical paths tend to be lower. Owing to the spectral inefficiency of available modulation formats, long-haul transmissions generally occupy wider bandwidth than short-hop connections do. On this basis, EONs can incur substantial unfairness regarding the transmission success rate and spectral efficiency, depending on the transmission distance. The RSA problem

which includes the flexibility of modulation level is called routing, modulation and spectrum allocation (RMSA) problem. The RMSA problem is also solved statically or dynamically by various researchers [28, 29].

As described above, the continuity and contiguity constraints of the RSA problem are introduced. The strictness of these constraints is based on the fact that EONs should not convert optical signals from the perspective of energy-efficient, high-speed and all-optical networking. This is called a transparent EON. In contrast, translucent EONs were proposed in [30] to provide further geographical scalability considering the reachability of modulation formats. The proposed translucent EON architecture with virtualized elastic regenerators (VERs) permits intermediate cost-effective signal regenerations. Reference [30] also mentions the possibility of spectrally efficient networking with optical regeneration. Figure 1.2 shows the concept of signal regeneration in EONs. In this context, some researchers have solved the regeneration placement (RP) problem in translucent EONs [31,32,33,34,35,36] by determining where each optical path should be regenerated. There is a requirement of RP algorithms to directly improve the spectral efficiency and the blocking probability in translucent EONs utilizing intermediate signal regeneration because the existing works mainly utilize the signal regeneration to compensate the signal degradation with additional power consumption.

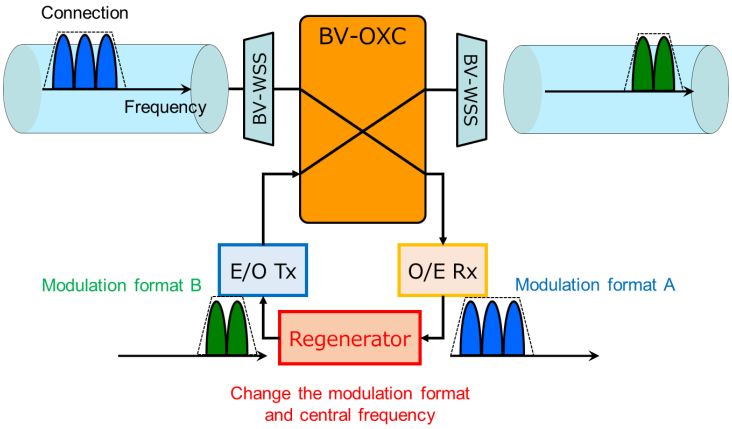

Figure 1.2: Concept of signal regeneration at the intermediate node of translucent EONs.

Considering the future core optical networks, SDM-EONs have to accommodate various

service applications. One of the important varieties of applications is a difference in their reservation conditions. Traditionally, it is considered that traffic requests in optical networks need to immediately reserve network resources in order to establish the transmission as soon as possible. On the other hand, there are some service applications that can tolerate a delay before the service start time. The former are called immediate reservation (IR) requests and the latter are called advance reservation (AR) requests. In such a case, it is possible to enhance the total resource utilization of optical networks by reserving future resources for AR requests. However, in SDM-EONs, the reservation flexibility of AR request causes resource fragmentation in the time domain. Moreover, the coexistence of IR and AR requests leads a lack of available resources for IR requests because AR requests can exploit future available resources before IR requests arrive. There are several researches considering coexistence of IR and AR requests [37, 38], and there are some infeasible points relating to the traffic inspection or modeling. Therefore, we need a service provisioning schemes which is suitable for a more realistic coexistent scenario in SDM-EONs.

While EONs can dramatically expand a capacity of optical networks, the rate of increase in the transmission capacity of the optical fiber has been gentle. This is because the transmission capacity approaches the physical limit of the traditional optical fiber. One of the physical limitations of the fiber capacity is related to the input power. The input power of the optical fiber is restricted mainly by two factors. The first is fiber fuse phenomenon [39]. When the input power in a fiber increases, the core of the fiber melts. This fiber fuse phenomenon continues until the input power of the fiber is lowered. Because a greater amount of transmitted signals yields a higher optical fiber power, the amount is limited. The second factor is signal degradation relating to the nonlinear optical effects [40]. Various nonlinear optical effects generate nonlinear interference among WDM signals. Therefore, to overcome the physical limitations of traditional optical fibers and further expand fiber capacity, novel innovative optical fibers are required [41].

In order to realize the further expansion of the fiber capacity, space-division multiplexing (SDM) has been intensively researched in the past few years [42]. Multicore fiber (MCF) is one of the new innovative fibers based on the SDM technology, and it is a strong candidate

of future optical fibers because of the simplicity of signal processing and easy replacement from the existing optical fibers. One of the most significant problems of MCFs is an physical impairment of transmission signals due to inter-core crosstalk (XT) because the signal degradation suppresses the expansion of transmission capacity of MCFs. Considerable researches on the design of MCFs have been reported in the past few years to pursue low inter-core XT and longer transmission distance [43, 44, 45, 46]. Most of the studies on MCFs have been tried to reduce XT of MCFs by contriving a structure of MCFs; for example isolated MCFs, whose XT is low enough. However, from the perspective of the cladding diameter, such an isolated structure tends to have a larger diameter than a non-isolated MCF. Therefore, a different way to reduce XT of MCFs is required. In several experiments, it was assumed that the signals of the same frequency were transmitted simultaneously at all cores in one MCF. Nevertheless, considering the network in total, there are many fibers that are not in such a high-crosstalk condition, because of traffic demands and resource allocations. Thus, XT in MCFs can be reduced by suitable network resource management, exploiting the available capacity.

Moreover, the appearance of SDM-based MCFs and an increase in the number of underlying optical fibers, which are aimed at expanding transmission capacity of optical networks, is expected to enlarge and complicate optical switching nodes in optical networks. In EONs broadcast-and-select and spectrum-routing are general optical switching node architectures shown in Fig 1.3, that have enough flexibility to realize fully elastic optical networks [47, 48]. The spectrum selective switch (SSS), which is also called bandwidth variable wavelength selective switch (BV-WSS) of a flexible WSS, is the most important signal processing module in the optical nodes of EONs [9]. This is because SSSs can filter spectra with an arbitrary width from input signals and switch them to arbitrary ports without signal replication, as shown in Fig. 1.4. In these architectures, SSSs are not only the main flexible signal processing module but also the dominant module in terms of power consumption. When optical switching nodes become complex and large-scale, cascaded SSSs dramatically increase the power consumption of these optical switching nodes owing to the limited port count of SSSs [49]. To suppress the increase in the number of signal processing modules, a hierarchical optical switching node architecture using small optical cross connects (OXCs) as subsystem

modules has been developed based on the traditional architectures [50]. This hierarchical node architecture divides the switching component into subsystems of smaller OXC and suppresses the increase in the number of cascaded SSSs. On the other hand, their subsystem-based partially restricted switching negatively affects the transmission success rate, and there is a trade-off between suppression of the modular cost and the transmission success rate. Therefore, it is necessary to establish a completely different node architecture to achieve cost reduction and successful transmission.

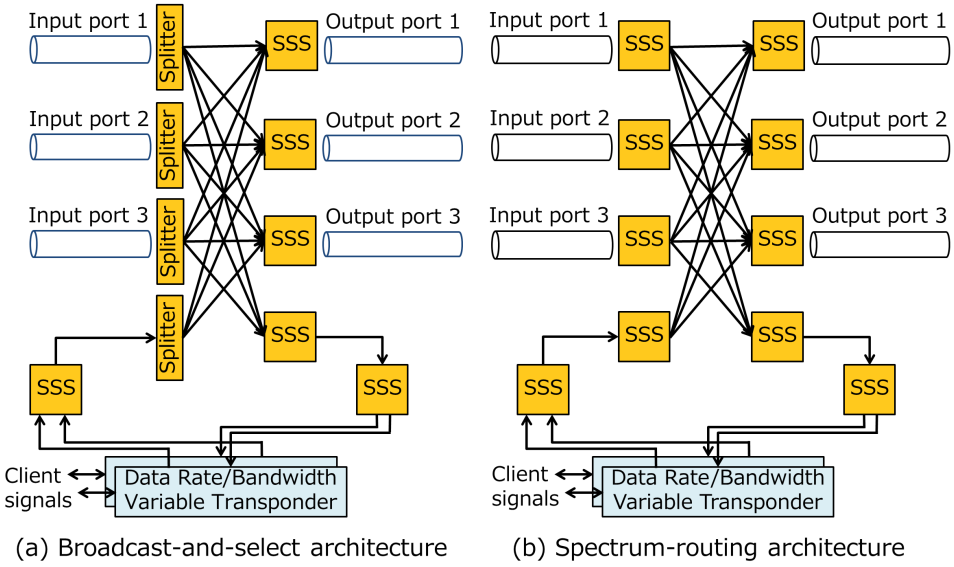

Figure 1.3: Traditional optical switching node architectures for EONs.

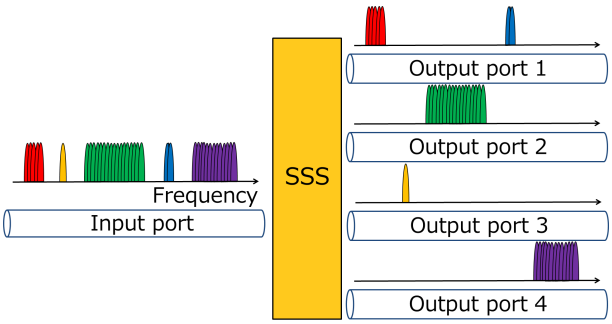

Figure 1.4: Concept of the SSS.

Reference [1] reduces the number of signal processing modules implemented in optical nodes by introducing a completely different novel optical node architecture which is called

an architecture on demand (AoD) node. In AoD nodes, an optical backplane, which is usually implemented using a large-port-count three-dimensional microelectromechanical system (3D-MEMS), interconnects input/output ports and signal processing modules in an arbitrary manner, as shown in Fig. 1.5. Use of an AoD node can reduce the number of signal processing modules by supplying just enough signal processing because these interconnections are dynamically constructed according to switching and signal processing requests. In other words, the AoD concept requires an appropriate resource allocation method (which creates an appropriate switching request) considering these interconnections in AoD nodes. Although AoD nodes have the great advantages, they also have two important challenges. The one is the scalability problem of the optical backplane. As shown in Fig.1.5, all the building modules implemented in an AoD node are connected to a central optical backplane (3D-MEMS). When the number of input/output ports and building modules are increased, the port count of 3D-MEMS required for the optical backplane is too large to be implemented. Using multiple 3D-MEMSs is a simple solution to this problem; however, in order to switch signals between multiple 3D-MEMSs freely, many 3D-MEMSs ports are used for intraconnections among them. A sophisticated AoD construction using multiple 3D-MEMSs is required because wasting the switching ports of a 3D-MEMS needs more 3D-MEMSs and increases the power consumption of AoD nodes. The other challenge is a trade-off between the switching granularity and the number of required modules. Although some studies have examined the energy efficiency of AoD nodes, reducing their power consumption depends on reducing the number of SSSs, assuming switching requests with coarse granularity, such as fiber switching. If EONs require fully flexible operation for all input/output ports of AoD nodes, they still require the same number of SSSs as that of traditional architectures.

As described above, a novel optical network architecture and transmission devices have been intensively researched based on the background of the explosive increase in the Internet traffic and the physical limit of the existing single-core single-mode fiber capacity. Space division multiplexed-elastic optical networks (SDM-EONs) are integration of the introduced novel techniques, and it is expected as a solution of the capacity problem of future optical networks. Towards the extremely large capacity, the SDM-EONs have to solve the various challenges

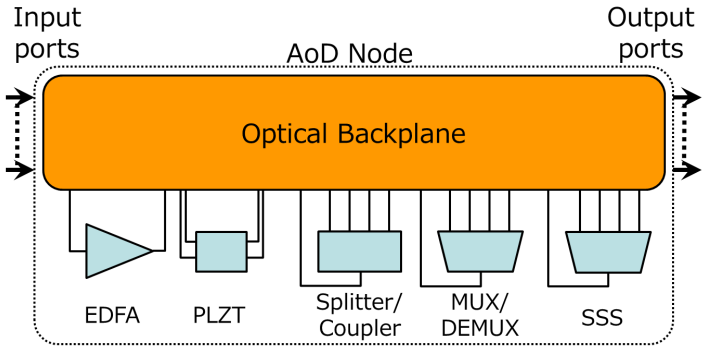

Figure 1.5: An AoD node architecture [1].

induced by their unique characteristics: complex management of fine-grained and spatially multiplexed spectrum resources, physical constraints relating to optical reaches of modulation formats and physical impairment in SDM-based optical fibers, and scalability of network equipments. In this dissertation, a dynamic path provisioning method is proposed with the object of further expansion in the capacity of SDM-EONs. The proposed optical path provisioning system is conducted by appropriately solving the RSA problem taking these unique characteristics into account.

First, this dissertation proposes a dynamic path provisioning method to mainly improve the performance of long-haul transmission in SDM-EONs. There are two proposals based on the two different spectrum assignment and regeneration placement (SARP) algorithms, respectively. The proposed algorithms divide a single long optical path into multiple short optical sub-paths at intermediate nodes where signal regeneration is implemented. The short optical sub-paths occupy fewer spectrum resources because more efficient modulation formats can be adopted compared to those required for long optical paths, and the continuity constraint is mitigated by allocating different FSs to different optical sub-paths. The proposed method not only improves accommodation rate of long-haul transmission but also improves that of overall SDM-EONs by allocating fewer spectrum resources. Moreover, the proposed method also has a novelty on the fairness issue of EONs because the main improvement provided by the proposed method is with regard to saving the performance degradation in long-haul transmission.

Second, this dissertation proposes a dynamic path provisioning method to reduce an amount of XT in MCFs. The path provisioning policy is divided into two predefinitions: the predefined

core prioritization for reducing XT in MCFs and the predefined core classification for reducing spectrum fragmentation. The proposed method firstly focuses on the theoretical formulation of XT in MCFs, and the fact that XT in MCFs is significant when the optical signals are transmitted on the same frequency in adjacent cores. The prioritization policy aims at reducing significant XT by selecting distant cores in MCFs as priority. Although the proposed method can provide optical paths with less XT in MCFs by the prioritization, the transmission success rate is slightly degraded because the prioritization is not ideal for the perspective of spectral efficiency. The classification policy aims at reducing spectrum fragmentation by orderly spectrum assignment based on the required bandwidths to compensate the degradation of transmission success rate.

The dissertation finally proposes a dynamic path provisioning method with energy-efficient node configuration in SDM-EONs. The proposed method has two important factors: a novel energy-efficient AoD node architecture and resource assignment method considering the proposed AoD node architecture. The proposed energy-efficient node architecture requires partially restricted spectrum allocation to adopt low-power-consumption modules for signal processing. Then, I also propose a novel on-demand resource allocation method suited for the proposed energy-efficient AoD nodes. The proposed resource allocation method simultaneously reduces the blocking probability of optical path set-up requests in the entire network because its allocation policy reduces spectrum fragmentation. Therefore, the proposed AoD node architecture and on-demand resource allocation method can improve both power consumption and traffic accommodation rate in SDM-EONs.

The rest of this dissertation is organized as follows. Chapter 2 explains the concept of EONs and the various algorithm to solve the RSA with RP problem in EONs. The dynamic SARP algorithms are proposed for path provisioning method in order to directly improve spectral efficiency of SDM-EONs. The performance of the proposed SARP algorithms is evaluated through the computer simulations in terms of the blocking probability and fairness. Chapter 4 explains the XT problem in MCFs in detail. The dynamic RSA algorithm is proposed for path provisioning method in order to reduce the amount of XT in SDM-EONs, in which MCFs are implemented. The performance of the proposed RSA algorithm is evaluated through the computer simulations in terms of the blocking probability, number of fragments, and crosstalk per

slot (CpS). Chapter 5 explains the configuration of switching nodes in EONs. The energy-efficient AoD node architecture is proposed, and the RSA algorithm which cooperate with the proposed node architecture is also proposed for path provisioning method in order to establish an energy-efficient total network system. The performance of the proposed system is evaluated through the computer simulations in terms of the blocking probability, qualitative scalability, quantitative scalability, total power consumption, and topological dependency. Chapter 6 confirms the validity of the proposed path provisioning methods based on the simulation results in the previous chapters. Finally, future works are addressed.

Chapter 2

Optical Path Provisioning with Regeneration Placement

2.1 Introduction

The rapid increases in the volume of Internet traffic requires the future optical core network to obtain higher spectral efficiency for larger network capacity. Elastic optical networks (EONs) have been studied as possible alternatives to overcome the inefficiencies of WDM technology [7,8]. In EONs, the unit of the assigned spectrum resource is smaller than that of the WDM network, and the unit is known as a frequency slot (FS). In an EON, spectrum resources are allocated by selecting the appropriate modulation format and number of FSs, depending on the required demand size and optical reach. From a networking perspective, it is essential that the routing and spectrum assignment (RSA) problem be solved to utilize EONs efficiently, and this requires the continuity and contiguity constraints to be satisfied [12]. The continuity constraint requires that each FS be assigned to the same optical path for all links along the transmission route, while the contiguity constraint requires that the FSs assigned to one optical path must be contiguous in the spectrum domain. However, it is difficult for long-haul connections to satisfy these two constraints. In addition, long-haul connections are inefficient in terms of their modulation formats [2]. Owing to the short reachability of a spectrally efficient modulation format, a long-haul connection tends to occupy wider bandwidth than a short-hop connection. On this basis, EONs can incur substantial unfairness regarding the transmission success rate and spectral efficiency, depending on the transmission distance. One solution to this unfairness

problem is to introduce signal regeneration at intermediate nodes, which can dramatically mitigate the continuity and modulation format constraints, although it leads to additional expense for equipment, power consumption, and transmission delay.

In this chapter, I propose novel dynamic spectrum allocation and regeneration placement (SARP) algorithms to improve the transmission performance and unfairness of long-haul connections. The proposed method divides a single long optical path into multiple sub-short optical paths connected by intermediate nodes where signal regeneration is implemented. The short optical sub-paths occupy fewer spectrum resources because more efficient modulation formats can be adopted compared to those required for long optical paths, and the continuity constraint of EONs is mitigated by allocating different FSs to different optical sub-paths. The proposed method not only improves the transmission success rate of long-haul connections but also improves that of the overall network by allocating fewer spectrum resources. There are three main contributions of this chapter. First, novel SARP algorithms are proposed that consider signal regeneration at intermediate nodes. Second, I provide performance evaluations of the proposed algorithm for various network environments. Third, I discuss the requirements of fairness in EONs.

The rest of this chapter is organized as follows. Section 2.2 explains transparent and translucent EONs. Section 2.3 proposes dynamic SARP algorithms that consider regeneration for fair EON transmissions. Section 2.4 evaluates the performance of the proposed method and discusses the fairness of EONs, and Section 2.5 concludes the chapter.

2.2 Network Architecture and Networking Problem

2.2.1 Elastic Optical Networks

Elastic optical networks (EONs) employ Orthogonal Frequency Division Multiplexing (OFDM) technology which is utilized in wireless communication. EONs can utilize spectrum resources more efficiently than traditional fixed-grid WDM networks by utilizing OFDM technology and modulation techniques [51]. An OFDM-based EON architecture was proposed as spectrum-sliced elastic optical path network (SLICE) in [7]. The concept of SLICE is to allocate spectrum resources flexibly for end-to-end optical paths against the traditional WDM networks which

adapt rigid spectrum width. This spectrum resource allocation is performed according to the traffic volume and user request.

Figure 1.1 shows the difference between traditional WDM networks and EONs. In traditional WDM networks, optical channels are aligned in fixed equal intervals. Therefore, the 10 Gbps optical path request needs the same bandwidths as the 100 Gbps optical path request. This spectrum resource allocation causes the inefficient utilization of spectra. Moreover, three optical paths of 100 Gbps are needed when a 300 Gbps optical path is requested. In this case, the spectrum resources between the optical paths are wasted. The main contribution of this network architecture is the efficient utilization of limited spectrum resources by ensuring the unit of spectrum allocation has fine granularity, and allocating only the minimum necessary bandwidth to each transmission request [7, 8, 9, 10].

In EONs, advanced modulation technologies are adopted in order to achieve high spectrum resource utilization and to reduce the transmitted symbol rate [8]. In EONs, optical signals with the various data rate can be generated by adjusting the modulation format. Basically, a higher-level modulation format with more bits per symbol is selected under the limitation of the minimum optical signal to noise ratio (OSNR) required to decode the data. M-Phase Shift Keying (M-PSK) and M-Quadrature Amplitude Modulation (M-QAM) are example of the familiar modulation format. Reference [8] describes the details of each modulation format as below.

- M-PSK: Phase-shift keying (PSK) is a modulation format that transmits data by modulating the phase of a transmitted signal. M-PSK is a multiphase modulation technique, and M is the number of phases which are utilized for encoding signals. Binary phase-shift keying (BPSK) is the simplest form of PSK; it can be called 2-PSK. BPSK supports 1 bit per symbol by utilizing two phases that are separated by 180°. Quadrature phase-shift keying (QPSK), which is also called 4-PSK, supports 2 bit per symbol because it utilizes four phases that are separated by 90°. Example constellation diagrams of M-PSK are illustrated in Fig. 2.1 (a). This figure includes 8PSK as a higher-order M-PSK formats.

- M-QAM: M-QAM is a modulation format that transmits data by modulating not only the

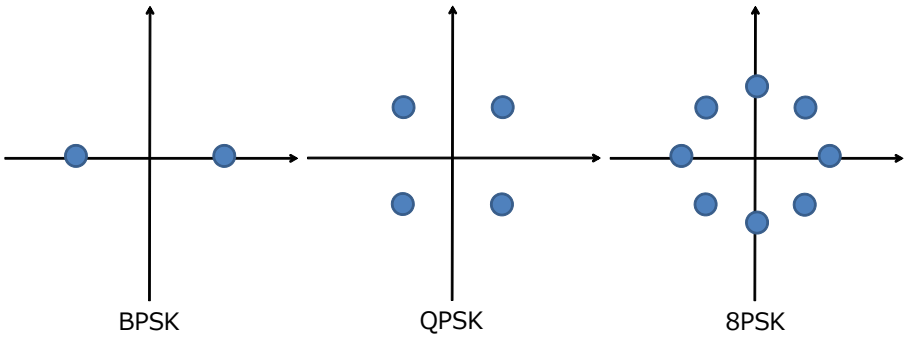

(a) Example constellation diagrams of M-PSK modulation

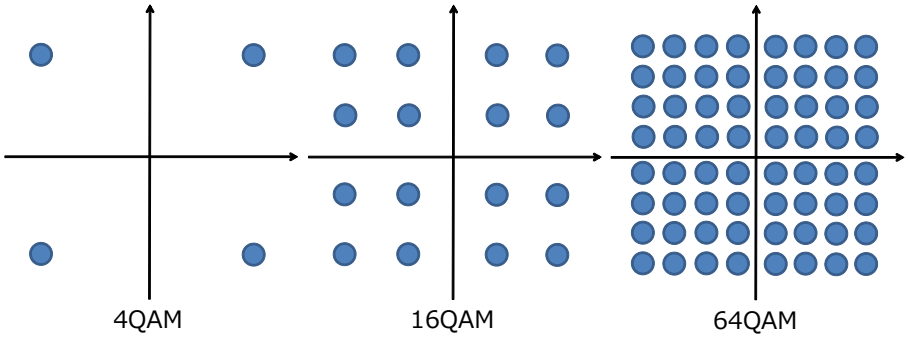

(b) Example constellation diagrams of M-QAM modulation

Figure 2.1: Example constellation diagrams of M-PSK and M-QAM modulation.

phase but also the amplitude of a transmitted signal in order to increase its symbol rate. In M-QAM, two M-level amplitude-modulated signals are multiplexed onto two carriers of the same frequency with phase shift of $90°$. 4QAM, 16QAM, and 64QAM are defined for 2, 4, and 6 bits/symbol, respectively. M-QAM can transmit data more efficiently than simple format which only modulates the amplitude or the phase of a reference signal. However, M-QAM is more affected by noise. Example constellation diagrams of M-QAM are illustrated in Fig. 2.1 (b).

The capacity of signals, which are modulated by these modulation formats, are explained as follows. When the capacity of a subcarrier modulated by BPSK supporting 1 bit/symbol is defined as C Gb/s, the capacity of subcarrier modulated 16QAM supporting 4 bits/symbol corresponds to $4C$.

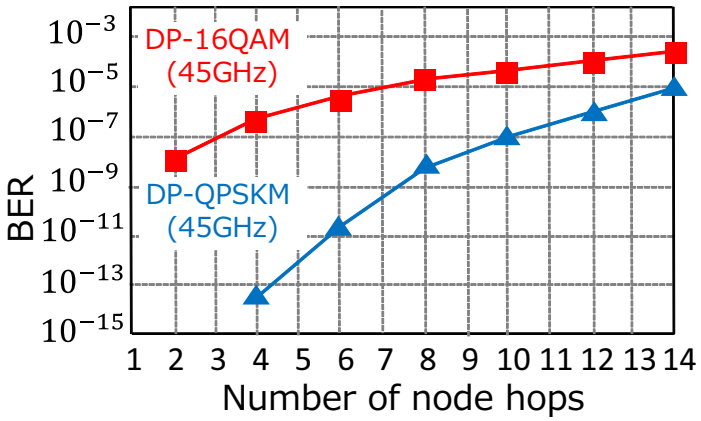

Figure 2.2: The relationship between the number of node hops and BER [2].

Figure 2.2 shows obtained bit error rate (BER) curves as a function of node hops for various 3dB widths of the filter, when single-carrier dual polarization (DP) 112 Gb/s 16-QAM and DP-QPSK signals are transmitted [2]. The offset between the center frequencies of the signal and optical filter is set to 2.5 GHz. Figure 2.2 shows that the larger the number of node hops is, the worse performance the BER indicates. The required signal to noise ratio (SNR) for BER scales linearly with OSNR, which in turn is dependent on the number of optical amplifiers traversed in the network [52]. Therefore, it is possible to utilize spectrum resources efficiently by selecting appropriate modulation format according to the transmission distance.

Spectrum resources in EONs are efficiently allocated with a flexible grid according to the physical requirement of each connection. This flexibility is provided by the fine-grained unit, or frequency slot (FS), used to assign spectrum resources in EONs. Because EONs can allocate the minimum necessary FSs to each connection depending on the required bandwidth, the spectral efficiency of EONs is higher than that of conventional WDM networks. The number of required FSs depends on the transmission distance of each connection. When a connection requires a short transmission distance, the network can select a spectrally efficient modulation format, such as 16-QAM or 64-QAM, although these modulation formats have short optical reaches. On the other hand, when connections require a long transmission distance, the network must select a spectrally inefficient modulation format, such as quadrature phase-shift keying (QPSK), because of the lower optical signal-to-noise ratio. Thus, the distance-adaptive spectrum assignment method in EONs reduces the need for spectrum resources [11, 2]. Simultaneously, there is the unfairness regarding the transmission success rate and spectral efficiency, depending on the transmission distance.

Considerable researches focusing on EONs have been undertaken [53, 54, 9, 10]. Reference [53] discusses signaling for elastically using spectrum resources per an ITU-T grid. Reference [54] proposed the Bandwidth Squeezed Restoration (BSR), which sets up backup links to mitigate link failure. This BSR framework classifies all transmissions either into the best effort type or not, and a back-up route is set up by adjusting the best effort transmission. Reference [9] discusses the building blocks and enabling technologies of EONs, such as the spectrum selective switch and bandwidth variable transponder. The benefits and the challenges of future EONs are summarized in Ref. [10].

2.2.2 Routing, Modulation and Spectrum Allocation Problem

The most important problem to solve when planning EONs is the RSA problem [9], which is equivalent to the routing and wavelength assignment (RWA) problem in rigid WDM networks. In traditional WDM networks, the RWA problem has one important constraint, which forces each connection to be assigned the same wavelength at all links for end-to-end all-optical transmission. This constraint is known as the wavelength continuity constraint. While the RSA

problem also has this spectrum continuity constraint, it also has one additional constraint related to spectrum allocation. In EONs, FSs must be contiguously allocated to one connection at all links. This constraint is known as the spectrum contiguity constraint. The RSA problem can be solved using a combination of route and spectrum that satisfies these two constraints. Moreover, the modulation format of FSs can be flexibly selected according to the transmission distance in EONs [11, 2].

Static approach

Various studies [12, 13, 22, 23, 24] have explored the RSA problem in EONs. Detailed RSA algorithms for EONs were proposed in [12, 13]. Other researchers [13] solved the RSA problem by using integer linear programming (ILP). The objective of ILP is to minimize the number of FSs that are assigned to at least one connection in the network under a static traffic matrix. The RSA problem can be solved by ILP when it is supposed that a network is small enough; for example, it has less than 10 nodes. However, the RSA problem is classified as NP-hard, and is too complex to solve computationally by ILP because there are too many variables: links, fibers, frequency, spatial channels in SDM optical networks, etc. Therefore, these authors proposed heuristic algorithms to solve the RSA problem for large networks. The heuristic approach in [12] divided the RSA problem into two sub-problems: routing and spectrum allocation. Reference [22] proposed two heuristic algorithms that maximized the reuse of spectrum resources. These algorithms assigned a higher priority to larger traffic demands because otherwise it was difficult to satisfy the continuity constraints. Reference [23] proposes two heuristic algorithms, maximizing the reuse of spectrum resources. In these algorithms, larger traffic demand has a higher priority because it is difficult to satisfy the continuity constraints of the RSA problem for such demand. Reference [24] considers “Time-varying” required transmission rate, and proposed spectrum expansion/contraction policies reduce blocking probability of networks by spectrum sharing. Reference [24] introduces theoretical calculation of blocking probability and compares it with dynamic network simulations.

Dynamic approach

These ILP-based static RSA solutions assume that a complete traffic matrix is provided in advance. However, in realistic optical networks, transmission requirements arrive dynamically and continuously. Therefore, it is important to adapt a dynamic approach to solve the RSA problem according to the rapidly changing network traffic [25,26,27,55,56,57,29]. In dynamic approaches, the optical paths are provisioned on-demand. Reference [25] experimentally evaluates efficient strategies in a GMPLS-controlled EON for dynamic source/PCE (path computation element) routing algorithms. Reference [26] presents an OpenFlow-based control plane for EONs for dynamic end-to-end path provisioning and IP traffic offloading. Reference [27] compares three types of dynamic spectrum allocation scenarios: fixed, semi-elastic, and elastic network scenarios. Reference [55] proposes semi-flexible grid networks in a dynamic network scenario. The semi-flexible grid network has almost the same blocking probability as conventional flexible grid networks, while the network system uses fixed grid interfaces. Reference [56] proposes zone-based spectrum assignment for dynamic RSA problem. In [57], a dynamic load-balancing RSA algorithm was proposed, which includes modulation format selection that considers the quality of transmission estimated based on the fiber nonlinearity effect and the impairment of intermediate nodes. Reference [29] proposes dynamic RMSA method considering multipath connection establishment. To further investigate the optical path selection process, the proposed online/offline path computation methods are compared.

Fragmentation problem

In EONs, spectrum fragmentation becomes serious problem that adversely affects the spectral efficiency of EONs [20, 19, 21, 58, 59, 60, 29, 61]. This problem arises because EONs flexibly allocate various amounts of bandwidth to connections, depending on the required modulation format and transmission distance, and the spectral resources become fragmented by the repetitive setup and release of these heterogeneous bandwidth requests. Although the sum of the available spectrum resources is sufficient, the continuity and contiguity constraints cannot always be satisfied due to fragmentation. Reference [19] proposes two heuristic algorithms for

ILP formulations of the network defragmentation problem in flexible optical WDM. Reference [21] proposes a network reconfiguration scheme that reroutes existing optical paths to reduce fragmentations. The studies reported in Refs. [58, 59, 60] attempted effective defragmentation in various ways. Reference [58] proposes two defragmentation algorithms using the *Path Connectivity* in flexible bandwidth networks. The *Path Connectivity* reveals the difficulty of transmitting traffic in the optical path on the basis of the spectral usage matrix. Reference [59] decomposes the RSA problem into multipath computation and spectrum assignment sub-problems. These sub-problems are handled sequentially in order to solve the proposed ILP model. Reference [60] experimentally evaluates the proposed fragmentation-aware routing and spectrum allocation algorithms in a software-defined network enabled by OpenFlow. In [29], the fragmentation ratio, which was based on the maximum size of the available slot blocks, was defined and evaluated. A detailed dynamic defragmentation algorithm based on connection reconfiguration, which permits the interruption of transmissions, was proposed in [61]. The connection reconfigurations can migrate traffic based on the proposed dependency graph model, and the proposed defragmentation timing selection minimizes the disruption time of the reconfigurations.

2.2.3 Regeneration Placement in Translucent EONs

In the previous subsection, I introduced the continuity and contiguity constraints of the RSA problem. The strictness of these constraints is based on the fact that EONs do not convert optical signals. This is called a transparent EON. In contrast, translucent EONs were proposed in [30] to provide further geographical scalability. The proposed translucent EON architecture with virtualized elastic regenerators (VERs) permits intermediate cost-effective signal regenerations for multiple optical channels with various modulation formats. Reference [62] also mentions the possibility of spectrally efficient networking with optical regeneration.

Some researchers optimized the regeneration placement (RP) problem in translucent EONs [31, 32, 33] by determining where each optical path should be regenerated. Reference [31] proposed a mixed-integer linear programming (MILP) formulation for the RSA with RP problem. The

objective of the MILP is minimizing the highest FS required to accommodate the network traffic. Due to the scalability limitations of the MILP approach, recursive heuristic algorithms were also proposed to solve the formulated MILP problem for realistic networks. The proposed heuristic approach divided the whole traffic matrix into small submatrices, and solved the MILP for each submatrix. Reference [32] also proposed a MILP formulation and heuristic algorithms for the RSA with RP problem. The objective of the MILP is minimizing the occupied spectral resources and maximize the spectral efficiency by regeneration. A weighting coefficient was introduced to control these contributions. Reference [33] formulated the routing, spectrum, transceiver, and regeneration allocation (RSTRA) problem as an ILP problem. In the RSTRA problem, the transceivers are used for transmitting/receiving optical signals from/at source/destination nodes or regenerations. Solutions to the RSTRA problem minimize the spectrum and transceiver usage based on a weighting coefficient. Reference [33] also proposed a metaheuristic algorithm based on the simulated annealing approach to solve the optimization problem.

To implement the solution to the RSA with RP problem in realistic dynamic networks, on-demand algorithms must be developed. References [34, 35, 36] are the studies that focus on the RSA with RP problem in dynamic translucent EONs. Reference [34] proposed an energy-aware multidomain service provisioning algorithm for the limited RP scenario, which supposes that regenerators are placed at the border nodes of domains. Reference [35] proposed an RSA algorithm that considered novel criteria of regenerations. Reference [35] also proposed an RP algorithm that showed possible improvements to the usage of regenerators in the proposed RSA algorithm. Reference [36] proposed energy-efficient RSA with RP algorithms. The power consumption models proposed in [36] include the power consumption of five elements: optical cross connects, IP routers, transponders, regenerators, and amplifiers. In the proposed algorithm, the RP problem is sequentially solved to satisfy the required bit error rate for the pre-searched available optical path and spectrum. Therefore, the RP algorithm in [36] provided an indirect approach to improving the spectral efficiency and blocking probability of dynamic translucent EONs.

In this chapter, I propose a joint algorithm to solve the combined problem of RMSA and RP.

Because the RMSA problem is classified as NP-hard, the combined problem is also classified as NP-hard, and it is impossible to compute an optimum solution. Then, I adopt a dynamic approach in order to consider realistic network scenarios. The proposed algorithm provisions optical paths with directly improving the spectral efficiency and reducing the blocking probability in translucent EONs utilizing intermediate signal regenerations, as shown in Fig. 1.2. The main improvement provided by the proposed method is with regard to long-haul connections, while it also reduces the unfairness of EONs.

2.3 On-Demand Spectrum Allocation and Regeneration Placement Dividing Optical Paths

2.3.1 The Concept of Path Division

In this section, I discuss how the proposed on-demand SARP algorithms improve the blocking probability and fairness of translucent EONs. The basic idea is to mitigate the two constraints by dividing spectrally inefficient long optical paths into multiple sub-short optical paths with signal regeneration. The path set-up example in Fig. 2.3 illustrates the efficiency of the path division for a connection requiring an optical path from node A to node D where the total transmission distance is 4,200 km. In Fig. 2.3(a), the transparent EON tries to establish the transmission with a single long-haul optical path using QPSK due to its optical reach. However, the connection request is rejected because the optical path cannot satisfy the continuity constraints between node C and node D. On the other hand, in Fig. 2.3(b), the translucent EON also tries to establish a transmission path from node A to node D. In the translucent scenario, the transmission is established by two optical sub-paths from node A to C and from node C to D while utilizing signal regeneration at node C. The path division in translucent EONs has two advantages. The first is the selection of 8-QAM as the high-level modulation format because optical sub-path A is short enough to adopt it, which reduces the number of required FSs between node A and C. The second is the mitigation of the RSA continuity constraint. Signal regeneration allows each optical sub-path to be assigned to different contiguous FSs. Based on this example, it is clear that path division can improve the spectral efficiency and reduce the blocking probability of long-haul transmissions with signal regenerations.

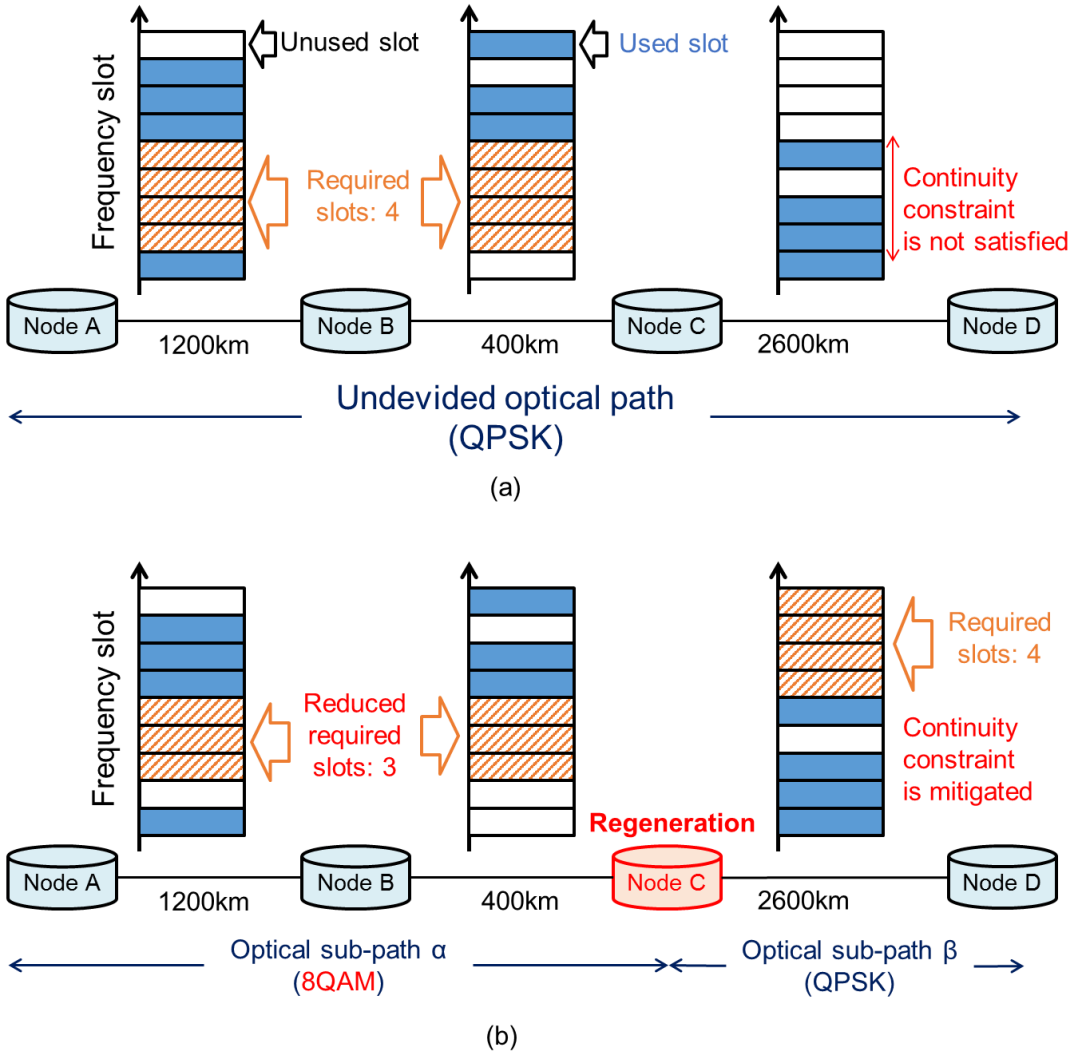

Figure 2.3: Comparison of two different path setup scenarios. (a) Transparent scenario w/o regenerations. (b) Translucent scenario w/ regenerations.

I propose two different SARP algorithms. The first is the "spectrally efficient SARP (SE-SARP) algorithm," which provides spectrum allocation with *proactive* RP to rejections of connection requests. The second is the "blocking aware SARP (BA-SARP) algorithm," which provide spectrum allocation with *reactive* RP to rejections of connection requests. The differences between these algorithms are related to both "how" and "when" the RP problem should be solved. A detailed description of these two algorithms is presented in the following sections.

2.3.2 Spectrally Efficient Spectrum Allocation and Regeneration Placement

The SE-SARP algorithm carefully divides the optical paths so that the highest-level modulation format can be adopted for each sub-path. The path division procedure is conducted proactively before solving the RSA problem to minimize the required bandwidth. This algorithm provides a simple sub-optimal dynamic solution because optical paths established by the algorithm always occupy as narrow bandwidth as possible. Although the SE-SARP algorithm has the highest spectral efficiency, a massive number of regenerations is required.

A flowchart of the overall on-demand path provisioning method in the SE-SARP algorithm is shown in Fig. 2.4. The process involves the following four steps. (1) When a new connection request arrives for a source-destination (SD) pair, the transmission route with the fixed shortest path is selected. The fixed shortest paths were calculated for all the SD pairs in advance. (2) After the routing process, the SE-SARP algorithm divides the end-to-end optical path into multiple optical sub-paths based on Alg. 2.1. The purpose of the path division in Alg. 2.1 is to allow for the highest possible modulation format in each optical sub-path. (3) Then, the available highest-level modulation format is selected for each optical sub-path according to the reach of the modulation format, and the number of required FSs is also calculated depending on the selected modulation format and demand size. (4) If there are no available FSs that satisfy the two constraints of the RSA problem for all optical sub-paths, the connection request is rejected. Otherwise, the proposed algorithm allocates FSs for the optical sub-paths according to a first-fit policy, and the connection request succeeds.

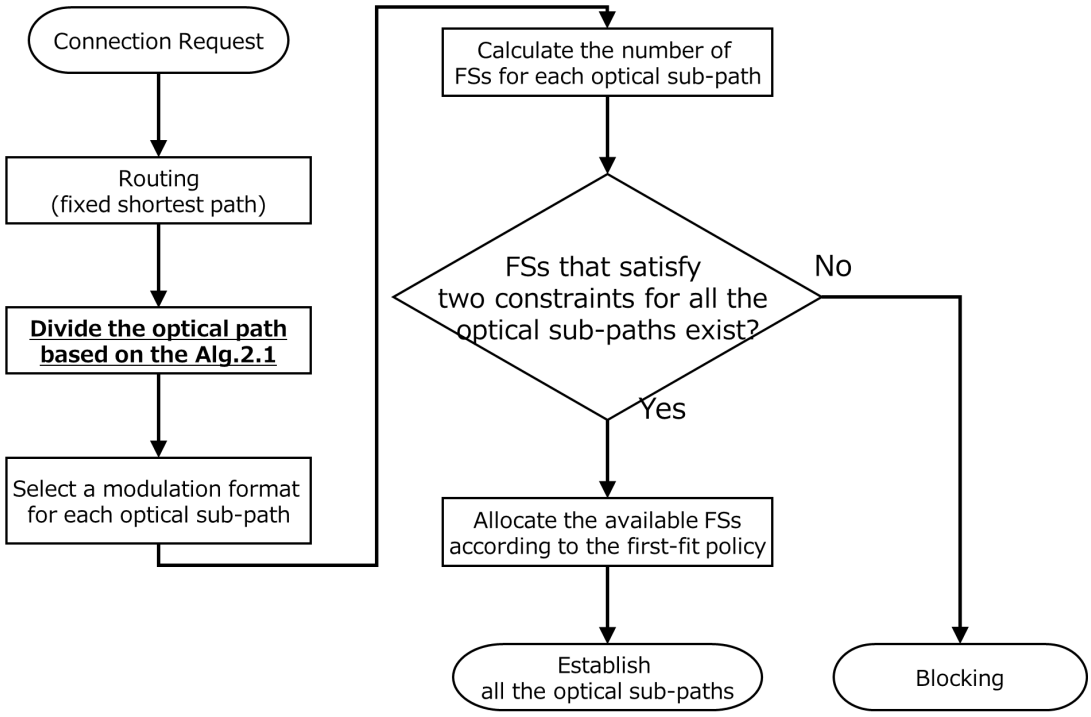

Figure 2.4: Flowchart of the SE-SARP algorithm.

Algorithm 2.1 Path division algorithm in SE-SARP

Require: network topology: $G(V, E)$, distance of link e: D_e, set of the links in the selected route: $\mathcal{R}$, reach of the highest-level modulation format: M.

Ensure: set of the nodes in which regeneration is placed: $\mathcal{V}_{RP}$.

$d \leftarrow 0$
for $k = 1$ **to** $|\mathcal{R}|$ **do**
  $e \leftarrow$ the k-th link of the selected route from the source node.
  if $D_e \geq M$ **then**
    $v \leftarrow$ the source-side edge node of the e ($k \neq 1$).
    $\mathcal{V}_{RP} \leftarrow v$
    $v \leftarrow$ the destination-side edge node of the e ($k \neq |\mathcal{R}|$).
    $\mathcal{V}_{RP} \leftarrow v$
    $d \leftarrow 0$
  else if $d = 0$ **then**
    $d \leftarrow D_e$
  else
    if $d + D_e > M$ **then**
      $v \leftarrow$ the source-side edge node of the e.
      $\mathcal{V}_{RP} \leftarrow v$
    else
      $d \leftarrow d + D_e$
    end if
  end if
end for
return $\mathcal{V}_{RP}$

2.3.3 Blocking Aware Spectrum Allocation and Regeneration Placement

The BA-SARP algorithm divides an optical path when a transparent single optical path cannot be allocated to a required connection. In this algorithm, the path division procedure is conducted reactively depending on the blocking of the connection request. In comparison to the SE-SARP algorithm, this algorithm provides a reasonable solution from the perspective of the required number of regenerations. The BA-SARP algorithm can improve the performance of translucent EONs, while suppressing excessive increases in the number of regenerations.

A flowchart of the overall on-demand path provisioning method with the BA-SARP algorithm is shown in Fig. 2.5. The process involves the following six steps. (1) When a new connection request arrives for a source-destination (SD) pair, the transmission route with the fixed shortest path is selected. The fixed shortest paths were calculated for all the SD pairs in advance. (2) After the routing process completes, the available highest-level modulation format is selected for the single end-to-end optical path, and the number of required FSs is also calculated depending on the selected modulation format and demand size. (3) If there are available FSs that satisfy the two constraints of the RSA problem, the connection request succeeds, and the proposed BA-SARP algorithm completes. (4) Otherwise, the BA-SARP algorithm divides the end-to-end optical path into two optical sub-paths based on Alg. 2.2. The purpose of the path division in Alg. 2.2 is to divide the optical path at the source-side edge node of the link in which available FSs cannot be found. When the links which qualifies the condition are different depending on the focused FSs, the algorithm selects the link that is the farthest from the source node. (5) After path division, the available highest-level modulation format is selected for each optical sub-path according to the reach of the modulation format, and the number of required FSs is also calculated depending on the selected modulation format and the demand size. (6) If there are no available FSs that satisfy the two constraints of the RSA problem for all optical sub-paths, the connection request is rejected. Otherwise, the proposed algorithm allocates the FSs for the optical sub-paths according to the first-fit policy, and the connection request succeeds.

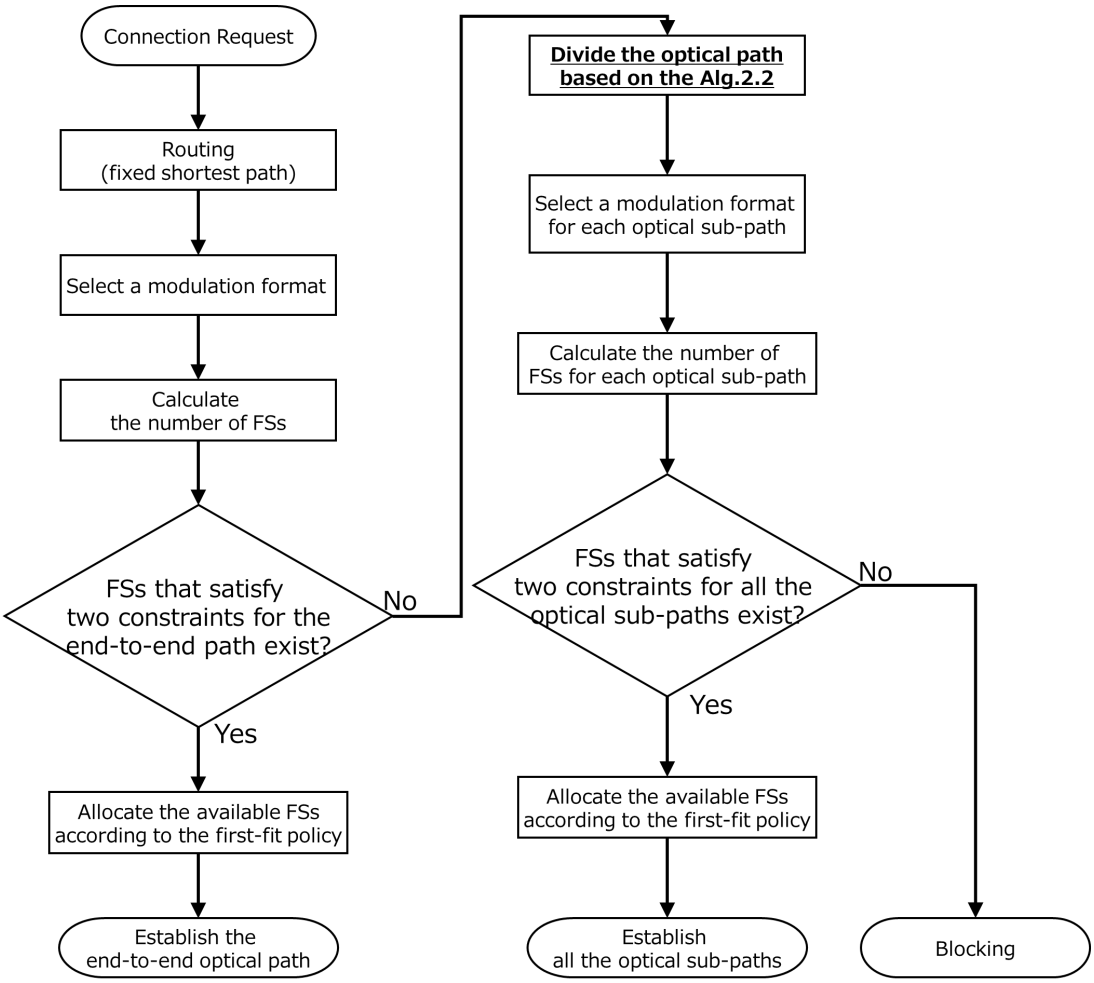

Figure 2.5: Flowchart of the BA-SARP algorithm.

Algorithm 2.2 Path division algorithm in BA-SARP

Require: network topology: $G(V, E)$, set of the links in the selected route: $\mathcal{R}$, Binary variable that equals 1 if i-th FS is not available in link e: $f_{e,i}$, set of $f_{e,i}$: $\mathcal{F}$, the number of required FSs: Δf.

Ensure: the node in which regeneration is placed: v.

```
l_max = 0
for i = 1 to |F| − Δf do
    l ← 0
    for k = 1 to |R| do
        e ← the k-th link of the selected route from the source node.
        if f_{e,i} + f_{e,i+1} + ··· + f_{e,i+Δf−1} = 0 then
            l ← l + 1
            continue
        else if l_max < l then
            l_max = l
            v ← the source-side edge node of the e.
            break
        end if
    end for
end for
return v
```

2.3.4 Spatial Channel Selection

I introduce simple fragmentation-aware (FA) policy regarding with spatial channel selection schemes for SDM-EONs. After solving the RSA with RP problem and deciding the selected FSs, SDM-EONs have to select the spatial channels of all links along the transmission route. In order to reduce the spectral fragmentation, the FA policy preferentially selects the spatial channels, in which the selected FSs are allocated without a gap between the focusing FSs and used FSs with regard to at least one of its upside and downside in a spectral domain. Otherwise, the FA policy selects spatial channels according to the first-fit policy.

2.4 Performance Evaluation

2.4.1 Simulation Model

I used my own C++ simulator to evaluate the proposed method. I adopted the JPN-12 (shown in Fig. 2.6 [63]) and US Backbone (shown in Fig. 2.7 [29]) topologies. The JPN-12 topology had 12 nodes and 17 links, while the US Backbone topology had 24 nodes and 43 links. Each link had eight optical fibers, which are spatial channels of SDM-EONs, for each direction. The

width of the FS was set to 12.5 GHz, and the total amount of spectrum resources per fiber was set to 4 THz (C band). Therefore, the number of FSs per fiber was $W = 320$. The connection requests were assumed to arrive according to a Poisson process with an average arrival rate λ, and the service time of each connection was assumed to follow a negative exponential distribution with an average $1/\mu$. Thus, overall traffic intensity is represented by λ/μ. The connection requests randomly required one source–destination (SD) pair; the traffic load (Erlang) means traffic intensity per SD pair, and it is represented by $\frac{i}{N\cdot(N-1)} \cdot \frac{\lambda}{\mu}$. The required demand size was randomly distributed between 12.5 and 200 Gbps. The number of required FSs was determined by the transmission distance and demand size, as shown in Table 2.1, which was based on [29]. Note that 32-QAM was only used in the JPN-12 topology. The "Transparent" method is introduced for comparison purposes, which allocates available spectra according to the first-fit policy of the FS index without regeneration.

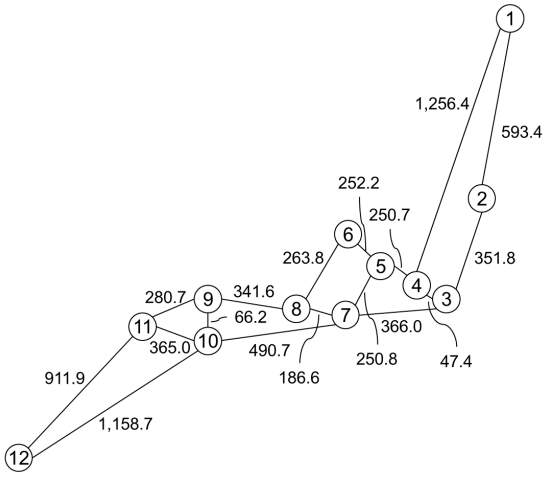

Figure 2.6: JPN-12 topology. The link distances are in kilometers.

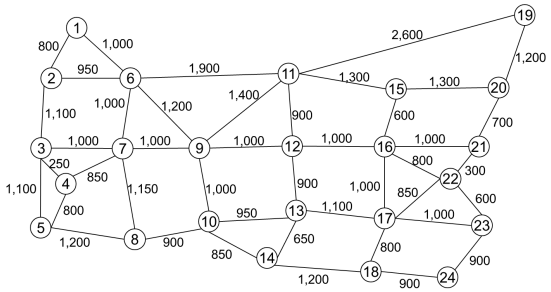

Figure 2.7: US Backbone topology. The link distances are in kilometers.

2.4.2 Bandwidth Blocking Probability

The bandwidth blocking probability (BBP) is used to evaluate the performance of the connection setups in EONs. In this chapter, the BBP is defined as the ratio of the total blocked demand size to the total required demand size.

Figures 2.8 and 2.9 depict the BBP of the overall network versus the traffic load. The BBP of

Table 2.1: Simulation parameters

Parameters	Values
Capacity of an FS	$12.5 \times m$ Gbps
Number of FSs for guard-band per connection	1
Transmission reach of BPSK ($m = 1$)	9600 km
Transmission reach of QPSK ($m = 2$)	4800 km
Transmission reach of 8-QAM ($m = 3$)	2400 km
Transmission reach of 16-QAM ($m = 4$)	1200 km
Transmission reach of 32-QAM ($m = 5$)	600 km

the overall network can be decreased by the two proposed SARP algorithms with path division. When the BBPs were several percent in the JPN-12 topology, the amount of accommodated traffic increased by approximately 3% and 34% for the BA-SARP and SE-SARP algorithms, respectively. When the BBPs were several percent in the US backbone topology, the amount of accommodated traffic increased by approximately 18% and 225% in the BA-SARP and SE-SARP algorithms, respectively. A comparison of these two figures indicates that the BBP reductions by the proposed methods are higher in large-scale networks. This is especially true for the BBP improvement of SE-SARP in the US backbone topology because it had longer-distance SD pairs than those in the JPN topology, and the cascaded regenerations in the SE-SARP algorithm provided greater spectral improvement.

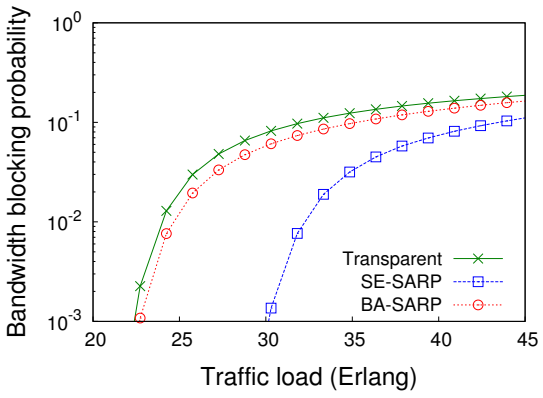

Figure 2.8: BBP of the overall network (JPN).

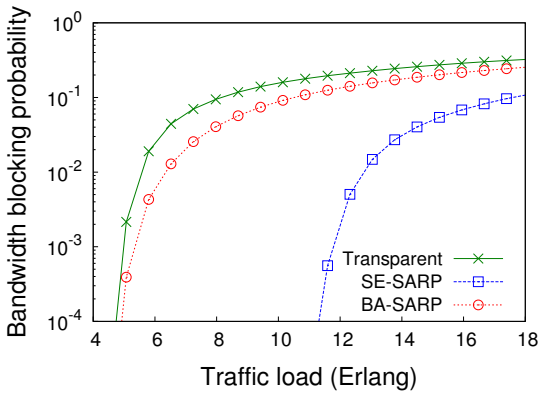

Figure 2.9: BBP of the overall network (US backbone).

2.4.3 Normalized Throughput and Fairness Index

I now introduce the normalized throughput (NTP) to evaluate the fairness of EONs. In this chapter, the throughput is defined as the sum of the demand size of the established connections per unit time. Reference [64] defined the normalized throughput to evaluate the performance of each base station in wireless networks. In Ref. [64] the normalized throughput of the i-th base station $T_{\mathrm{norm},i}$ is defined as

$$T_{\mathrm{norm},i} = \frac{T_i}{L_i}, \tag{2.1}$$

where T_i and L_i is the throughput and traffic load of i-th base station, respectively. I also introduce a fairness index (FI) to more directly evaluate the fairness of EONs. The FI is originally defined in [65], and Ref. [64] extended the definition to evaluate the fairness for throughput of base stations. Utilizing the NTP, the FI F is defined in [64] as follows.

$$F = \frac{\left(\sum_{i=1}^{N_{\mathrm{BS}}} T_{\mathrm{norm},i}\right)^2}{N_{\mathrm{BS}} \cdot \left(\sum_{i=1}^{N_{\mathrm{BS}}} T_{\mathrm{norm},i}^2\right)}. \tag{2.2}$$

Note that N_{BS} is the number of base stations in the network. I utilize these definitions by replacing the term "base station" with "SD pair."

The NTP of each SD pair is shown in Figs. 2.10 and 2.11 when the overall-network traffic load was 6400/10000 Erlang, which means traffic load was $48.48\ldots/18.11\cdots$ Erlang, in the JPN-12/US backbone topology. The horizontal axes show the SD pairs which are sorted in the ascending order of the distance of their fixed shortest paths. In the transparent EON, most of the long-distance SD pairs had low throughput because it was more difficult to satisfy the spectrum continuity constraint over long distances than it was for the short-distance SD pairs. This was also because the highest-level modulation format was frequently unavailable for them; thus, the required bandwidth tended to be wider. The proposed methods primarily improved the throughput of long-distance SD pairs, which is typically poor in transparent EONs. Conversely, some of the short-distance SD pairs in the proposed methods had lower throughput than those in the transparent EON. Figures 2.12 and 2.13 show the FI for the NTP of SD pairs. The results

show that the proposed methods that had high performance in terms of their BBP evaluations also scored high on the FI. To summarize the results and discussions in Sections 2.4.2 and 2.4.3, the proposed SARP algorithms primarily improved the performance of long-haul transmissions and improved the fairness of EONs related to the SD pairs.

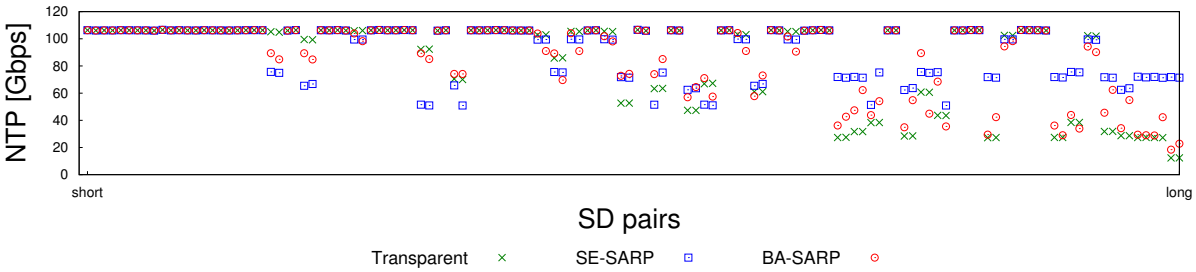

Figure 2.10: NTP of the SD pairs (JPN).

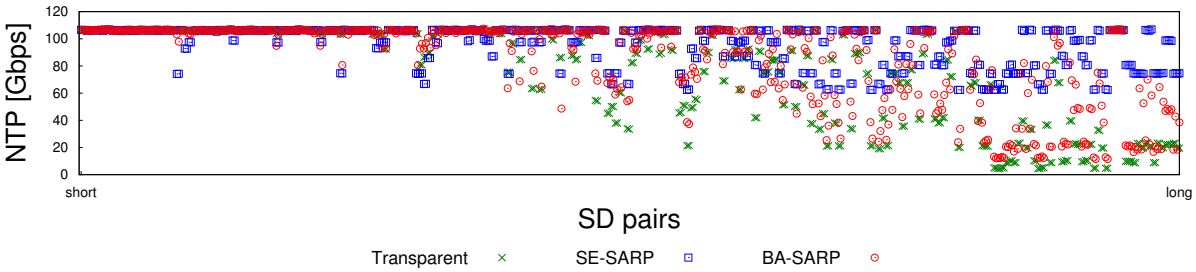

Figure 2.11: NTP of the SD pairs (US backbone).

2.4.4 Maximum Number of Regenerations

The maximum number of regenerations (MNR) was evaluated to assess the performance of regeneration placement. The MNR is defined as the maximum number of regenerations simultaneously utilized in the overall network or in each node throughout the simulation trials.

Figures 2.14 and 2.15 depict the MNR of the overall network versus the traffic load. The MNR of both proposed methods linearly increased with regard to the traffic load. The SE-SARP algorithm performed better than the BA-SARP algorithm from the perspective of the BBP; however, these results show that the BA-SARP algorithm required fewer regenerations.

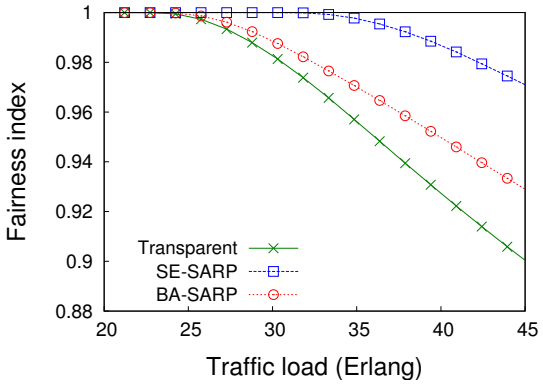

Figure 2.12: Fairness index for NTP of SD pairs (JPN).

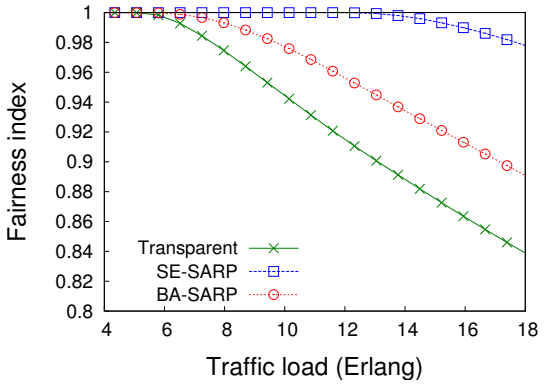

Figure 2.13: Fairness index for NTP of SD pairs (US backbone).

The difference in the MNR performance was significant in large-scale networks, as was the case for the BBP performance.

Figures 2.16 and 2.17 depict the MNR of each node when the traffic load was 6400/10000 in US backbone/JPN-12 topology. The results of these evaluations indicate the number of regenerators that were required in each node to achieve the BBP performance shown in the previous subsection. The comparison of the two proposed methods in these figures demonstrates that the nodes that required many regenerators were the same for both methods, and the required number of regenerators for each node varied widely. In particular, Fig. 2.17 indicates that more than 70% of the total number of regenerators were located at only three nodes in the BA-SARP method in the US backbone topology.

2.4.5 Discussion

In this subsection, I discuss which algorithm performed better. I introduce the BBP improvement (BBPI) parameter to this discussion to represent the degree to which the BBP was improved per each required regeneration. The BBPI of the SE-SARP I_{SE} is defined as follows.

$$I_{SE} = \frac{1 - \frac{P_{SE}}{P_{TP}}}{N_{SE}}. \tag{2.3}$$

Note that P_{SE} is the BBP of the SE-SARP, P_{TP} is the BBP of the "Transparent," and N_{SE} is the MNR of the SE-SARP. The BBPI of the BA-SARP I_{BA} is similarly defined utilizing the BBP

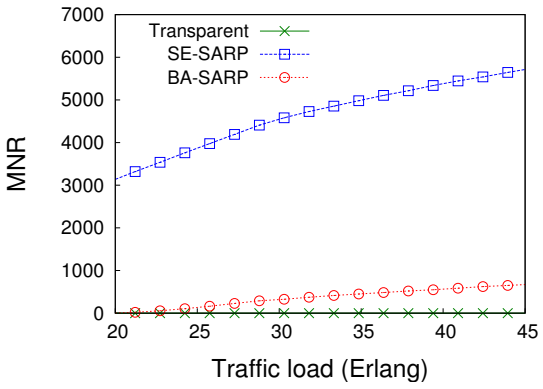

Figure 2.14: MNR of the overall network (JPN).

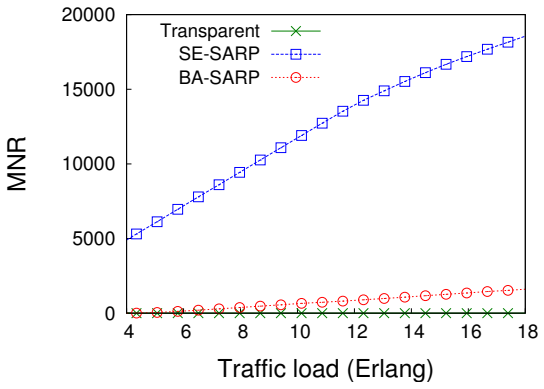

Figure 2.15: MNR of the overall network (US backbone).

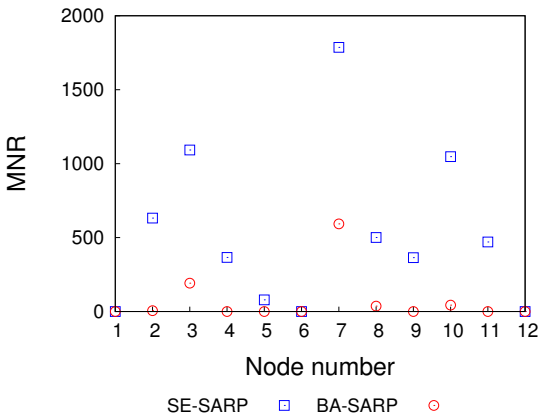

Figure 2.16: MNR of each node (JPN).

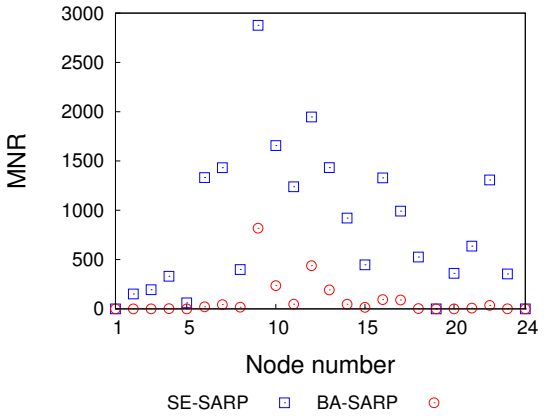

Figure 2.17: MNR of each node (US backbone).

of the BA-SARP, the BBP of the "Transparent," and the MNR of the BA-SARP. The BBPIs of both algorithms are shown in Figs. 2.18 and 2.19. These results indicate that the BA-SARP algorithm is superior to the SE-SARP in terms of the efficient utilization of regenerations. It should be noted that there are some constraints related to the cost and scale of each node in realistic EONs, although these constraints are not addressed in this chapter. Therefore, my results show that the BA-SARP algorithm is more practical than the SE-SARP algorithm.

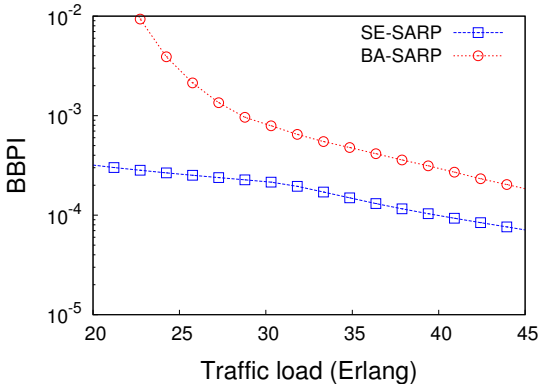

Figure 2.18: BBPI of the overall network (JPN).

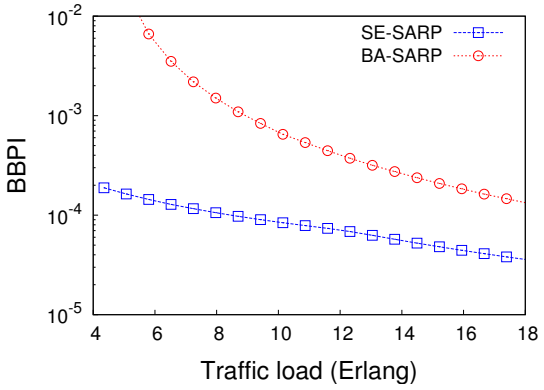

Figure 2.19: BBPI of the overall network (US backbone).

2.5 Conclusion

To address capacity challenges in large scale core optical networks, translucent EONs, which regenerate the optical path at intermediate nodes, have been proposed and investigated. In terms of spectral efficiency, the regenerated shorter optical paths have significant advantages related to the selection of modulation format and continuity constraint of the RSA problem. In this chapter, I investigated the dynamic RSA with RP problem in translucent EONs, and focused on the improvement of the spectral efficiency by RP. In my proposed spectrally efficient or blocking-aware SARP algorithms, the path division method utilizing optical regeneration improved the performance of long-haul transmissions by allowing the selection of higher-level modulation formats and changes in the signal frequencies. I evaluated the proposed method using extensive computer simulations, and found that the proposed method could reduce the BBP of the overall network. The improvement was particularly effective for long-haul transmission requests;

therefore, the throughput of SD pairs in translucent EONs can be made fairer. In conclusion, I determined that the BA-SARP algorithm was a more practical method than the SE-SARP algorithm because the BBP improvement per required regeneration was higher.

Chapter 3

Optical Path Provisioning Considering a Variety of Reservation

3.1 Introduction

The elastic optical network (EON) was introduced by [7] as a promising technology to increase the transmission capacity of optical networks because it can flexibly exploit spectrum resources by selecting modulation formats based on both the requested bit rates and optical reach [2]. However, despite recent improvements in spectrum utilization by EONs, the future increases in traffic in backbone networks will soon exhaust the expanded transmission capacity. Space division multiplexing (SDM) technologies, including multi-fibers, -cores, and -modes, have been investigated extensively in order to accommodate more network traffic. At the network level, the routing and spectrum assignment (RSA) problem is the most important issue that affects SDM-based EONs where the aim is to make full use of limited resources. In EONs, repeatedly setting up and taking down connections with various bandwidth sizes in order to satisfy the continuity and contiguity constraints in a dynamic network environment yields many fragmentations, which are non-contiguous small pieces within the spectral resources. These fragmentations lead to the waste of spectrum resources.

Traditionally, each traffic request needs to reserve network resource to establish a connection immediately after it arrives. On the other hand, it is important to handle requests that can be reserved in advance in order to enhance the quality of service (QoS) for applications that can tolerate a delay before the start of service such as large data transfer [66]. The former are called immediate reservation (IR) requests and the latter are called advance reservation (AR) requests.

The time flexibility of AR requests makes spectrum fragmentation more influential in terms of the time domain as well as the frequency domain. Moreover, in networks that support the coexistence of IR requests and AR requests, it is difficult to reserve spectrum resources for IR requests because a lack of resources is caused by AR requests, which can reserve future spectrum resources. It leads to a large number of IR request blockings, and as a result, significant service degradation of IR requests. However, the desired service level of each type of requests for the network operator depends on the difference between them such as service charge. Therefore, control of the service level in terms of the Bandwidth Blocking Probabilities (BBPs) [67] of IR and AR requests based on the intention of the network operator is a challenging issue.

In this chapter, I propose a dynamic RSA method for reducing spectrum fragmentation, which also ensures the service level control of IR requests and AR requests in SDM-EONs. To combat spectrum fragmentation, this method classifies the frequency domain into multiple prioritized areas and common areas based on the number of frequency slots required, thereby aligning the utilized spectrum resources in an appropriate manner. To cope with IR service degradation by AR requests, the method only allows IR requests to select a route among K-shortest-paths. Furthermore, spectrum areas dedicated to IR requests are established on the frequency domain, where their widths are controlled dynamically according to both the desired ratio of BBPs and the actual ratio of BBPs between IR and AR requests, thereby control the service level.

The remainder of this chapter is organized as follows. Section 3.2 describes related research into EONs and resource allocation methods for IR and AR requests. Section 3.3 proposes a novel dynamic RSA method, which reduces spectrum fragmentation and simultaneously improves the service level control of IR and AR requests. Section 3.4 presents performance assessments of the proposed method and I give my conclusions in Sec. 3.5

3.2 Service Classification and Network Environments

3.2.1 Immidiate Reservation and Advance Reservation Requests

Traffic requests can be classified into two types: immediate reservation (IR) and advance reservation (AR) requests. IR requests allocate bandwidth and start data transmission immediately

after the request arrival time. By contrast, AR requests can reserve future resources in advance and actually allocate the bandwidth at the service start time. The concept of AR requests for optical networks was initially proposed in [68]. AR requests are expected to provide better QoS for applications that require large amounts of bandwidth and where the service start time can be delayed for a certain amount of time, such as off-site backups and grid computing [69]. Furthermore, AR requests can be beneficial for efficient network resource usage compared with IR requests because of the flexibility in the time domain.

The RSA problem is the most important issue that affects EONs from the perspective of networking. To effectively use the flexibility of AR requests in the time domain, numerous studies have investigated RSA schemes for AR requests as well as RSA for IR requests. In [70] and [71], ILP formulations were presented for the RWA problem with static traffic based on the multicast of AR requests in rigid WDM networks, while a dynamic multicast RWA algorithm was presented in [72]. Dynamic RSA including the adaptive selection of modulation formats for AR requests in EONs was initially proposed in [73]. In [74], a method was proposed to reduce spectrum fragmentation in terms of the time domain and the frequency domain by combining the two dimensions. These studies assumed a network where only AR requests are generated but it is also important to concurrently serve IR requests to diversify network applications.

In optical networks that support the coexistence of IR and AR requests, it is difficult to reserve spectrum resources for IR requests, as shown in Fig. 3.1, because AR requests tend to reserve spectrum resources in advance. Therefore, the current resources available for IR requests are wasted. The pre-reservation characteristic of AR requests leads to a much higher bandwidth blocking probability (BBP) for IR requests compared with that for AR requests. If the network operator intends to just improve spectrum utilization, AR requests should have higher priority than IR requests and IR service degradation by AR requests does not matter. On the other hand, in networks where service charge for IR requests is higher than that for AR requests, the network operator may try to improve the IR service level instead of spectrum utilization. In addition, network operators may try to ensure different service levels for IR and AR requests considering uneven IR traffic profiles [38]. In this scenario, I address the service level (namely, BBPs) control of IR and AR requests according to the intention of the network

operator.

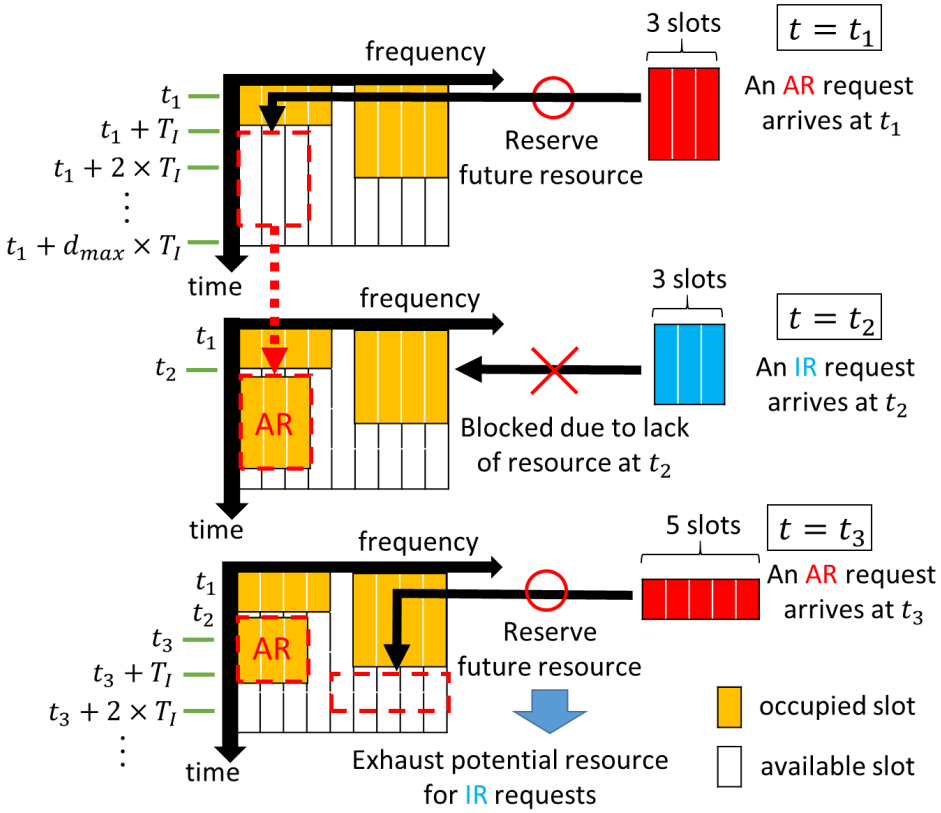

Figure 3.1: Challenge due to the coexistence of IR and AR requests. The used symbols are explained in Sec. 3.2.2.

In [75], a method was proposed for blocking AR requests and increasing resources for IR requests when the network utilization exceeds a certain rate. This method assumes traditional, rigid WDM networks. Thus, it is important to reduce spectrum fragmentation to apply this method to EONs. Some recent studies have discussed the coexistence of IR and AR requests in EONs [37, 38]. Specifically, in [37], a method was proposed for dynamic holding time-aware routing, modulation, and spectrum assignment (RMSA), which comprises two phases of RMSA for arriving requests and the re-optimization of scheduled AR requests that are not in service. In this study, they aimed to reduce the entire blocking probability by reducing two-dimensional fragmentations but they did not consider the service level of IR and AR requests. Moreover, holding time-awareness for all IR and AR requests may be infeasible in networks with various applications. In [38], the aim was to minimize the conflict among currently provisioned IR and pre-reserved AR under the assumption that AR requests had higher priority than IR requests.

The model of IR and AR requests as well as the occurrence of conflict was different from the network environments assumed in the present study.

3.2.2 Network Environments

In this chapter, I suppose each fiber has multiple isolated cores, therefore the effect of crosstalk or mode-coupling can be negligible. A network comprises $(V,\ E)$, where V is the set of network nodes and E is the set of network links. Every link has N_{space} multiple independent spatial channels $\mathbf{S}$ ($\mathbf{S} = S_1, S_2, ..., S_{N_{space}}$). Every core has C as the bandwidth capacity and C is divided into N_{slot} slots in terms of the number of frequency slots. A frequency slot has $M \times \frac{C}{N_{slot}}$ as the transmission capacity, where M is the modulation level (e.g. $M = 1$ when binary phase-shift keying (BPSK), $M = 2$ when quadrature phase-shift keying (QPSK)).

An IR request comprises four tuples, black$(s,\ d,\ b,\ \Delta,\ t_{arrival})$, where s and d are the source and destination nodes, respectively, b is the required bit rate, Δ is the holding time of the request, and $t_{arrival}$ is the request arrival time. A network contains IR requests with both specific and unknown service durations. The value of Δ for the requests with unknown holding times is assumed to be infinity and the bandwidth reserved by the requests is released at the actual end of service.

Compared with an IR request, an AR request has another tuple $(s,\ d,\ b,\ \Delta,\ t_{arrival},\ d_{max})$, where d_{max} is the maximum delay tolerated by the AR request for the service starting from $t_{arrival}$ in terms of the number of time interval. For simplicity, I assume the service start time of AR requests is discrete from $t_{arrival}$ with the time interval of T_I. Therefore, the set of time $\{t_{arrival},\ t_{arrival} + T_I,\ t_{arrival} + 2 \times T_I,\ ...,\ t_{arrival} + d_{max} \times T_I\}$ is the candidate start time for the AR request. AR start time is discrete but the other tuples including Δ, $t_{arrival}$, and T_I are continuous. Thus, the network is operated in a continuous-time manner.

Similar to IR requests, I employ two types of AR requests in specific start time and specific (or unknown) duration (STSD or STUD) models with a flexible window as described in [69].

3.3 On-Demand Routing and Spectrum Allocation Considering a Variety of Reservation

3.3.1 Concept of the Proposed Method

I propose a novel dynamic RSA method for reducing spectrum fragmentation as well as controlling the service level of IR requests and AR requests in multi-core EONs. This method configures prioritized areas based on the required frequency slots to reduce spectrum fragmentation. Each prioritized area is divided into two sub-areas: one dedicated to IR requests (IR-dedicated sub-area) and another that is shareable for both IR and AR requests (shareable sub-area). IR-dedicated sub-areas maintain the spectrum resources for IR requests even if the reservations for AR requests increase. Note that I set not AR-dedicated sub-areas but shareable sub-areas because AR requests can be easily allocated compared with IR requests due to flexibility in the time domain. In addition, the border of the IR-dedicated and shareable sub-areas is moved dynamically to obtain the desired ratio for the BBPs of IR and AR requests. Each prioritized area and sub-area follow the same spectrum division in all the cores of the network at all times because this helps to satisfy the continuity constraints on a transmission route in RSA. This method is called AR-Limited (AR-L).

AR requests can reserve future resources in advance, but IR requests can only reserve the resources at the request arrival time. Therefore, in general, relatively fewer resources are potentially available for IR requests than AR requests. This method makes more resources available to IR requests than AR requests in terms of the routing for each request. In particular, this method allows only IR requests to select a route among K candidate routes which are precomputed by the K-shortest-path algorithm, while AR requests can only use the shortest-length route, which increases the spectrum resources available for IR requests.

The proposed method reserves the available resources that are found first, whereas many previous methods ([73], [74], [37], [38]) search for all of the possible resources. Methods that search for all of the possible resources can reduce spectrum fragmentation based on a broad view of the network resources, but they have much higher computational complexity. By contrast, the proposed method pre-defines prioritized areas based on the number of frequency

slots. Allocating connection requests in the corresponding prioritized areas suitably arranges utilized spectrum resource without search for all of the possible resources. It means unoccupied resources likely get the just-enough size for later incoming requests, resulting in reduced spectrum fragmentation.

I propose another RSA method that configures common areas in addition to prioritized areas to reduce spectrum fragmentation. This method is called AR-L-Common (AR-L-C). In AR-L, if a prioritized area is fully occupied, overflowed requests are allocated in other prioritized areas. It generates spectrum fragmentation in other prioritized areas and subsequently fragmentation occurs in the area. To cope with this situation, AR-L-C configures a common area in addition to prioritized areas in order to accommodate overflowed requests in prioritized areas. If there is a common area, spectrum fragmentation likely occurs not in prioritized areas but in the common area, which ensures resource alignment in prioritized areas. In addition, generally, there are differences in the total bandwidth (the number of frequency slots) on each link that users request. This difference makes it difficult to reduce spectrum fragmentation by configuring prioritized areas, which follow the same spectrum division for each unit of frequency slots throughout the network links. The common area helps to relieve the effects of the difference in the total bandwidth required for each link.

Figure 3.2 shows the difference between AR-L and AR-L-C with prioritized areas and a common area, including the corresponding IR-dedicated and shareable sub-areas in the two domains of frequency and core. Note that Fig. 3.2 represents a virtual resource design example for proposed RSA and the detailed resource allocation is not considered here. The relative size of each prioritized area is computed statically based on the statistical characteristic of the topological bottleneck link (TBL) in the target topology, which follows [76]. TBL is defined as the link to which the most connection requests are assigned when all the source and destination pairs have the same arrival rate, and the shortest path is always selected. The size of each prioritized areas is statically fixed.

In order to mitigate the excessive restriction of AR allocation, the common area is kept available for both IR and AR requests (shareable sub-areas).

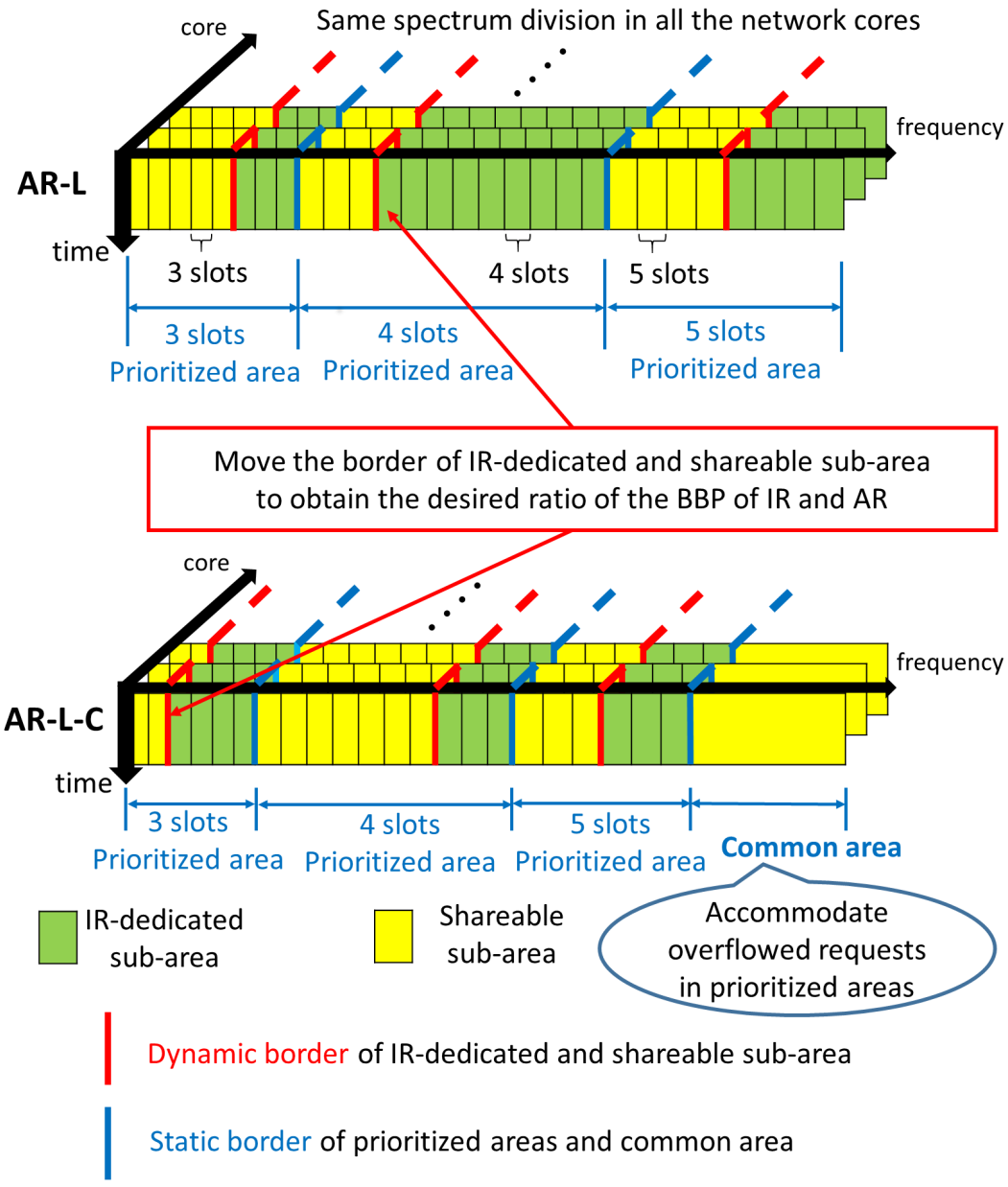

Figure 3.2: Virtual resource design of the proposed methods. All the areas and the sub-areas follow the same spectrum division in the network including the core domain due to the continuity constraint on the transmission route in RSA.

3.3.2 Symbols

The symbols used in my proposed algorithm are described in Table I. Among them, α, β, γ are the parameters of my method. The details are described in the next section.

Table 3.1: Symbols used in pre-definitions

Symbols	Description
w	required number (width) of frequency slots
d_w	divisor of w
f_i	i-th frequency slot
$P_{IR\ (\gamma)}$	BBP of IR requests with γ samples
$P_{AR\ (\gamma)}$	BBP of AR requests with γ samples
U_{IR}	utilization ratio of IR-dedicated sub-areas on the TBL in the network
α	desired ratio of the BBP of AR relative to that of IR
β	threshold for the utilization ratio in IR-dedicated sub-areas
γ	number of samples used for border movement
$\mathbf{R}$	set of candidate transmission routes
$r_i\ (\in \mathbf{R})$	the i-th route of R
K	number of candidate routes for K-shortest-path algorithm
$\mathbf{L^r}$	set of the links with r in order from the source to destination
l_i^r	i-th link of r from the s to d
$\mathbf{B^w}$	set of spectrum blocks (w continuous FSs)
$\mathbf{B_i^w}\ (\in \mathbf{B^w})$	i-th spectrum blocks for w slots
$\mathbf{S^A}$	set of allocated cores for a request
S_i^A	allocated core on the i-th link of a route

3.3.3 Configuration and Movement of the Border between IR-Dedicated and Shareable Sub-areas

IR-dedicated and shareable sub-areas are initialized by dividing each prioritized area based on the statistical traffic matrix of the IR and AR requests. The border of these sub-areas is moved dynamically to control the BBPs of IR and AR requests based on the parameter α, where α is statically set by the network operator as the desired ratio of BBP of AR requests relative to that of IR requests.

The border is moved to the same location on all of the links in the network when IR or AR

requests are blocked. If an IR request requiring w slots is blocked and Eq. (3.1) is satisfied, the border in the corresponding prioritized area is moved by w slots in a suitable direction to increase the IR-dedicated sub-areas over all the network links. Note that $P_{IR\ (\gamma)}$ is the BBP for IR requests with γ samples and $P_{AR\ (\gamma)}$ is that for AR requests. IR requests have K candidate routes and each of them may have different w. I assume w for blocked IR requests is the number of required slots when the shortest path is selected.

$$\frac{P_{AR\ (\gamma)}}{P_{IR\ (\gamma)}} < \alpha. \tag{3.1}$$

From the perspective of network resource utilization, IR-dedicated sub-areas should be well occupied when an AR request is blocked. Therefore, if an AR request is blocked and Eq. (3.2) is satisfied, the border is moved by w slots in a suitable direction to increase the shareable sub-areas in all the network links regardless of the BBP of each traffic request. Note that U_{IR} is the utilization ratio for IR-dedicated sub-areas on the TBL in the network.

$$U_{IR} < \beta. \tag{3.2}$$

Even if Eq. (3.2) is not satisfied, the border is moved to increase the shareable sub-areas in all the network links if Eq. (3.3) is satisfied.

$$\frac{P_{AR\ (\gamma)}}{P_{IR\ (\gamma)}} > \alpha. \tag{3.3}$$

In this chapter, each border is located at the same position in the core domain in light of the continuity constraint in the transmission route. However, spectrum utilization may be improved by individually setting borders per core considering the congestion of each link, which is my future work.

3.3.4 Proposed RSA Algorithms

Next, I describe the detailed individual RSA algorithms for IR and AR requests. Algorithms 3.1 and 3.2 show the procedures of the proposed RSA based on prioritized areas for IR and AR requests, respectively, after a connection request arrives.

RSA for IR requests

Firstly, when the network operation starts, K routes for all the source-destination pairs are computed beforehand. When an IR request arrives, precomputed K routes from s to d become candidate routes $\mathbf{R} = \{r_1, r_2, ..., r_K\}$ in ascending order of the route length. A modulation format with the highest-level of M is selected for each candidate route based on its route length. The number of required frequency slots w is determined according to the selected modulation format and the required bit rate b. Considering the contiguity constraint in the frequency domain on the route r_i, the candidate spectrum blocks $\mathbf{B^w} = \{\mathbf{B_1^w}, \mathbf{B_2^w}, ..., \mathbf{B_{N_{slot}-w+1}^w}\}$ are initially defined with elements that are continuous w slots in the frequency domain ($\mathbf{B_1^w} = \{f_1, f_2, ..., f_w\}, \mathbf{B_2^w} = \{f_2, f_3, ..., f_{w+1}\}, ...$). After the initialization mentioned above, the proposed method starts by searching for an available spectrum block B_i^w from the lowest index to the highest (First-Fit policy), preferably in the prioritized area for w slots. If a core is found where the same spectrum block is unoccupied for the duration of possible data transmission at every link on the transmission route r_i, the bandwidth is allocated using the resources for the request. If no available resources are found in the prioritized area on r_i, the method does not search in the common area or non-prioritized area for w on r_i, but instead it searches the prioritized area on r_{i+1} for the IR request. Searching the non-prioritized area for w slots after checking all of the resources in the prioritized area is helpful for assigning spectrum resources in the corresponding prioritized area as much as possible, which reduces spectrum fragmentation. If there are no available resources in the prioritized area on any candidate route, the RSA procedure (lines 3–20 of Alg. 3.1) is repeated in the prioritized areas for d_w, where d_w is a divisor of w, because it makes no fragmentation. Note that if there are candidates for d_w, d_w is selected in the descending order. Next, the common area (only for AR-L-C) and the prioritized areas except for w and d_w slots are searched. The request is blocked if no available resources are found in any areas, which indicates a lack of spectrum resources for IR requests. Therefore, if Eq. (3.1) is satisfied, the border between IR-dedicated and shareable sub-areas in the prioritized area for w slots is moved by w slots in a direction that increases the IR-dedicated sub-areas on all the links throughout the network.

RSA for AR requests

The basic RSA procedure for AR requests is similar to that for IR requests. The main differences are in the parts related to sub-area coverage, routing, and searching in the time and frequency domains, as follows.

- Search in the time domain

  AR requests have the time flexibility compared to IR requests, meaning that RSA for AR requests needs to consider when to reserve bandwidth. The proposed RSA tries to reserve spectrum resources as soon as possible after the request's arrival in order to utilize current resources and to reduce the average delay until the service start for AR requests. (line 3 in Alg. 3.2)

  AR requests whose service start time is specifically fixed in advance (e.g. video conferencing) can be allocated with the proposed algorithm if $t_{arrival}$ and d_{max} is set to the service start time and 0, respectively. However, the BBP of these AR services should be worse than that of delay-tolerant AR services due to the difference of flexibility in the time domain. Thus, in order to ensure the service level control including the AR services with fixed-start time, a more sophisticated algorithm of RSA and border movement, which is out of scope in this chapter, will be studied.

- Sub-area coverage

  IR requests can search all of the spectrum blocks, including both IR-dedicated and shareable sub-areas. However, the resources for AR requests are limited to the shareable sub-areas (line 4 in Alg. 3.2).

- Routing

  AR requests can search only a specific route from s to d, whereas the proposed method provides routing options to IR requests. This approach aims to equalize the dimensions of the solution space, which includes the route, frequency, and core for IR requests, as well as the time, frequency, and core for AR requests to provide flexible control of the BBPs.

- Search in the frequency domain

AR requests search for an available spectrum block from the highest to the lowest index (Last-Fit policy) in the frequency domain, in contrast to the First-Fit policy for IR requests. The spectrum search from the inverse direction for each request in the frequency domain separates the potential resources for each request, which makes it easier to move the border between IR-dedicated and shareable sub-areas. Figure 3.3 shows an example of order of search-point in the proposed algorithm based on the three domains of core, frequency and time individually for IR and AR requests. AR requests can reserve bandwidth from the search-point time if selected B_i^w is unoccupied for the holding time Δ from that time on the transmission route r.

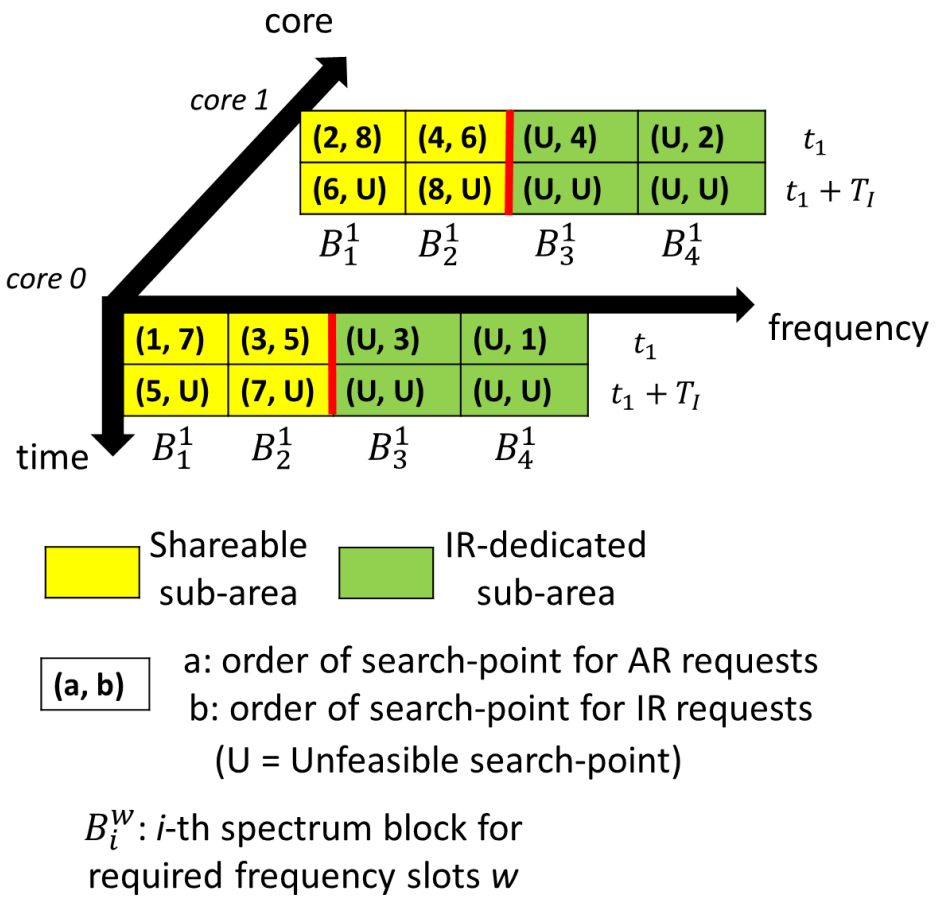

Figure 3.3: Order of search-point in the proposed algorithm.

3.3.5 Complexity Analysis

The time complexity of the proposed RSA for an IR request is $\mathcal{O}(K \times |\mathbf{B^w}| \times |\mathbf{L}| \times |\mathbf{F}|)$, which is due to the for-loop in Lines 3–20 of Alg. 3.1. I assume K at most 5 or so, which is also assumed in [37], [38].

Algorithm 3.2 shows that the time complexity of the proposed RSA for an AR request is $\mathcal{O}(d_{max} \times |\mathbf{B^w}| \times |\mathbf{L}| \times |\mathbf{F}|)$ with the for-loop in the time domain instead of the for-loop for routing IR requests.

Algorithm 3.1 RSA for IR requests

Require: IR request $(s,\ d,\ b,\ \Delta,\ t_{arrival})$
Ensure: RSA solution (route, spectrum block, set of cores) or request blocking
1: Compute $\mathbf{R}$ between $s - d$
2: Determine w for each route and $\mathbf{B^w}$
3: **for all** $r_i (\in \mathbf{R})$ **do**
4: **for all** $\mathbf{B_j^w}$ in the prioritized area **do**
5: **for all** $l_p^{r_i}$ **do**
6: **for all** S_q on $l_p^{r_i}$ **do**
7: **if** $\mathbf{B_j^w}$ of S_q on $l_p^{r_i}$ available for $[t_{arrival}, t_{arrival} + \Delta]$ **then**
8: $F_p^A \leftarrow S_q$
9: break
10: **end if**
11: **end for**
12: **if** $S_p^A ==$ Null **then**
13: break
14: **end if**
15: **end for**
16: **if** $|\mathbf{S^A}| == |\mathbf{L^{r_i}}|$ **then**
17: **return** $(r_i, \mathbf{B_j^W}, \mathbf{S^A})$
18: **end if**
19: **end for**
20: **end for**
21: Repeat lines 3–20 in the prioritized areas for d_w slots
22: Repeat lines 3–20 in the common areas (for AR-L-C)
23: Repeat lines 3–20 in the prioritized areas except for w and d_w slots
24: Block the request
25: **if** Eq. (ref1) is satisfied **then**
26: Move the border to increase the IR-dedicated sub-area in the prioritized area for w slots
27: **end if**

Algorithm 3.2 RSA for AR requests

Require: AR request $(s,\ d,\ b,\ \Delta,\ t_{arrival},\ d_{max})$
Ensure: RSA solution (time, spectrum block, set of cores) or request blocking
1: Compute the specific r between $s - d$
2: Determine w and $\mathbf{B^w}$
3: **for** $t_{arrival} + t \times T_I$ such that $0 \leq t \leq d_{max}$ **do**
4: **for all** $\mathbf{B_i^w}$ in the shareable sub-area in the prioritized area **do**
5: **for all** l_p^r **do**
6: **for all** S_q on l_p^r **do**
7: **if** $\mathbf{B_i^w}$ of S_q on l_p^r available for $[t_{arrival} + t \times T_I, t_{arrival} + t \times T_I + \Delta]$ **then**
8: $S_p^A \leftarrow S_q$
9: break
10: **end if**
11: **end for**
12: **if** $S_p^A ==$ Null **then**
13: break
14: **end if**
15: **end for**
16: **if** $|\mathbf{S^A}| == |\mathbf{L^r}|$ **then**
17: **return** $(t, \mathbf{B_j^W}, \mathbf{S^A})$
18: **end if**
19: **end for**
20: **end for**
21: Repeat lines 3–20 in the prioritized areas for d_w slots
22: Repeat lines 3–20 in the common areas (for AR-L-C)
23: Repeat lines 3–20 in the prioritized areas except for w and d_w slots
24: Block the request
25: **if** Equation (3.2) or (3.3) is satisfied **then**
26: Move the border to increase the shareable sub-area in the prioritized area for w slots
27: **end if**

3.4 Performance Evaluation

3.4.1 Simulation Model

I evaluated the performance of the proposed RSA method based on computer simulations using my own C++ simulator. I sampled 10^8 connection requests in total for IR and AR requests. The JPN-12 topology [63] and USA topology shown in Figs. 3.4 and 3.5 were employed as the test networks. The JPN-12 topology has 12 nodes and 16 fiber links, whereas the USA topology has 28 nodes and 45 fiber links. Each fiber link was bidirectional and there were eight cores per direction ($N_{space} = 8$). I adopted the above homogeneous model because the evaluation in this chapter focused on the performance of prioritized areas for fragmentation and dynamic

border movement for the service level control of IR and AR requests. Therefore, more realistic network model where each link has different number of cores according to traffic demand [77] will be adopted in my future work. I set the width of a frequency slot as 12.5 GHz and the total spectrum resources per core comprised 4 THz (C-band). Therefore, the number of frequency slots per core N_{slot} was 320. The inter-arrival time of each connection followed an exponential distribution. The holding time Δ for IR and AR requests followed an exponential distribution with 10 as the average. Required bit rate b was uniformly distributed within the range between 12.5 Gbps and 200Gbps. The guard band size was 1 frequency slot. The modulation format with the highest modulation level of M was selected based on the route length, as shown in Table 3.2 [29]. The required frequency slots were determined among 2, 3, 4, 5, or 6 according to the selected modulation format and the required bit rate. Note that the requests which cannot be allocated with the highest-level modulation format (e.g. more than 187.5 Gbps and more than 4800 km) were not generated in the simulations. The number of candidate routes K was 3. The relative size of each prioritized area was computed according to the required ratio for each slot on the topological bottleneck link (TBL) under the condition that a request generates for each bit rate at the interval of 12.5 Gbps between 12.5 Gbps and 200 Gbps for all the source-destination pairs and the shortest-path is always selected.

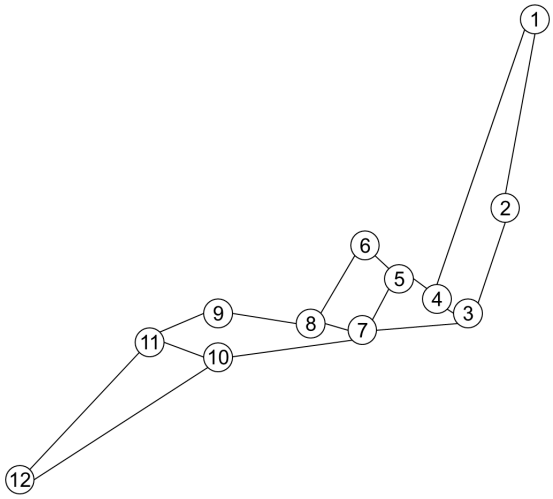

Figure 3.4: JPN-12 topology.

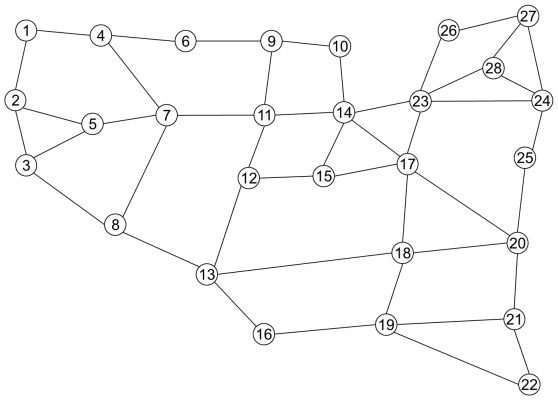

Figure 3.5: USA topology.

Source and destination nodes were selected randomly. The interval of AR search in the time

domain T_I was 1.0. An integer value from 1 to 10 was selected with equal probability as d_{max}. The load of the traffic requests, referred to "traffic load," was defined as the ratio of the required bandwidths for the TBL relative to its capacity. "Traffic load" satisfied the following equation:

$$\text{traffic load} = \frac{\lambda \times SP_{\text{BN}} \times BW_{\text{ave}} \times \Delta_{\text{ave}}}{SP_{\text{all}} \times N_{space} \times N_{slot}}, \tag{3.4}$$

where SP_{BN} is the number of shortest paths through the TBL, BW_{ave} is the average number of required frequency slots, Δ_{ave} is the average holding time, λ^{-1} is the average inter-arrival time of path set-up requests throughout the entire network, SP_{all} is the number of shortest paths for all source and destination pairs, N_{space} is the number of cores per link, and N_{slot} is the number of frequency slots per core.

I used the fragmentation ratio (FR) [78] as a metric of spectrum fragmentation for each number of slots on multi-core optical networks. $FR_{(E_i,w)}$ indicates the fragmentation of the slots on a particular link E_i in terms of w slots, and it is computed according to the following steps.

1. Every slot on E_i including all cores is marked as 1 if occupied or 0 if available.

2. $F_{B_i^w}$ is marked as 0 if all the slots in B_i^w are occupied or available, or as 1 otherwise for every spectrum block of continuous w slots. Note that $F_{B_i^w}$ indicates whether spectrum fragmentation occurs in B_i^w.

3. The sum of $F_{B_i^w}$ obtained from step (2) is computed for all the spectrum blocks of continuous w slots.

4. $FR_{(E_i,w)}$ is normalized in the range of (0–1) by dividing the sum obtained from step (3) by $|\mathbf{B^w}|$ in E_i.

FR_w^{net} indicates the fragmentation of the slots in the entire network in terms of w slots and it is computed according to the following equation.

$$FR_w^{net} = \frac{\sum_{E_i \in \mathbf{E}} FR_{(E_i,w)}}{|\mathbf{E}|}. \tag{3.5}$$

FR is computed at 10 time points, which are selected randomly based on a simulation and their average is used as the final value.

I compared the proposed method with the following three RSA methods.

- Unidirectional Allocation (UA)

  UA employs first-fit to search the frequency domain for both IR and AR requests, but without configuring the prioritized and common areas based on the frequency slots required. UA follows the core, time and frequency orders of search-point as shown in Fig. 3.6 to prevent the spread of reservations for AR requests in the frequency domain because the widespread reservation of the frequency domain limits the resources available for IR requests.

- Prioritized Unidirectional Allocation (PUA)

  PUA configures the prioritized areas based on the frequency slots required without a common area. The bandwidth is divided for each prioritized area in the same manner as AR-L.

- Unidirectional Allocation-Multi Route (UA-MR)

  UA-MR allows only IR requests to select a route among K routes from the source to destination using the K-shortest path algorithm, but without configuring the prioritized areas.

The parameters in the proposed method, i.e., α, β, and γ, were 1, 0.7, and 10^6, respectively. Each data point has a confidence interval of 95%.

Table 3.2: Relationship between modulation format and maximum transmission reach

Modulation format	Maximum transmission reach
BPSK ($M = 1$)	9600 km
QPSK ($M = 2$)	4800 km
8-QAM ($M = 3$)	2400 km
16-QAM ($M = 4$)	1200 km

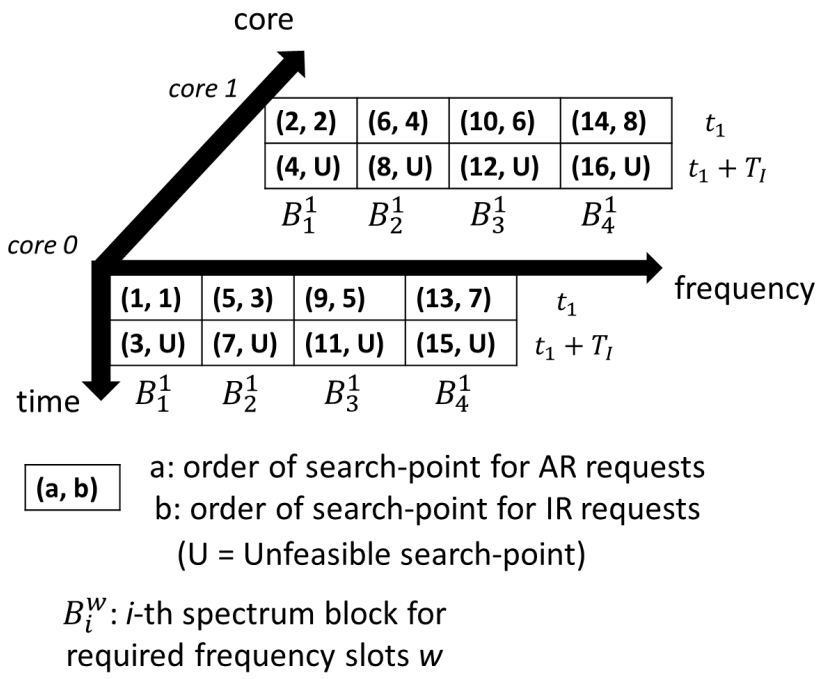

Figure 3.6: Order of search-point in UA.

3.4.2 Common area width

Figures 3.7 and 3.8 show the relationships between the BBPs (IR, AR and total of them) and the width of the common areas for AR-L-C when traffic load was fixed at 0.85 and IR and AR requests were generated with equal probability. Note that the common area widths were not plotted with the constant interval on the horizontal axis. This is because the relative size of each prioritized area for w slots depends on statistical traffic information on the TBL in each topology. In addition, it should have multiples of w slots and the remaining slots were included into the common areas. The total BBPs were the lowest with 20 and 29 common area widths for USA and JPN-12 topology, respectively. It indicates the common areas improve the spectrum utilization because they prevent fragmentation from occurring in prioritized areas and mitigate the difference in traffic for each link. In both topologies, the BBPs of IR and AR separated when the common area widths were greater than certain values. This is because all the resources in the common areas are kept available for both IR and AR requests (shareable sub-areas) in order not to excessively limit the resources for AR requests. Therefore, as the common area widths are greater, it gets more difficult to control BBPs for IR and AR requests by the border movement in

prioritized areas. In the later results, I adopted 20 and 29 as the common area width for AR-L-C in USA and JPN-12 topologies, respectively.

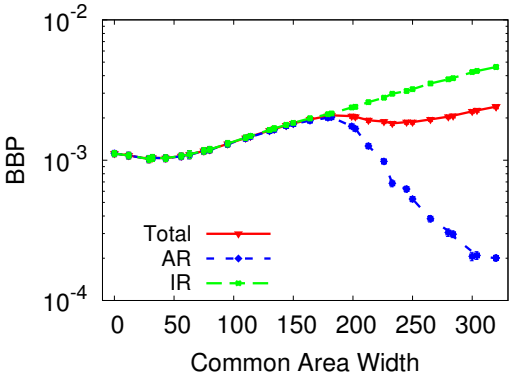

Figure 3.7: Common area width vs. BBP (JPN-12).

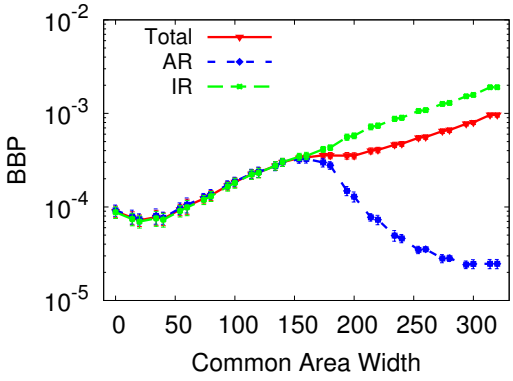

Figure 3.8: Common area width vs. BBP (USA).

3.4.3 Total Bandwidth Blocking Probability

Figures 3.9 and 3.10 show the total BBPs with the two proposed methods and the three comparison methods when the IR and AR requests were generated with equal probability. The BBPs were higher with the JPN-12 topology than the USA topology due to the definition of the "traffic load." In the previous subsection, I defined the traffic load as the expected utilization ratio of the TBL capacity, which means that the load of the entire network depends on some factors related to the topology configuration such as the number of network links and the degree of the nodes. The entire network load depended on the topologies, but the two proposed methods reduced the BBP with both the USA and JPN-12 topologies compared with the other methods. There are two main reasons for this improved total BBP. First, the proposed methods configure prioritized areas for each number of slots required in the frequency domain, which helps to reduce spectrum fragmentation. Second, these methods provide IR request options during routing and more potential resources are available than the comparison methods.

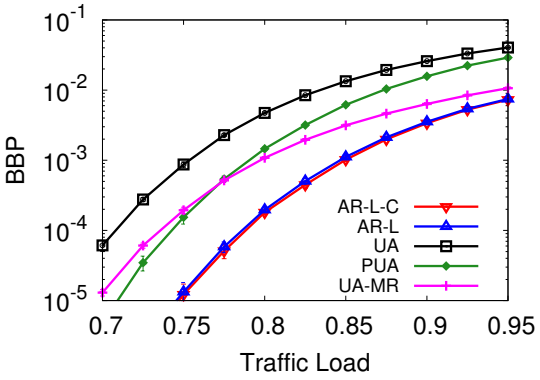

Figure 3.9: BBP for total traffic (JPN-12).

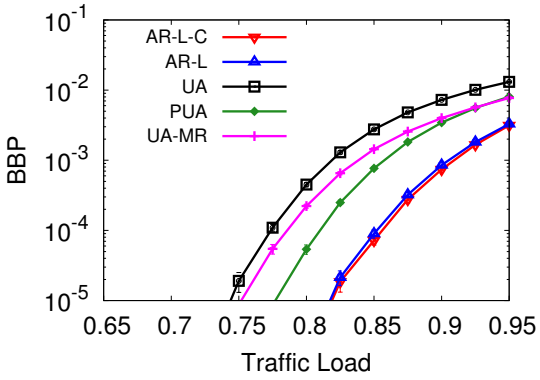

Figure 3.10: BBP for total traffic (USA).

3.4.4 Individual Bandwidth Blocking Probability

Figures 3.11 and 3.12 compare the individual BBPs for IR and AR requests with the five methods when the traffic load was fixed at 0.85. The BBPs of IR requests in UA, PUA, and UA-MR were much higher than those of AR requests because current resources for IR requests were likely pre-reserved by AR requests. In contrast, at many ratios of AR-requested traffic relative to the traffic load in the entire network, AR-L and AR-L-C had nearly the same BBPs for IR and AR requests by dynamic control of the border between the IR-dedicated and shareable sub-areas based on the desired ratio of $\alpha = 1$ (i.e., the desired BBPs for IR and AR requests were same.). However, when AR ratio was relatively small or large compared to IR requests in AR-L and AR-L-C, especially in USA topology, the BBP of the requests which generated less frequently tended to be higher than that of the other. The reason is the difference in the number of samples for each request. The proposed methods use BBPs of γ samples for the border movement decision. If the AR ratio of the traffic load is 0.1, (i.e. the IR ratio of the traffic load is 0.9), it means the arrival rate of IR requests is 9 times larger than that of AR requests. Therefore, the weight of a sample for border movement decision was much different for each type of requests. It resulted in the separation of the BBPs of IR and AR requests throughout the simulations.

Figures 3.13 and 3.14 show the individual BBPs of IR and AR requests when an integer value from 1 to maximum d_{max} was selected with equal probability for an AR request. Even

if the maximum d_{max} was changed, the two proposed methods controlled the BBPs of IR and AR requests according to the desired ratio α. However, the proposed methods did not improve the BBP of AR requests so much because they follow the BBPs of IR requests. The BBPs of AR requests for UA and UA-MR did not improve or even got worse when maximum d_{max} was large. This is because the resource search order of them. These methods follow the core, time, and frequency orders of search-point as shown in Fig. 3.6. Thus, they tends to search for future resources even when current resources on the frequency and core domain are available, which leads to the waste of current resources. Although PUA follows the same search order as UA and UA-MR, it reduces spectrum fragmentations with prioritized areas. Reduction of fragmentation in the frequency domain also helps to reduce fragmentation in the time domain. Therefore, PUA effectively utilized the resources in the time domain, which leaded to the improvement in the BBPs of AR requests.

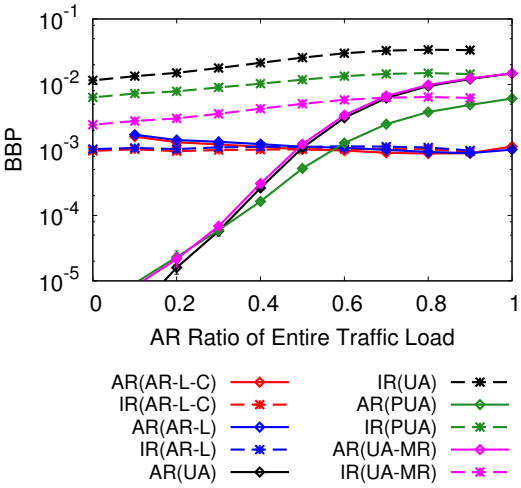

Figure 3.11: AR ratio of traffic load vs. BBPs for IR and AR requests (JPN-12).

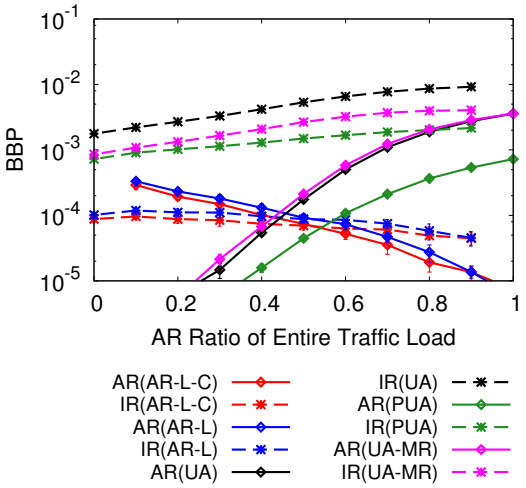

Figure 3.12: AR ratio of traffic load vs. BBPs for IR and AR requests (USA).

3.4.5 Bandwidth Blocking Probability vs. the Desired Ratio

Figures 3.15 and 3.16 show the relationships between the BBPs and α which is the desired ratio of BBP of AR requests relative to that of IR requests. In both topologies, the ratio of the BBPs of IR and AR was controlled according to α. However, as α got larger, the total BBP of IR and AR requests got higher. The reason is the difference in potential resources for IR and AR

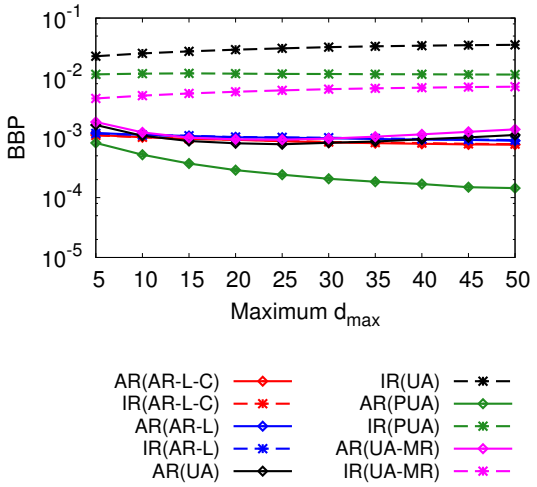

Figure 3.13: Maximal d_{max} vs. BBPs for IR and AR requests (JPN-12).

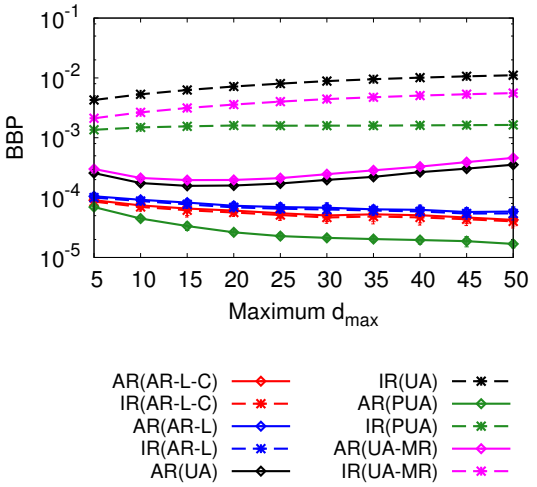

Figure 3.14: Maximal d_{max} vs. BBPs for IR and AR requests (USA).

requests. IR requests have smaller potential resources than AR requests because IR requests cannot search in the time domain. Therefore, when the proposed methods tried to lower the BBPs of IR requests, relatively many AR requests were blocked. In order to cope with this situation, the number of candidate routes K for IR requests should be more increased.

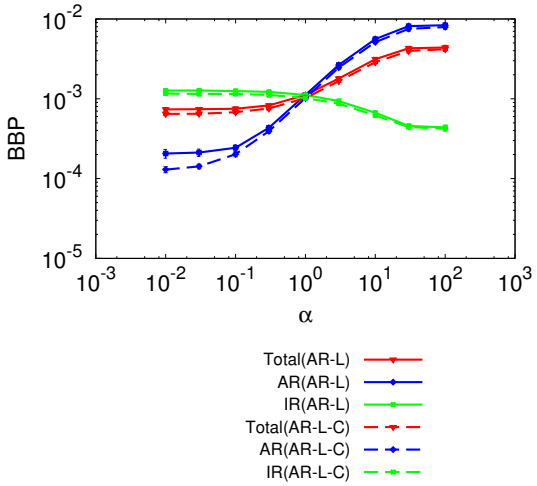

Figure 3.15: α vs. BBPs (JPN-12).

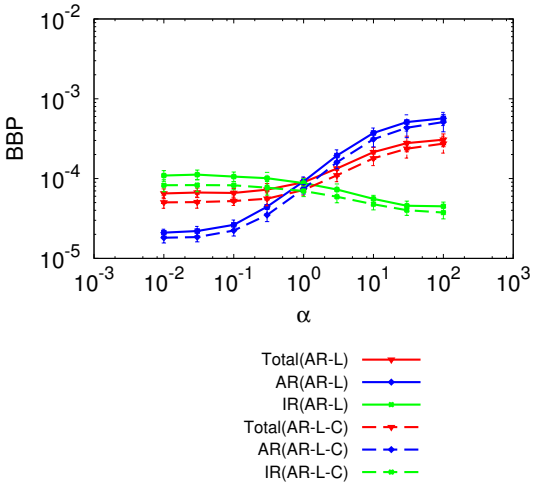

Figure 3.16: α vs. BBPs (USA).

3.4.6 Snapshots of TBL Usage and FR

Figures 3.17 and 3.18 show snapshots of the resource usage on cores in the TBLs under the USA and JPN-12 topologies, respectively, immediately after the arrival of 10^6 requests. The traffic load was fixed at 0.85 and the IR and AR requests were generated with an equal probability. AR-L, AR-L-C, and PUA ordered the spectrum resources for each number of requests by configuring the prioritized areas, whereas UA and UA-MR scattered all requests in the frequency domain. In addition, I validated that the spectrum resources available for IR and AR requests were basically separated by IR-dedicated and shareable sub-areas with AR-L and AR-L-C. The prioritized areas allowed AR-L, AR-L-C, and PUA to reduce spectrum fragmentation, i.e., to achieve a lower FR on the TBL than the other methods, as shown in Figs. 3.19 and 3.20. Figures 3.21 and 3.22 also confirm that these methods improved the FR throughout the entire network compared with the other methods.

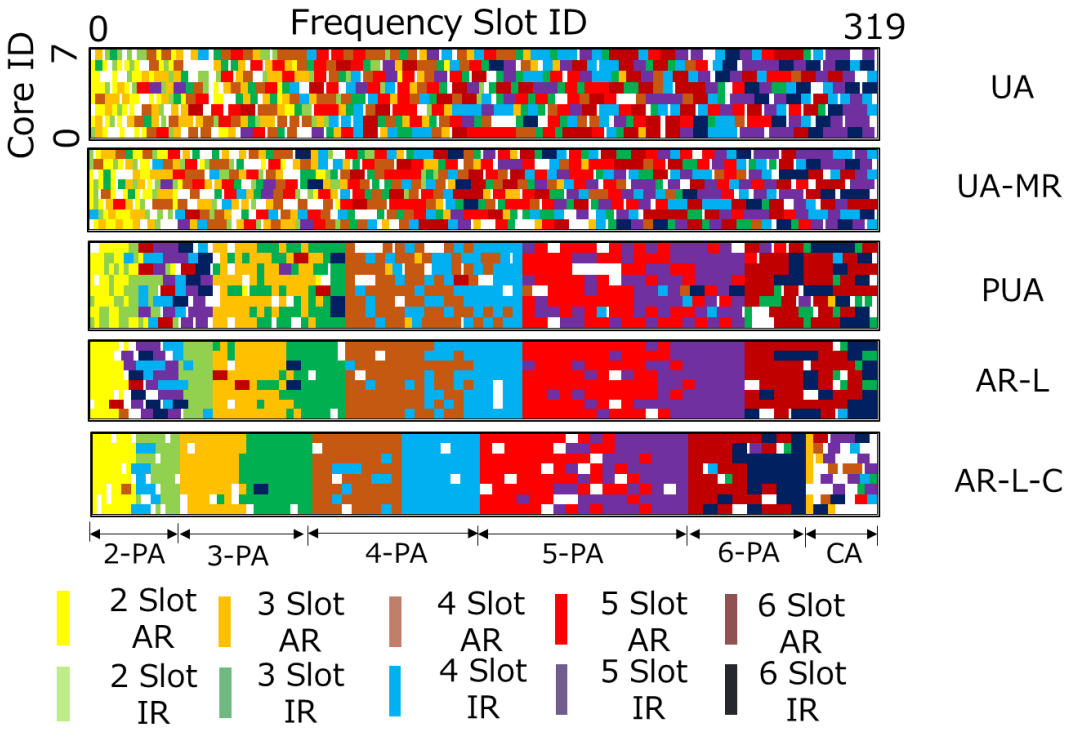

Figure 3.17: Snapshot of the TBL (JPN-12 topology). n-PA is the prioritized area for n slots. CA is the common area.

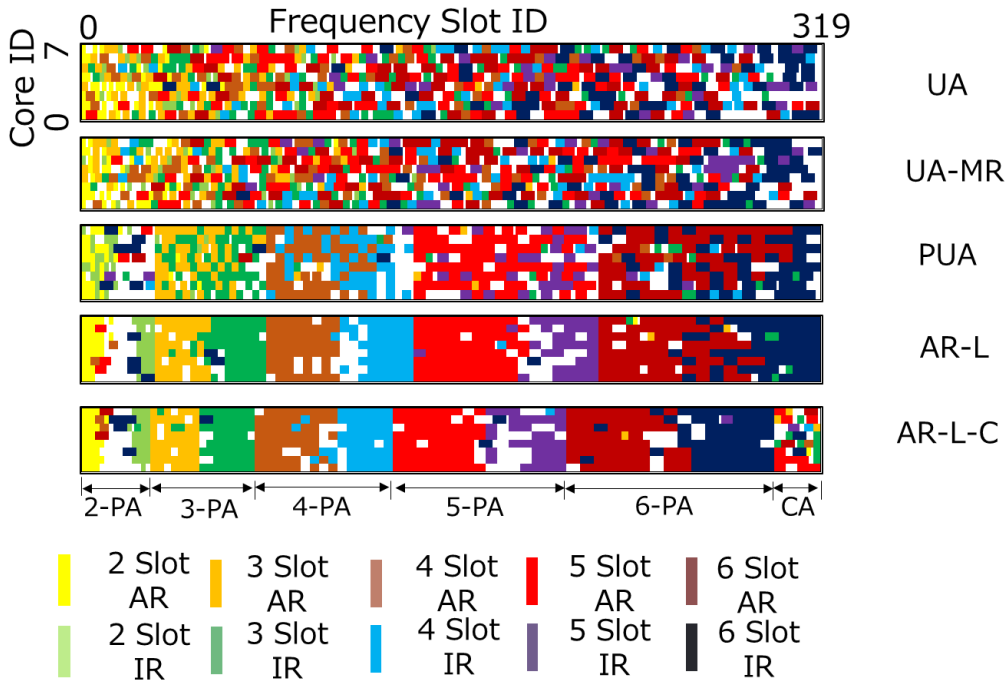

Figure 3.18: Snapshot of the TBL (USA topology). n-PA is the prioritized area for n slots. CA is the common area.

3.4.7 Initial delay of AR requests

Figures 3.23 and 3.24 show the average initial delays for AR requests from their request arrival time until the start of the service time. The proposed methods reduced the average initial delay for AR requests due to two main reasons. First, the proposed methods search for available resources in the order of core, frequency, and time, which means that these methods try to assign resources as soon as possible. By contrast, the comparison methods follow the order of core, time, and frequency. Note that these methods do not try to spread the reservations for AR requests in the frequency domain because widespread reservation in the frequency domain limits the resources available for IR requests. The difference in the search order was one of the main reasons for the different results obtained. Second, the proposed methods search for resources from different directions inside prioritized areas according to the type of requests in the frequency domain. This separates the resources available for IR and AR requests, which helps to prevent AR requests from reserving future resources that are currently being used for IR requests.

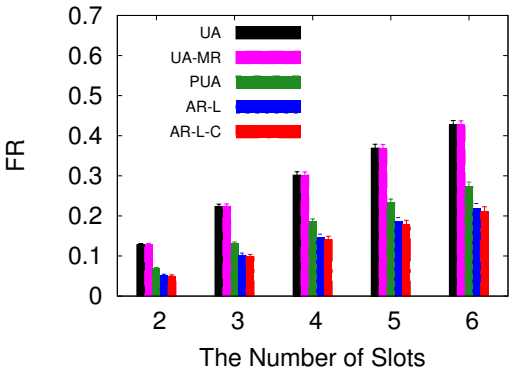

Figure 3.19: FR of the TBL (JPN-12).

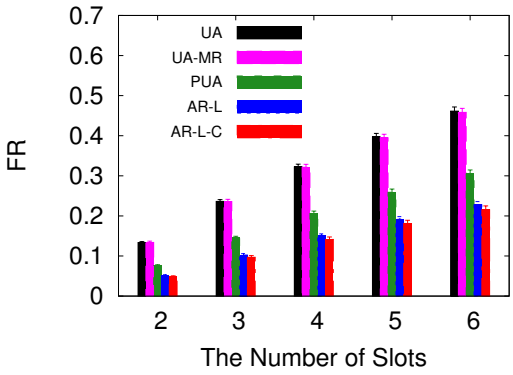

Figure 3.20: FR of the TBL (USA).

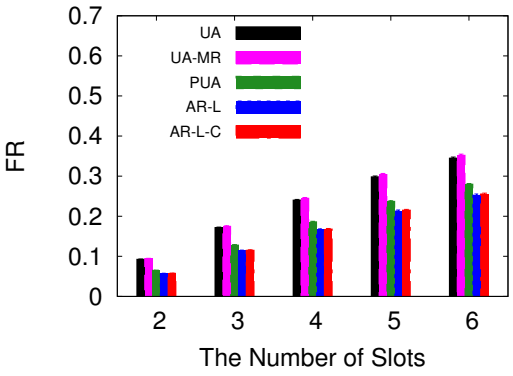

Figure 3.21: FR of the entire network (JPN-12).

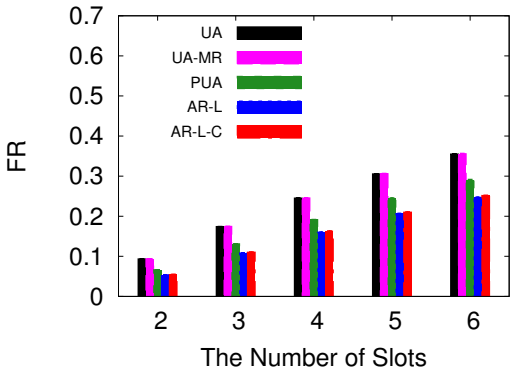

Figure 3.22: FR of the entire network (USA).

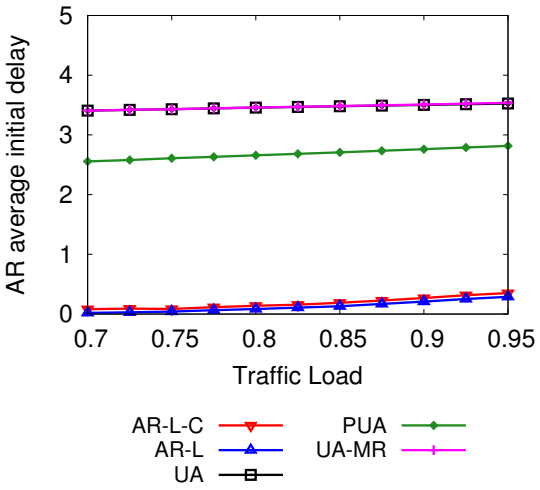

Figure 3.23: AR initial delay (JPN-12).

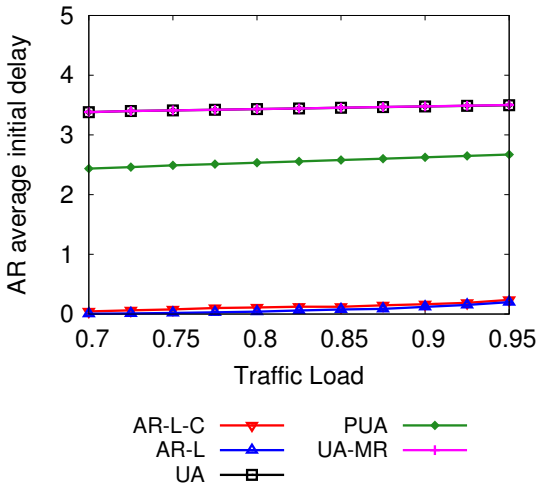

Figure 3.24: AR initial delay (USA).

3.5 Conclusion

SDM-EONs are expected to provide great improvements in terms of the transmission flexibility and capacity. I investigated the problem of IR service degradation in EONs that support both IR and AR requests. I proposed two methods to reduce spectrum fragmentation and to ensure the service level control of IR requests and AR requests. I introduced prioritized areas to reduce spectrum fragmentation by ordering spectrum resources in the spectral and spatial domains. In addition, I divided the prioritized areas into IR-dedicated and shareable sub-areas, with dynamic control of the border between the two sub-areas in order to the BBP. I evaluated the proposed methods based on computer simulations. I verified that the proposed methods obtained improvements in terms of the BBP, service level control of IR and AR requests, spectrum fragmentation, and AR initial delay.

Chapter 4

Optical Path Provisioning Reducing Crosstalk of Multicore Fibers

4.1 Introduction

Owing to the recent advancements in network architectures, the transmission capacity of existing optical fibers is soon expected to reach its physical limit. In order to realize the further expansion of the fiber capacity, space division multiplexing (SDM) has been intensively researched in the past few years [42]. Multicore fiber (MCF) is one of the new innovative fibers in SDM technology. One of the most significant problems of MCF is the physical impairment of transmission signals due to inter-core crosstalk (XT). Many MCF structures have been proposed to reduce the XT [46], and their performance has been tested by experiments [79]. In several experiments, it was assumed that the signals of the same frequency were transmitted simultaneously at all cores in one fiber. Nevertheless, considering the overall network, there are many fibers that are not in such a high-XT condition, because of dynamic traffic demands and resource allocations. Thus, the XT in MCFs can be reduced by suitable network resource management.

Filling spectra without a gap, as by the first-fit policy, realizes simple and effective resource utilization in general elastic optical networks (EONs) because of its characteristic of fewer spectral fragmentation. However, such a concentrating policy tends to yield more XT in MCF because it is important to avoid spectrum overlapping in adjacent cores in order to reduce the XT. In Ref. [80], we showed the fundamental evaluation of this trade-off in a SDM-EONs. It is expected that the novel resource management method will improve the network efficiency by

considering both the fragmentation in EONs and the XT in MCFs.

In this chapter, I propose a dynamic spectrum and core allocation method using a classification of cores based on the required bandwidths. The fundamental concept has been roughly presented in [81]. There are several different bandwidth connections in EONs; the proposed method dynamically assigns the same bandwidth connections to the same cores. This uniform connection assignment decreases the blocking probability owing to the reduction in the spectral fragmentation. Moreover, by introducing a priority of core selection based on the non-complex qualitative evaluation of the XT in MCF, the proposed method can reduce the XT in MCF.

The remainder of this chapter is organized as follows. Section 4.2 explains related work regarding SDM technology. Section 4.3 proposes a dynamic spectrum and core allocation that reduces XT and spectral fragmentation simultaneously. Section 4.4 evaluates the performance of the proposed method, and Section 4.5 concludes the chapter.

4.2 Issues in Space Division Multiplexing

4.2.1 The Limit of Traditional Fibers

Many researchers have aimed for more efficient utilization of EONs. Consequently, it is said that the channel bit rate of optical fibers will increase to 1 Tbps [82], and the transmission capacity per fiber will also increase. Nevertheless, the rate of increase in the transmission capacity of the optical fiber is reduced. This is because the transmission capacity approaches the physical limit of the existing single-mode fiber. One of these physical limits is related to input optical power. Input optical power is mainly limited by two factors as follows.

- Fiber fuse phenomenon

  Because of the increase of transmission capacity of a traditional fiber, optical power of a transmitted signal also increases. When optical power increases in surplus, an optical fiber waveguide is destructed and the destruction is propagated to a source of light. Although the cause of fiber fuse phenomenon is unrevealed, this phenomenon continues until optical power is lowered [39].

- Nonlinear optical effect [40]

When optical power increases, nonlinear optical effects such as self phase modulation, cross phase modulation and four wave mixing are generated. These effects degrade quality of an optical signal.

These factors give the upper limit of optical power. Then, signal to noise ratio (SNR) of an optical signal and Shannon limit lead the upper limit of transmission capacity per bandwidth. Therefore, to overcome the physical limitations of the existing fiber and further expand fiber capacity, innovative novel fibers are required [41].

4.2.2 Novel SDM-Based Optical Fibers

Reference [42] indicates that SDM using MCFs is expected to improve the physical limitations dramatically. MCF is one of the innovative new fibers in SDM technology, and it is a strong candidate of future optical fibers because of simplicity of signal processing and easy replace from the existing optical fibers. MCFs have multiple waveguides (cores) per fiber and an independent signal is transmitted in each core. Thus, MCFs can expand transmission capacity dramatically. In MCFs, multiple cores are arranged closely, and therefore inter-core XT degrades transmission signals. In order to further expand the transmission capacity, it is essential to reduce the XT by considering a structure of MCFs. From the perspective of the connecting and laying MCFs, MCFs require uniform mode field diameter and chromatic dispersion. From the perspective of avoiding signal degradation, MCFs require wide effective core area. Figure 4.1 shows the optical multi-input multi-output (MIMO) transmission using MCF.

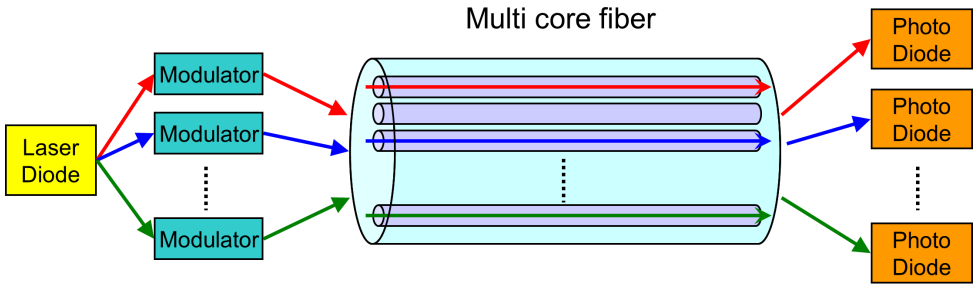

Figure 4.1: The optical MIMO transmission using MCFs

Considerable research on the design of MCFs has been reported in the past few years [43, 44, 45, 46]. Reference [43] proposes the new concept of heterogeneous MCFs. The cores in

heterogeneous MCFs differ slightly in their physical characteristics. These physical differences diminish the optical power transferred among the cores, and heterogeneous MCFs can increase the core density. Reference [44] proposes quasi-homogeneous solid MCFs. Because the quasi-homogeneous structure realizes a drastic power-conversion efficiency, the fabricated quasi-homogeneous solid MCF exhibits a very small XT. Reference [45] investigates a method to enlarge the effective area of optical fibers without increasing the XT. Reference [46] proposes an analytical method to determine the coupling coefficient value between two adjacent trench-assisted non-identical cores and proposes heterogeneous trench-assisted MCFs. Using novel MCFs, many transmission experiments have been conducted. Regarding experimental demonstrations using MCFs, Ref. [83] succeeded in 1.01-Pbps transmission over 52 km with a 12-core fiber, and Ref. [79] succeeded in 110.9-Tbps transmission over 6,370 km with a 7-core fiber and an erbium-doped fiber amplifier. Recently, Ref. [84] succeeded in 105.1 Tbps transmission over 14,350 km with a 12-core fiber, and its capacity-distance product of 1.51 Pb/s·km is approximately 1.5 times as large as a previous result. Basically, an optical switching node structure for MCFs is slightly different from traditional ones for existing single core fibers. MCFs are demultiplexed in SDM domain by fan-in/fan-out devices, and each core is connected to each input/output port of switching nodes as existing single core fibers [79].

4.2.3 Inter-Core Crosstalk of Multicore Fiber

In order to expand transmission capacity of MCFs, inter-core XT in MCFs is an essential problem. Recently, the XT mechanism in MCF has been practically uncovered [85, 86, 87, 88, 89]. Reference [85] shows that the bend characteristics and fabrication variations have a crucial impact on the XT in MCF by statistically averaging with a short fiber segment. Reference [86] formulates the coupled-mode equation considering the bending effect and confirms a quantitative agreement between the simulated and measured results. According to this formulation, the XT in MCF is stochastic value. Reference [87] revises the coupled-mode theory and coupled-power theory for MCF. The simulation results based on these two theories agree well with the measurement results. Reference [88] formulates the amount of XT based on the coupled-mode and coupled-power theories considering the random fluctuation in the longitudinal direction.

The formulation gives the amount of the 7-core MCF's XT between the center core and one of the outer cores as follows:

$$X^{(7)} = \frac{1 - \exp\left(-7h^{(7)}z\right)}{1 + 6\exp\left(-7h^{(7)}z\right)}. \tag{4.1}$$

This formulation indicates that the amount of XT in 7-core MCF $X^{(7)}$ is dependent on the power-coupling coefficient of 7-core MCF $h^{(7)}$ and transmission distance z. Reference [88] also indicates that the formulation agrees well with the experimental results according to the wavelength dependence of the XT. Reference [89] proposes new methods for measuring the XT statistically by sweeping the wavelength. These methods can measure extremely low XT in MCF, and it is confirmed that the stochastic behavior of the XT is dependent on the polarization state. As previously stated, the conventional method for reducing the XT involves contriving the low-XT structure of the MCF as an isolated MCF. However, from the perspective of the cladding diameter, such an isolated structure tends to have a larger diameter than a non-isolated MCF. Therefore, it is also required to reduce the XT in MCF without depending on the contrived structure. Since the XT in the MCF is dependent on the transmission distance and frequency of signals, as indicated by the aforementioned research, my proposal reduces the XT by contriving resource management from the perspective of networking.

There has been little research on networking with MCFs in EONs. References [90] integrates various transmission granularities of EONs with SDM into new multidimensional hierarchical networking model. Based on this networking model, multidimensional coded-modulation can improve signal bit error rate by increasing Euclidean distance between constellation points. Reference [91] presents the EON with MCFs considering a new optical node structure. The network consists of two MCFs and four programmable Architecture on Demand (AoD) all-optical nodes that can switch with 6000-fold bandwidth granularities. Reference [92] demonstrates software defined networking control plane for EON with MCFs. In this control plane, bandwidth and quality of transport (*i.e.* bit error rate) are appropriately allocated for service requests.

In order to conduct completely efficient networking, it is essential to consider the XT impairment in MCFs. While some references show various formulations of MCF's XT (e.g. in Ref. [88]), they are valid only in restricted conditions with regard to experimentation. It is

required to model the XT simply so as to improve the efficiency of the EON with MCF by resource management. We proposed the fundamental concept of network resource management in EONs with MCF [80]. The simulation results in [80] indicate that the XT can be reduced by networking through the simplified modeling of the XT. In [81], we also propose advanced resource allocation in EONs with MCFs. However, these resource allocation methods partially depend on the structure or the number of MCFs. In this chapter, I propose general network resource management that is adaptable to the MCFs regardless of the structure and the number of cores. The transmission success rate is generally degraded if a spectrum utilization scheme aims at reducing XT, for example, allocating spectra randomly. My proposed method can improve both transmission success rate and XT by utilizing spatial channels in SDM-EONs.

4.3 On-Demand Spectrum and Core Allocation Reducing Crosstalk

4.3.1 Outline

In this section, I propose a spectrum and core allocation method to provide appropriate optical paths for EONs with MCFs. When a connection request is generated between a source-destination pair, an optical path is established in order to transmit data through the connection according to the flowchart in Fig. 4.2. Firstly, the shortest hop route is selected for the connection. The shortest hop route is calculated in advance for each source-destination pair using Dijkstra's algorithm. Next, the number of frequency slots required for the connection is calculated according to the route. After determining the spectrum resource status in all links along the route, I check whether the frequency slots and cores are available while satisfying the continuity and contiguity constraints of the RSA problem. If no such suitable combination of frequency slots and cores exists, the connection is rejected. Otherwise, available frequency slots and cores are selected from the candidates by the proposed method or other compared methods. Finally, the optical path is established.

My proposed policy is divided into two predefinitions: the predefined core prioritization for reducing the XT and the predefined core classification for reducing the fragmentation. In the remainder of this section, I explain these two predefined polices as well as the procedures

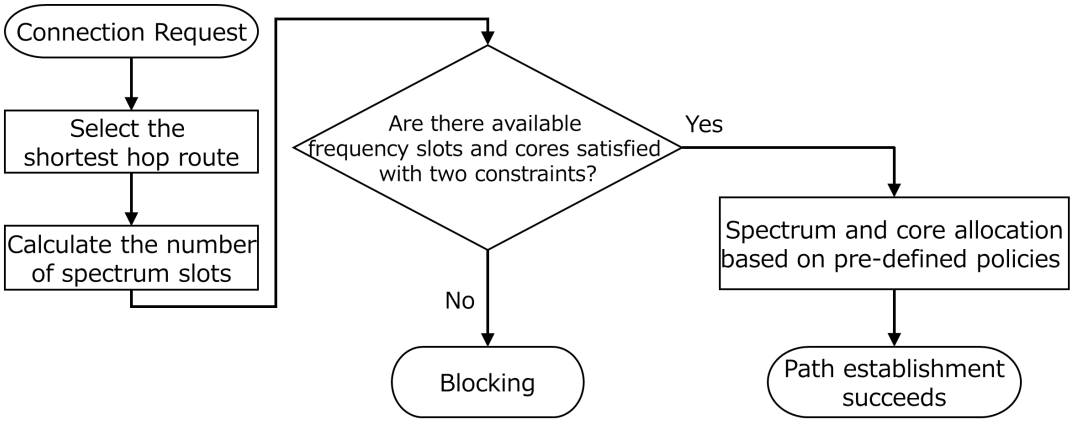

Figure 4.2: Flowchart of a dynamic resource allocation.

of the proposed dynamic spectrum and core allocation. The symbols used in my proposed predefinitions are summarized in Table 4.1.

Table 4.1: Symbols used in the preefinitions

Symbols	Description
n	The number of cores.
x_{ij}	Binary variable; it equals to 1 if core i and core j is adjacent, otherwise it equals to 0. $(1 \leq i, j \leq n)$
D_{ij}	The distance between core i and core j.
N_i	The number of adjacent cores for core i.
C_i	The cost of core i in the prioritization. It is initialized to 0 in advance.
$\mathcal{I}$	The set of cores.
$\mathcal{P}$	The set of cores' priority.
$P_i(\in \mathcal{P})$	The index of i-th prioritized core.
$\mathcal{R}$	The set of links which belong to the selected route.
$S^{(i)}$	The score of i-th candidate frequency slots in the score calculation.
$S_j^{(i)}$	The score of j-th link on the selected route for i-th candidate frequency slots.

4.3.2 Pre-defined Core Prioritization Reducing Crosstalk

When the distance between two cores is small, inter-core XT occurs among the cores in a MCF. The actual signal spectrum is not flat in frequency domain and the impact of the XT is different with the frequency; the impact is larger at the center frequency. In this chapter, the signal spectrum is assumed to be flat in frequency domain and the impact of the XT is same regardless

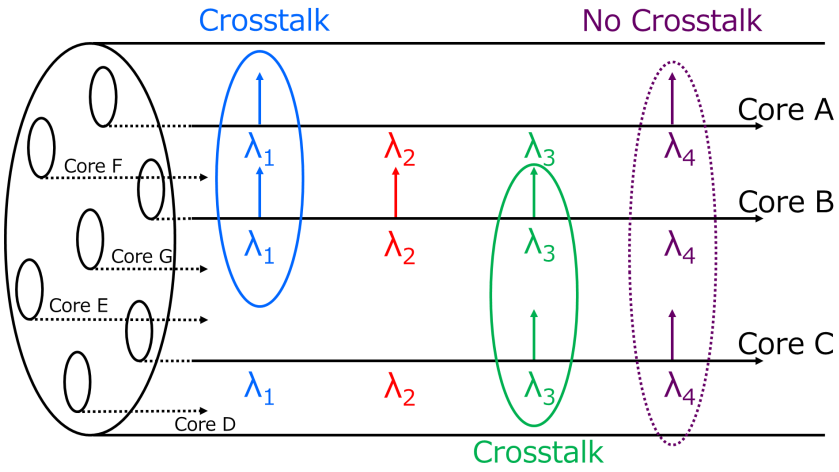

Figure 4.3: An example of the XT in my assumption.

of frequency position. Even if I simplified the XT by assuming flat signals, the XT index newly introduced is safely valid because of relative evaluation.

XT in MCFs is generated by the propagation of optical signals between cores due to an evanescent wave. Because an evanescent wave decays exponentially with the traveled distance, there is quite a difference between the amount of adjacent cores' XT and that of non-adjacent cores' XT. Existing experimental researches [93, 94] also measure the amount of XT between adjacent cores of MCFs. Then, from the perspective of frequency, the amount of XT is depends on propagation constants of transmitted optical signals. When the two optical signals have the same propagation constant, the one optical signal's evanescent wave is generated in the other optical signal in phase with each other. Thus, the optical power is transferred to each other, and the amount of XT increases. Utilizing a refractive index of core n, a wavenumber of a propagated signal in vacuum k_0, and a propagation angle θ_m, a propagation constant β is defined as follows,

$$\beta = nk_0 \cos\theta_m. \tag{4.2}$$

If f means frequency,

$$\beta = n\frac{2\pi}{f}\cos\theta_m \tag{4.3}$$

because $k_0 = \frac{2\pi}{f}$. Therefore, a propagation constant is dependent on signal's frequency, and a large XT effect occurs when signals are transmitted in adjacent cores with the same frequency.

I assume that the XT only occurs between adjacent cores when the same frequency slot is used in both cores in an EON with MCFs in this chapter. In fact, my XT assumption is the simplest modeling scheme. Recently, there are several researches that focus on the XT-aware networking scheme with calculating the detailed amount of XT [95, 96]. My proposed method is based on the simple crosstalk model in order to reduce computational complexity. References [95, 96] try to evaluate the detailed amount of XT.

Figure 4.3 shows an example of the XT in my assumption. In this figure, the important XT is that in λ_1 or λ_3 because λ_1 and λ_3 are used by two adjacent cores. Although λ_4 is also used by multiple cores, the cores A and C (using λ_4) are not adjacent. The distance between non-adjacent cores is longer than that between adjacent cores. Therefore, I do not take such non-adjacent cores' XT into account.

The first predefined policy aims at reducing the important XT by a prioritization of core selection based on the aforementioned assumption. Procedure 4.1 shows the pseudo-code of the proposed predefined core prioritization for reducing the XT in n-core fibers. The low $P_k \in \mathcal{P}$ indicates a high priority.

Figure 4.4 provides an example of predefining the priority of core selection in a 7-core MCF according to Procedure 4.1. Firstly, all of the costs C_i are initialized to zero at step 0. At step 1, core 1 is selected as first prioritized core, and the costs of adjacent cores (C_2, C_6 and C_7) are incremented. At step 2, cores 3, 4, and 5 have the lowest cost, and cores 3 and 5 are the nearest to core 1, which is selected in the previous step. Core 4 is selected in this case. In the final step of the algorithm, all of the cores are prioritized, and the priority can reduce the XT in the MCF. Figure 4.5 shows examples of the predefined priorities of MCFs with different structures and numbers of cores.

4.3.3 Pre-defined Core Classification Reducing Fragmentation

In EONs, there are various connections with different required bandwidths. It is important to solve the problem of fragmentation in the spectrum resource domain because many different bandwidth connections arrive and leave. The second predefined policy aims at reducing the

Procedure 4.1 Core Prioritization

Require: Structure of MCFs, x_{ij}, D_{ij}, and N_i.

Ensure: The priority of core selection, $\mathcal{P}$.

for $k = 1$ **to** n **do**
  $\mathcal{I}' \leftarrow \left\{ i \in \mathcal{I} \middle| C_i = \min_{i \in \mathcal{I}} (C_i) \right\}$
  $\mathcal{I}'' \leftarrow \left\{ i \in \mathcal{I}' \middle| N_i = \min_{i \in \mathcal{I}'} (N_i) \right\}$
  if $k = 1$ **then**
    Select arbitrary $i (\in \mathcal{I}'')$.
  else
    $\mathcal{I}''' \leftarrow \left\{ i \in \mathcal{I}'' \middle| D_{iP_{k-1}} = \min_{i \in \mathcal{I}''} \left(D_{iP_{k-1}} \right) \right\}$
    Select arbitrary $i (\in \mathcal{I}''')$.
  end if
  $P_k \leftarrow i$
  for $l = 1$ **to** n **do**
    if $x_{P_k l} = 1$ **then**
      $C_l + +$
    end if
  end for
  $C_{P_k} \leftarrow \infty$
end for
return $\mathcal{P}$

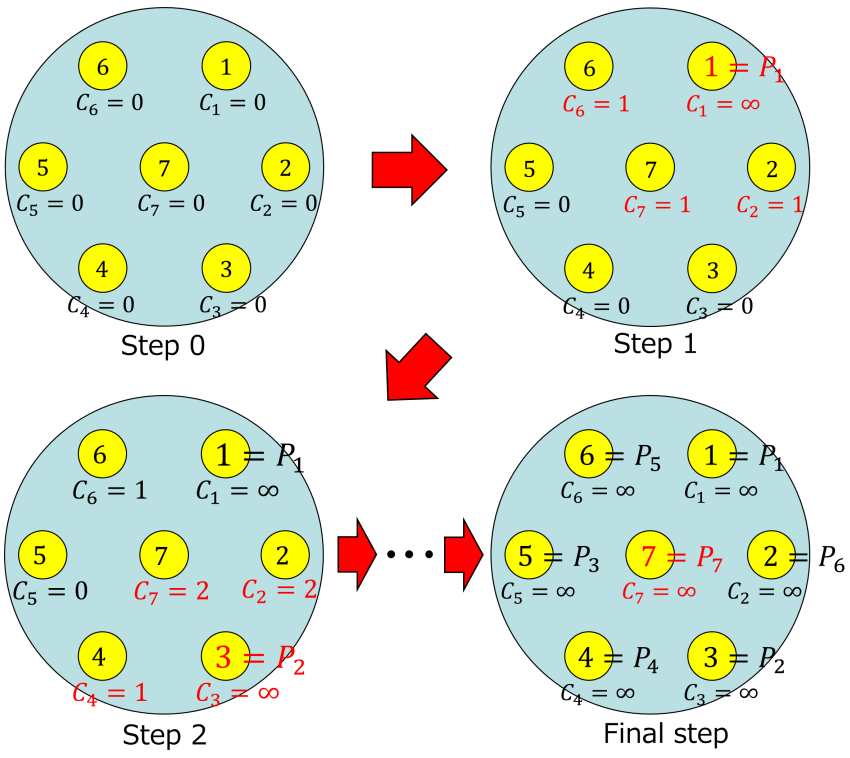

Figure 4.4: An example of pre-defining the priority of core selection in 7-core fiber.

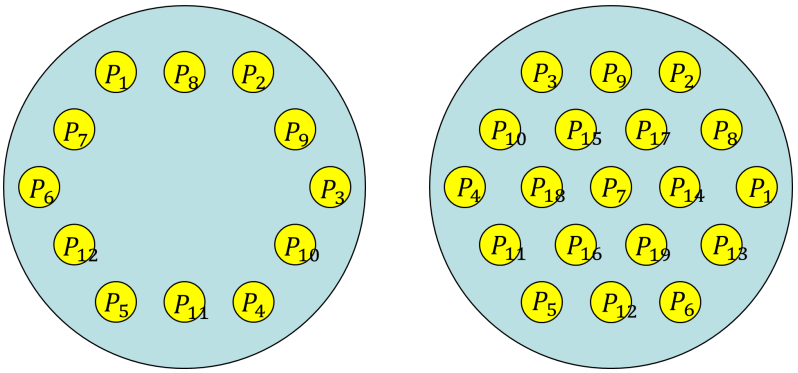

(a) Pre-defined priority (12MCF) (b) Pre-defined priority (19MCF)

Figure 4.5: The pre-defined priority patterns of core selection in different MCFs.

fragmentation according to the core classification based on the bandwidths of the required connections.

Figure 4.6 shows an example of spectrum utilization in an EON with MCFs. Figure 4.6(a) shows the spectrum utilization with no core classification, and Fig. 4.6(b) shows the spectrum utilization based on my predefined core classification. My policy classifies MCF cores per the number of required frequency slots (FSs). The classified cores are defined as those for which the connections requiring the same bandwidth are preferentially allocated. In Fig. 4.6(b), cores 1 and 2 are the classified cores for the connections requiring three FSs. It is clear that there are no spectral fragmentations in the classified core as long as the core has one type of connection about requiring bandwidth. However, when there is no available classified core for the required connection's bandwidth, cores classified for different bandwidths are possibly used as core 7 in Fig. 4.6(b). Therefore, this concept is slightly similar to multi-layer WDM networks in some respects but different in others.

In general, there are m types of bandwidth connections in an EON with n-core fibers. I suppose that the average ratio of the number of each type of existing connections is known from statistical information. The classified cores are prepared in turns in the descending order of the values of this ratio. An example of predefined core classification is illustrated in Fig. 4.7. This classification is based on the priority in Fig. 4.4. Connections require three types of bandwidth, *i.e.*, three, four, or five FSs in this example. Note that this example is specific to the adopted network topology (JPN-12 topology in Fig. 3.4). In Fig. 4.7, there are three classified cores

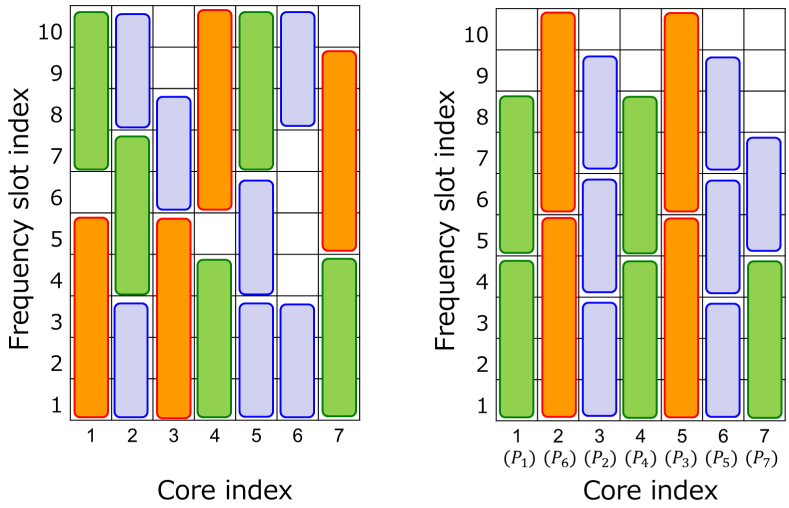

(a) No classification (b) Pre-defined core classification

Figure 4.6: An example of spectrum utilization.

for connections requiring four FSs and two classified cores for connections requiring three or five FSs. Although there are only 3 types of bandwidths which is required by connections in this example, one classified core can be preferentially used by two or more types of bandwidth connections when m is more than n.

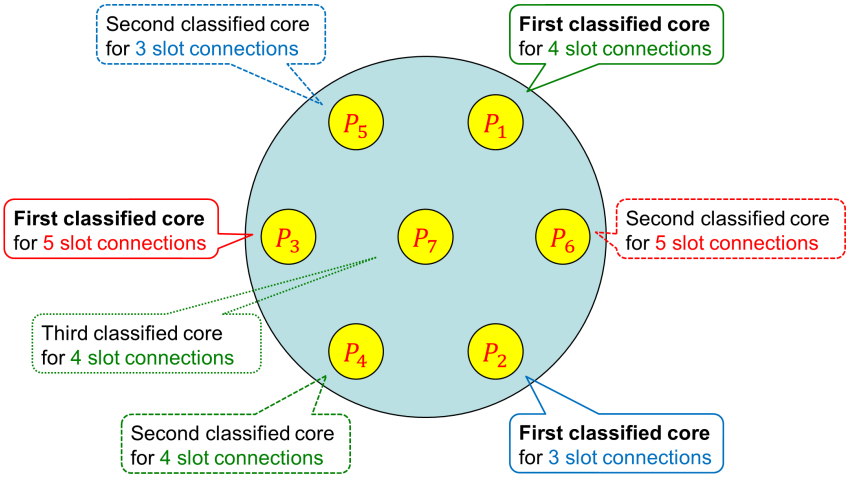

Figure 4.7: The example of pre-defined core classification for 7-core fiber.

4.3.4 Procedure of Dynamic Spectrum and Core Allocation

The proposed method allocates the spectrum and core per the required connections dynamically according to two predefined policies. It is assumed that all of the nodes in an EON with MCF

have the capability of free switching from core to core. This capability divides the core allocation problem into respective sub-problems for each link. I also employ a Path Computation Element (PCE) in order to solve the RSA problem.

After the route and corresponding modulation format are selected, the number of required FSs for the target requested connection is calculated. By checking the status of all links in the selected route, a list of the FSs satisfying two continuity constraints in the RSA problem is created. The proposed method calculates a score for each candidate of FSs, as Procedure 4.2. Procedure 4.2 shows the pseudo-code for the score calculation of one candidate of FSs. For the i-th candidate of available slots, the score $S^{(i)}$ represents the worst core allocation among the selected route. More desirable core allocations yield lower scores. After calculating the score for each candidate of FSs, the proposed method allocates the FSs with the lowest score. When there are multiple slots with the lowest score, the FSs with minimum index are allocated to the connection. Finally, one core is selected in each link according to the following steps.

Procedure 4.2 Score Calculation

Require: $\mathcal{P}$, $\mathcal{R}$ and the i-th candidate of FSs.
Ensure: The FSs' score, $S^{(i)}$.

for j-th link of the selected route **do**
  Check an available core P_k with the lowest k.
  if P_k is the classified core prioritized for the same bandwidth as current connection **then**
    $S_j^{(i)} \leftarrow P_k$.
  else
    $S_j^{(i)} \leftarrow 2n - P_k$.
  end if
end for
$S^{(i)} \leftarrow \max_{j \in \mathcal{R}} \left(S_j^{(i)} \right)$.
return $S^{(i)}$

Core selection procedure

Step 1 Select one core with the highest predefined priority from among the classified cores prioritized for the same bandwidth as current connection.

Step 2 If no core is selected in Step 1, select one core with the lowest predefined priority from among the classified cores for the other bandwidths.

4.4 Performance Evaluation

4.4.1 Simulation Model

I used my own C++ simulator for a simulation to evaluate the proposed method. The proposed method is evaluated in two different ways. The one is named as "Classification", and the other is named as "Proposal." The "Classification" is the method which adopts only Core Classification and core prioritization follows first-fit in this method. The "Proposal" adopts both Core Prioiritization and Core Classification. I adopted the JPN-12 topology and USA topology shown in Figs. 3.4 and 3.5. The JPN-12 topology has 12 nodes and 16 links. Each link has one MCF for each direction. I simply suppose that all links have a single MCF. I select three types of MCFs: the number of cores is 7-, 12- or 19-. The structures of these MCFs are shown in Refs. [79, 83, 97], respectively. I set the width of FS is 12.5 GHz and the total spectrum resource per core is 4 THz (C-band). Therefore, the number of FSs per core as $W = 320$. I assume that connection requests have a constant service time and that their inter-arrival time follows an exponential distribution. Connections are requested between the randomly selected source and destination. The traffic load represents the spectrum utilization of the "bottleneck link." The "bottleneck link" is the link in which the most optical paths are assigned when all pairs of source and destination have same arrival rate and shortest paths are always selected. The average inter-arrival time of the entire network μ satisfies the following formulation, where SP_{all} is the number of shortest paths for all pairs of source and destination, SP_{BN} is the number of shortest paths through the bottleneck link. BW_{ave} is an average number of required FSs, T_{ave} is an average service time, and N_{FS} is the number of FSs per link.

$$\mu = \frac{SP_{\text{BN}} \times BW_{\text{ave}} \times T_{\text{ave}}}{\text{Traffic load} \times SP_{\text{all}} \times N_{\text{FS}}}. \tag{4.4}$$

I assume that connections require 112 Gbps transmission. A different modulation format is applied to the generated connections according to the number of hops in order to compensate filter narrowing effect. The number of required FSs is dependent on the selected modulation format. The maximum number of hops in the JPN-12 topology is five and that in USA topology is seven. Table II shows the parameter set-up for the adopted topology scaled from the set-up

in Ref. [2]. The proposed method is compared with the simple spectrum and core allocation methods: "First-fit" and "Random." The "First-fit" method allocates available FSs and cores such that the indexes of the allocated FSs are minimized. The "Random" method arbitrarily allocates available FSs and cores.

Table 4.2: Number of FSs

# of hops			
JPN-12	USA	Modulation format	# of slots
1,2	1,2,3	DP-16-QAM	3
3,4	4,5	DP-QPSK	4
5	6,7	DP-QPSK	5

4.4.2 Blocking Probability

Figures 4.8, 4.9 and 4.10 show the blocking probabilities of an EON with 7, 12, and 19 core MCFs for JPN-12 topology, respectively. The core classification form is exemplified in Fig. 4.7 in particular in the case that JPN-12 topology and 7-core MCFs are adopted. Compared with the "First-fit" and "Random," these results show that the "Proposal" can improve the blocking probability to the same degree, regardless of the number of cores. There is a difference between "Classification" and "Proposal" because the spectrum allocation in low-prioritized cores is less sophisticated than that of "Proposal." From the comparison of these figures, the large number of cores reduces the blocking probability owing to the statistical multiplexing effect.

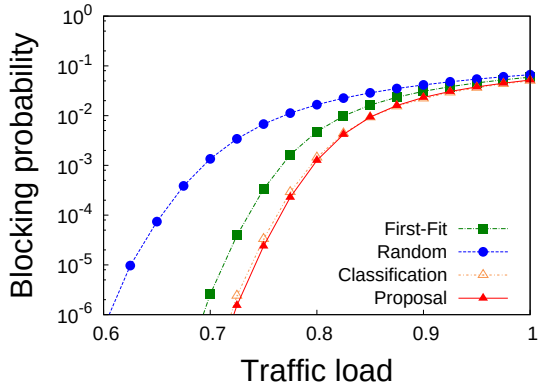

Figure 4.8: Blocking probability (JPN-12, 7-core MCF).

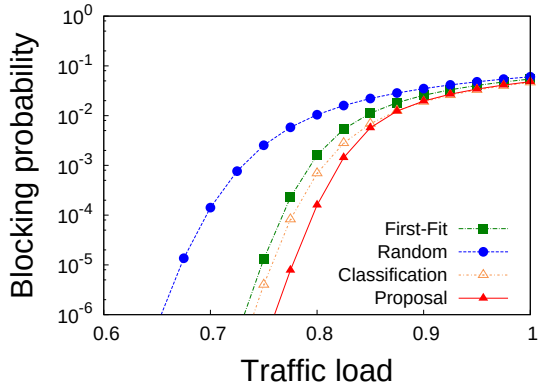

Figure 4.9: Blocking probability (JPN-12, 12-core MCF).

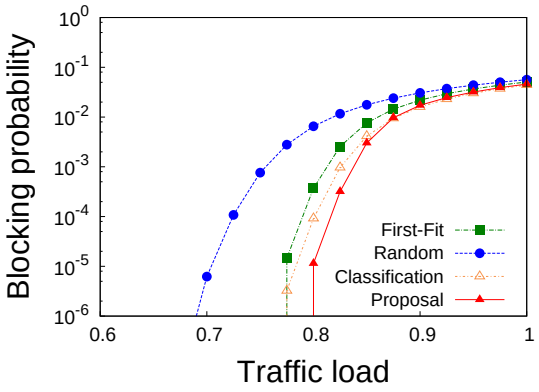

Figure 4.10: Blocking probability (JPN-12, 19-core MCF).

4.4.3 Fragmentation

The worse performances of the "First-fit" and "Random" with respect to the blocking probability are caused by the spectrum fragmentation shown in Figs. 4.11 and 4.12. Figures 4.11 and 4.12 indicate the average number of one- or two-slot fragments in the entire network for JPN-12 topology with 7-core MCFs. In my simulation condition, these focused one- or two-slot fragments are dead spectrum resources because the smallest number of required FSs is three. Therefore, the number of such fragments directly impacts the blocking performance. The proposed method can drastically reduce these fragments because of the pre-classification policy.

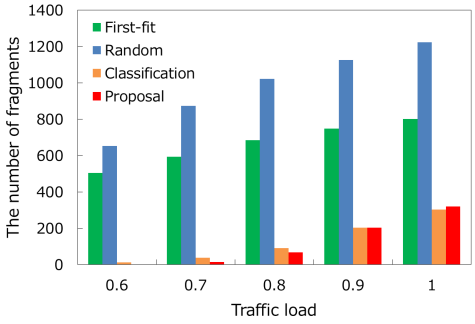

Figure 4.11: The number of fragments (1 slot).

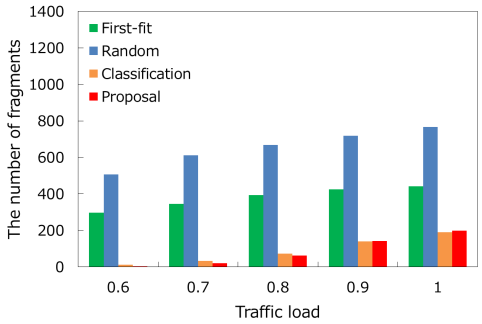

Figure 4.12: The number of fragments (2 slots).

4.4.4 Crosstalk per Slot

Figures 4.13, 4.14 and 4.15 show "Crosstalk per Slot (CpS)" in the proposed and compared methods for JPN-12 topology. These figures differ in the number of cores in the MCFs. The "CpS" is defined as follows. First, I define the "Arrangement of Crosstalk (AoC)" as the pairs of used FSs which have same frequency and located in adjacent cores. In other words, AoC is the arrangements of FSs which generate XT. Therefore, CpS is formulated as follows:

$$\mathrm{CpS} = \frac{\text{The number of AoCs}}{\text{The number of used frequency slots}}. \tag{4.5}$$

Note that from the definition, that CpS is a relative measure depending on fixed MCF structure. Thus, CpS should not be used for the comparison between different MCF structures but for the comparison of spectrum and core allocation methods under a fixed MCF structure. Qualitatively, the higher CpS spectrum and core allocation method shows, the worse its blocking probability becomes. Although there is a trade-off between the blocking probability and the CpS in the "First-fit" or "Random," the "Proposal" succeeds in improving both performances. "Proposal" can reduce the XT by less than half of the "First-fit" value, regardless of the number of cores. These XT reductions mainly depend on the prioritization policy of my proposed method. Therefore, two compared methods can also reduce XT to the same degree by adopting the prioritization policy. The XT reductions in "Classification" is smaller than these in "Proposal" because "Classification" does not adopt my proposed prioritization policy. However, "Classification" outperforms the other two compared methods because classification policy orderly disperses core allocations. For every proposed and compared method, the CpS in 12-core MCF is far smaller than that in other MCFs. This is because the maximum CpS in 12-core MCF is two, whereas that in 7-core MCF and 19-core MCF is six.

4.4.5 Topological Independncy

Figures 4.16 and 4.17 show the blocking probability and CpS for USA topology with 7MCF, respectively. The blocking probability and CpS shown in the figures are similar characteristics to that for JPN-12 topology. This means the effectiveness of the proposed method even in more densely meshed network with different traffic.

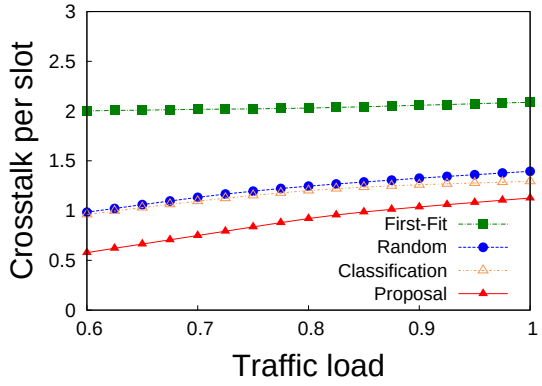

Figure 4.13: Crosstalk per slot (JPN-12, 7-core MCF).

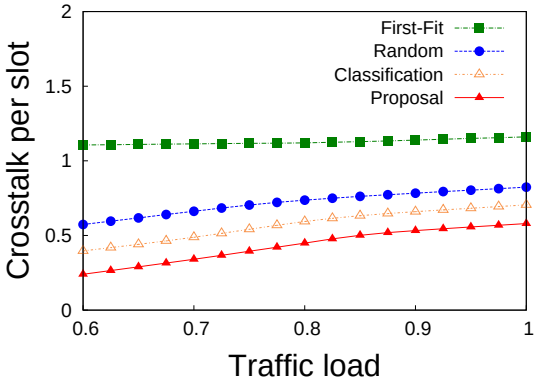

Figure 4.14: Crosstalk per slot (JPN-12, 12-core MCF).

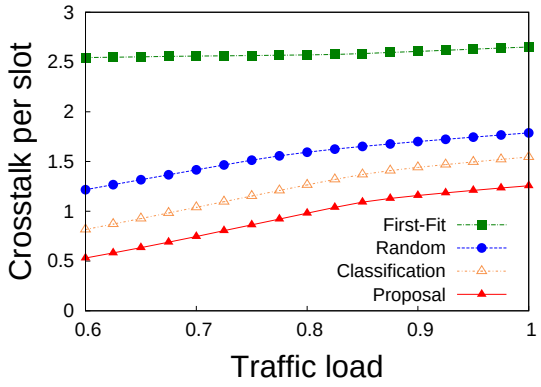

Figure 4.15: Crosstalk per slot (JPN-12, 19-core MCF).

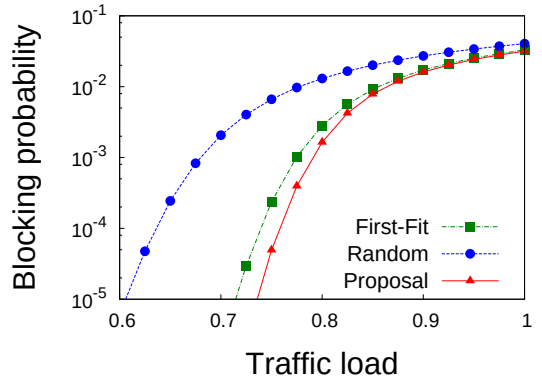

Figure 4.16: Blocking probability (USA, 7-core MCF).

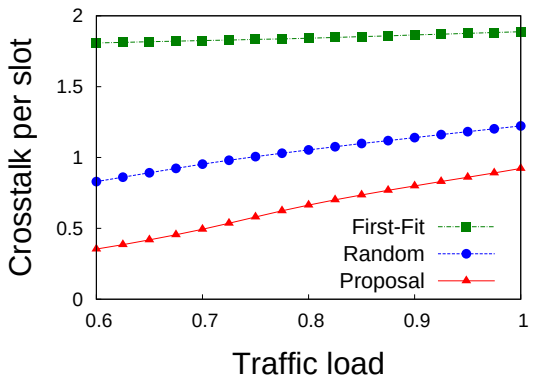

Figure 4.17: Crosstalk per slot (USA, 7-core MCF).

4.4.6 Spectrum Utilization

Figures 4.18 and 4.19 show the states of the spectrum utilization in a bottleneck link and a low load link, respectively. The adopted topology is JPN-12 topology and each MCF has 7 cores. The "low load link" is the link which has almost half traffic in a "bottleneck link." Each subfigure shows the snapshot of the spectrum utilization state for "First-fit," "Random," or "Proposal." In these figures, used FSs are colored. The blue, green, and red squares represent the FSs allocated to the connections requiring 3, 4, and 5 FSs, respectively. Figures 4.18(a) and 4.19(a) show that the "First-fit" method generates relatively less fragments according to its spectrum allocation filling without gap. This is why the "First-fit" shows higher CpS than taht of "Random" regardless of the number of cores. Figures 4.18(b) and 4.19(b) show that the "Random" method generates the most fragments because of its disordered allocation. This is why the "Random" shows the highest blocking probabilities regardless of the number of cores. In contrast, in Figs. 4.18(c) and 4.19(c), it is clear that the predefined classification reduces the fragmentations owing to the harmonious operation in the spectrum and core allocation. Note that there is a difference between the number of prepared classified cores and the number of classified cores required based on traffic requests. From the perspective of XT, my proposed method keeps large blanks in the cores with low priority in order to reduce the XT. The tendency is verified in the other link which have less traffic as shown in Fig. 4.19. The simulation results show that the proposed method can simultaneously improve both the XT in MCFs and the blocking probability of the total network. Moreover, these improvements are not dependent on the number of MCF cores.

4.5 Conclusion

An EON with MCFs is expected to realize great improvements in transmission flexibility and capacity. However, this presents the problem of the inter-core XT in MCFs. In this chapter, I proposed an "on-demand" spectrum and core allocation method in order to reduce the XT in MCFs from the perspective of networking. I introduced two predefined policies in order to reduce not only the XT in MCFs but also the blocking probability of overall networks. The

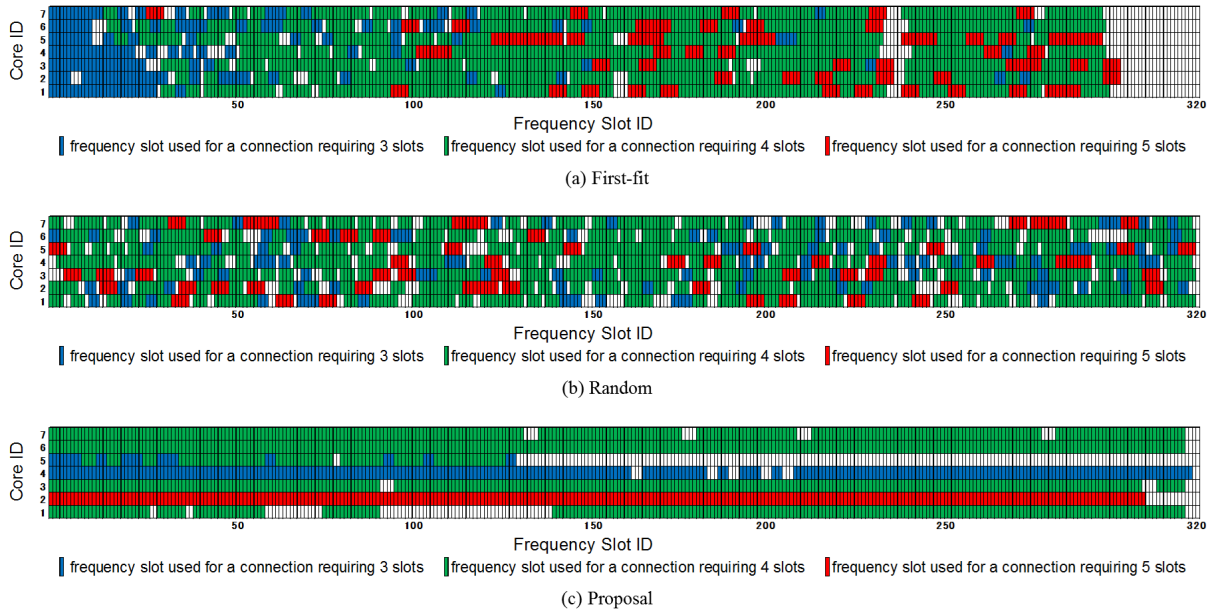

Figure 4.18: Spectrum utilization in a bottleneck link (traffic load = 0.7, JPN-12, 7-core MCF).

Figure 4.19: Spectrum utilization in a low load link (traffic load = 0.7, JPN-12, 7-core MCF).

first is a predefinition of a core selection priority for reducing the XT, and the second is a predefinition of a core classification for reducing the spectrum fragmentations. I evaluated the proposed method using extensive computer simulations. The proposed method can improve both the blocking probability and XT, which typically exhibit a trade-off relation.

Chapter 5

Energy-Efficient and Cooperative Node Configuration

5.1 Introduction

Optical fibers based on space division multiplexing (SDM) technology are important novel transmission devices that can expand the transmission capacity of core optical networks beyond the physical limit of traditional optical fibers [42,98,99]. The appearance of SDM-based optical fibers and an increase in the number of underlying optical fibers, which are aimed at expanding transmission capacity of optical networks, are expected to enlarge and complicate optical switching nodes in future core optical networks. Broadcast-and-select and spectrum-routing are general optical switching node architectures that have enough flexibility to realize fully-elastic optical networks [47, 48]. In these architectures, the spectrum selective switch (SSS) is not only the main signal processing module but also the dominant module in terms of power consumption. When optical switching nodes become complex and large-scale, cascaded SSSs dramatically increase the power consumption of these optical switching nodes owing to the limited port count of SSSs [49].

To suppress the increase in the number of signal processing modules, a hierarchical optical switching node architecture using small optical cross connects (OXCs) as subsystem modules has been proposed [50]. This hierarchical node architecture divides the switching component into subsystems of smaller OXC and suppresses the increase in the number of cascaded SSSs and erbium-doped fiber amplifiers (EDFAs). On the other hand, their partially restricted switching negatively affects the transmission success rate, and there is a trade-off between suppression

of the modular cost and the transmission success rate. Therefore, it is necessary to establish a completely different node architecture to achieve both cost reduction and successful transmission. Reference [1] also reduces the number of signal processing modules implemented in optical nodes by introducing a completely different novel optical node architecture which is called an architecture on demand (AoD) node. In AoD nodes, an optical backplane, which is usually implemented using a large-port-count three-dimensional microelectromechanical system (3D-MEMS), interconnects input/output ports and signal processing modules in an arbitrary manner, as shown in Fig. 1.5. Use of an AoD node can reduce the number of signal processing modules by supplying just enough signal processing because these interconnections are dynamically constructed according to the switching and signal processing request. In other words, the AoD concept requires an appropriate resource allocation method (which creates an appropriate switching request) considering these interconnections in AoD nodes.

In this chapter, I propose a novel energy-efficient network system that consists of a novel node architecture and resource assignment method considering an AoD node architecture in SDM-EONs. First, I discuss the proposal of energy-efficient AoD node architecture that can reduce power consumption of optical switching nodes. This proposed node architecture requires partially restricted spectrum allocation to adopt low-power-consumption modules for signal processing. Then, I also propose a novel on-demand resource allocation method to provide appropriate optical paths suited for the proposed energy-efficient AoD nodes. The proposed resource allocation method simultaneously reduces the blocking probability of path set-up requests in the entire network because its allocation policy reduces spectral fragmentation. Therefore, the proposed AoD node architecture and on-demand resource allocation method can improve both the power consumption and the blocking probability in SDM-EONs. There are mainly three contributions in this chapter. The first contribution is a novel energy-efficient optical node architecture based on AoD concept. The second contribution is a new resource assignment method realizing energy-efficient AoD nodes by appropriately arranging spectra. The third contribution is improving power consumption and blocking rate of connections in SDM-EONs.

The rest of this chapter is organized as follows. Section 5.2 introduces optical node architectures for EONs including both traditional static node architectures and an AoD node architecture. Section 5.3 explains the proposed energy-efficient AoD node architecture, which incorporates low-power-consumption modules. Section 5.4 proposes an on-demand routing and spectrum allocation method suitable for the energy-efficient AoD node architecture. Section 5.5 evaluates the performance of the proposed method. Section 5.6 concludes this chapter.

5.2 Optical Node Architecture for EONs

5.2.1 Traditional Optical Node Architectures for EONs

In EONs, optical switching nodes need to handle transmission signals with greater flexibility and finer granularity than in traditional WDM networks. The SSS, which is also called bandwidth variable wavelength selective switch (BV-WSS) of a flexible WSS, is the most important signal processing module in the optical nodes of EONs [9]. The SSS can filter spectra with an arbitrary width from input signals and switch them to arbitrary ports without signal replication, as shown in Fig. 1.4. The flexibility of spectrum selection in the SSS realizes flexible networking in EONs.

Two traditional optical node architectures based on SSSs are proposed for EONs, as shown in Fig. 1.3 [47, 48]. In the broadcast-and-select architecture, the input signals are replicated in splitters and broadcast to all output ports. On each output port, the appropriate spectra are selected using an SSS, and the multiplexed signal is transmitted through the output port. However, the replication by these splitters seriously degrades the transmission signals when the scale of a node is large [100, 101]. In the spectrum-routing architecture, the input signals are first demultiplexed by an ingress SSS without replication. Then, these demultiplexed signals are routed to different output ports and finally combined, also by an egress SSS, at the output port. The spectrum-routing architecture does not produce signal degradation by splitters, unlike the broadcast-and-select architecture, but the spectrum-routing architecture is more costly than the broadcast-and-select architecture because the number of SSSs is doubled.

In both architectures, the cost of optical nodes is a serious problem. When the number of input/output ports of an optical node is large, for example because multicore fibers (MCFs)

are adopted, SSSs with the same port count are required in these traditional node architectures. However, the port count of an SSS is limited, for example, 20 for a current commercial SSSs. If traditional node architectures require a higher port count than this limit, cascaded SSSs are usually implemented for these architectures, explosively increasing the number of required SSSs for optical nodes. The increase in the number of SSSs required for Spectrum Routing node is formulated as follows. It is supposed that Spectrum Routing node supports $P \times P$ switching and each SSS supports $1 \times P_{\mathrm{SSS}}$ multiplexing/demultiplexing. If one SSS block in Fig. 1.3 needs to supply multiplexing/demultiplexing with more than P_{SSS} ports, the block is implemented by cascaded multiple SSSs. It is defined that cascaded N_{Cas} SSSs supply a $1 \times P_{\mathrm{Cas}}$ multiplexing/demultiplexing. When the SSS block is implemented by 2-step cascaded SSSs ($1 \leq N_{\mathrm{Cas}} \leq P_{\mathrm{SSS}} + 1$),

$$P_{\mathrm{Cas}} = (N_{\mathrm{Cas}} - 1) \times P_{\mathrm{SSS}} + P_{\mathrm{SSS}} - (N_{\mathrm{Cas}} - 1). \tag{5.1}$$

Because $P \leq P_{\mathrm{Cas}}$,

$$\begin{aligned} P &\leq (N_{\mathrm{Cas}} - 1) \times P_{\mathrm{SSS}} + P_{\mathrm{SSS}} - (N_{\mathrm{Cas}} - 1), \\ &= N_{\mathrm{Cas}} \cdot (P_{\mathrm{SSS}} - 1) + 1, \\ N_{\mathrm{Cas}} &\geq \frac{P-1}{P_{\mathrm{SSS}} - 1}, \\ N_{\mathrm{Cas}} &= \lceil \frac{P-1}{P_{\mathrm{SSS}} - 1} \rceil. \end{aligned} \tag{5.2}$$

Therefore, The total number of SSSs required in Spectrum Routing node N_{SR} is calculated as follows.

$$N_{\mathrm{SR}} = 2 \times P \times N_{\mathrm{Cas}} = 2 \cdot P \cdot \lceil \frac{P-1}{P_{\mathrm{SSS}} - 1} \rceil. \tag{5.3}$$

To overcome the substantial increase in power consumption of the traditional optical node, other optical node architecture is required to mitigate such a cost increase due to the use of cascaded SSS.

5.2.2 Architecture on Demand Nodes

AoD concept was introduced mainly as a solution to the problem of limited flexibility in traditional node architectures due to the hard-wired arrangement of modules [1]. The optical backplane in AoD nodes (Fig. 1.5) is usually implemented using large-port-count optical switches such as a 3D-MEMS, which interconnects input/output ports and diverse building modules such as the SSS, multiplexer (MUX), demultiplexer (DEMUX), EDFA, PLZT devices, and so on. These interconnections in the optical backplane are dynamically reconfigured according to the request for switching and signal processing. Moreover, it is easy to add extra functions (e.g., wavelength conversion) because the arrangement of these building modules is not fixed. Therefore, an AoD node has greater flexibility and upgradability than other static optical node architectures.

Multi-granular transmission in the space/frequency/time domain has been demonstrated using AoD nodes and MCFs [91]. An experiment demonstrated great flexibility of AoD node in MCF-based EONs with over 6000-fold bandwidth granularity. Reference [102] defines the flexibility of node architectures on the basis of the entropy of the system and compares those of AoD nodes and traditional static node architectures of EONs. The advantage on the flexibility of AoD nodes has been proved both theoretically and experimentally. Reference [103] first demonstrated WDM inter-data center network (DCN) transmission using AoD nodes. In this model, clustered DCNs are connected through metro/core networks, and inter- and intra-cluster transmission is conducted according to the AoD concept.

Moreover, the flexibility of AoD nodes can also be used to reduce the power consumption of optical nodes. Because AoD nodes are dynamically constructed according to the switching and signal processing request, they can use just enough modules, although traditional architectures constantly require a fixed maximum number of hard-wired modules regardless of the request. It is possible that the use of AoD nodes can reduce the number of implemented modules and the power consumption. References [104, 105] include a power consumption analysis for AoD nodes. Reference [104] shows that using AoD nodes can reduce the total power consumption

of the network by more than 25% using a heuristic algorithm to construct AoD nodes. Reference [105] numerically analyzes the benchmark of power consumption reduction according to the granularity of the switching request.

Despite these great advantages, AoD nodes also have some challenges. In this chapter, the two important problems of AoD nodes are addressed. One is the scalability problem of the optical backplane. As shown in Fig.1.3, all the building modules implemented in an AoD node are connected to a central optical backplane (3D-MEMS). When the number of input/output ports and building modules are increased, the port count required for the optical backplane is too large to be implemented by a single 3D-MEMS. Using multiple 3D-MEMSs is a simple solution to this problem; however, in order to switch signals between multiple 3D-MEMSs freely, many 3D-MEMSs ports are used for intraconnections between them. A sophisticated AoD construction using multiple 3D-MEMSs is required because wasting the switching ports of a 3D-MEMS requires more 3D-MEMSs and increases the power consumption of AoD nodes. The other problem is a trade-off between the switching granularity and the number of required modules. Although some studies have examined the energy efficiency of AoD nodes, reducing their power consumption depends on reducing the number of SSSs, assuming switching requests with coarse granularity, such as fiber switching. If EONs require fully flexible operation for all input/output ports of AoD nodes, they require the same number of SSSs as traditional architectures.

5.2.3 Routing and Spectrum Assignment Problem for Architecture on Demand Nodes

When AoD nodes are implemented for EONs, the RSA problem and resource allocation method become more serious concerns. AoD nodes dynamically construct themselves and supply the signal processing functions according to the switching requests; therefore, the arrangement of allocated spectra (which is the result of resource allocation) affects the AoD node configurations [1]. Several studies have examined a dynamic resource allocation method considering the construction of AoD nodes [95, 106]. Reference [95] numerically analyzes RSA solutions in MCF-based EONs that reduce intercore crosstalk of MCFs considering AoD nodes. The

proposed RSA strategy also reduces the number of SSSs and amplifiers in AoD nodes. Reference [106] proposes a redundant optical node configuration method based on AoD nodes for restoration from component failure. It also addresses a routing algorithm that improves the lightpath availability by increasing the fiber switching requests. However, these studies assume not a dynamic but a static model of performance evaluation. It is necessary to study about a dynamic resource allocation method considering AoD node configuration. References [107, 108] includes my fundamental dynamic resource allocation method considering the monetary cost of AoD nodes, but the proposed resource allocation methods and node architectures still have the problem of scalability and feasibility.

5.3 Energy-Efficient Architecture on Demand Nodes

5.3.1 Concept

First, the concept of the proposed energy-efficient AoD node is introduced. Note that in this chapter, although EONs are assumed to be equipped with MCFs, the proposed node architecture and resource allocation method can also be applied to an EON that has multiple single-core single-mode fibers in one link.

In the proposed energy-efficient AoD node architecture, a large proportion of the SSSs is replaced by an array-waveguide-grating-based MUX/DEMUX to reduce power consumption. A MUX/DEMUX is a fixed grid signal processing module whose output/input ports and wavelength channels are in a one-to-one correspondence. Spectra with the same bandwidth need to be allocated in a transmission signal if it is processed by a MUX/DEMUX. Figure 5.1 shows the difference between traditional spectrum allocation and the proposed spectrum allocation considering energy-efficient AoD nodes. The proposed spectrum allocation method simplifies the signal processing modules in the proposed energy-efficient AoD nodes. It is explained in detail in the next section.

Figure 5.1(a) shows the traditional non-uniform spectrum allocation in EONs. When MCFs are installed in EONs, each input or output port of the optical nodes is connected to a core of MCFs. Because of the repeated setup and release of connection having diverse bandwidth, the spectrum resources of EONs are fragmented; therefore, the efficiency of spectrum utilization is

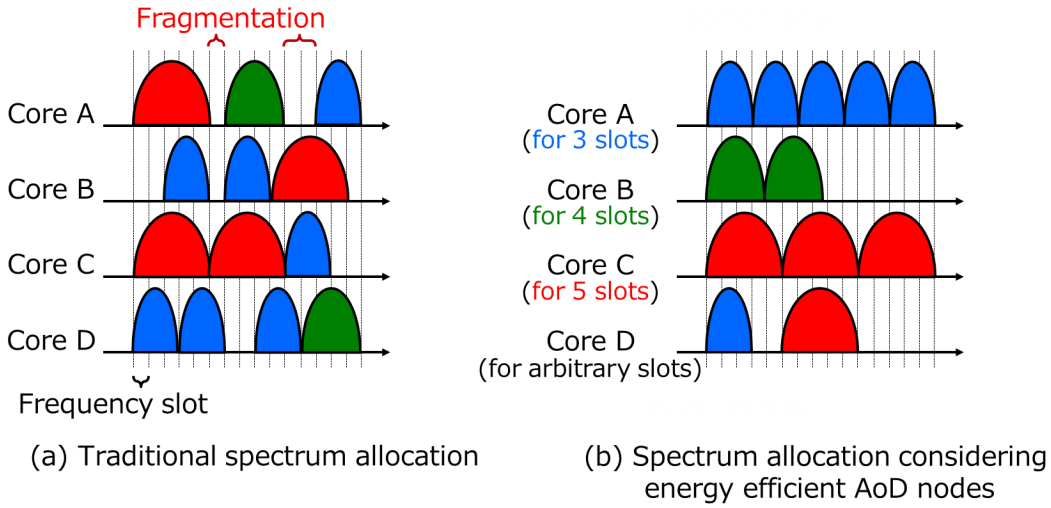

Figure 5.1: Example of spectrum allocation considering energy efficient AoD nodes.

decreased. On the other hand, the proposed uniform spectrum allocation shown in Fig. 5.1(b) can reduce the spectrum fragmentation by classifying connections according to the required bandwidth. Moreover, in terms of the node architecture, this uniform spectrum allocation also makes it possible to replace flexible SSSs with fixed-grid MUX/DEMUXs according to the dynamic and adaptive construction of AoD nodes. In this chapter, cores in which connections requiring the same bandwidth are allocated [such as core A, B, and C in Fig. 5.1(b)] are called *dedicated cores*, and cores in which connections requiring arbitrary bandwidth are allocated [such as core D in Fig. 5.1(b)] are called *common core*. The number of common cores and dedicated cores is statically established before network operation begins; however, the number of dedicated cores for the λ slots is set dynamically. First, a connection requiring an arbitrary number of FSs can be allocated to an empty dedicated core. Once the connection is allocated to the empty dedicated core, subsequent connections requiring the same number of FSs must be allocated to that dedicated core.

5.3.2 Architecture

The architecture of the proposed energy-efficient AoD nodes is shown in Fig. 5.2. Note that two dotted lines are the examples of optical switching and they are explained in the next paragraph. Optical switching in this AoD nodes is divided into three phases as shown in Fig. 5.2. This is

because the number of required switching port is too high to be constructed if the implementation depends on the single central Optical Backplane. Signals are switched in this architecture as follows. First, input signals are switched to appropriate signal processing modules in the core switching phase. If input signals are from common cores, then such signals having various spectral width are processed by an SSS in the waveband switching phase. In this part, spectra with the same width are grouped and switched to the corresponding DEMUXs. Note that the color of the MUX/DEMUXs in my figures represents the supported spectral width. On the other hand, if the input signals are from dedicated cores, then, skipping the waveband switching phase, such signals are directly switched to the corresponding DEMUXs in the wavelength switching phase. In the wavelength switching phase, switched input signals from dedicated cores and the corresponding waveband group from an SSS are demultiplexed into wavelength channel in DEMUXs. Each wavelength channel is switched to the corresponding MUX, which is connected to an appropriate output port according to the switching request.

Figure 5.2 also shows examples of signal switching and processing. The blue dotted line represents a connection requiring three FSs, and its switching request is from a dedicated core to a dedicated core. The input signal in a dedicated core for three FSs is first demultiplexed by a blue-colored DEMUX in Fig. 5.2 (which is for three FSs) after the core switching phase and then delivered to a blue-colored MUX through the wavelength switching phase. The signal is finally delivered to the output dedicated core, which is for three FSs. The green dotted line represents a connection requiring four FSs, and its switching request is from a dedicated core to common core. The input signal in a dedicated core for four FSs is first demultiplexed by a green-colored DEMUX (which is for four FSs) after the core switching phase and then delivered to a green-colored MUX through the wavelength switching phase. Next, the signal is delivered to an SSS through the waveband switching phase. In this SSS, the signal is combined with other signals that have different spectral width, and finally delivered to the output common core.

The proposed architecture in Fig. 5.2 have the same number of input/output ports, however, this architecture also supports the case that the numbers of input/output ports are different. In such a case, the scale of the 3D-MEMSes, which are used for wavelength switching, depends on the higher port-count.

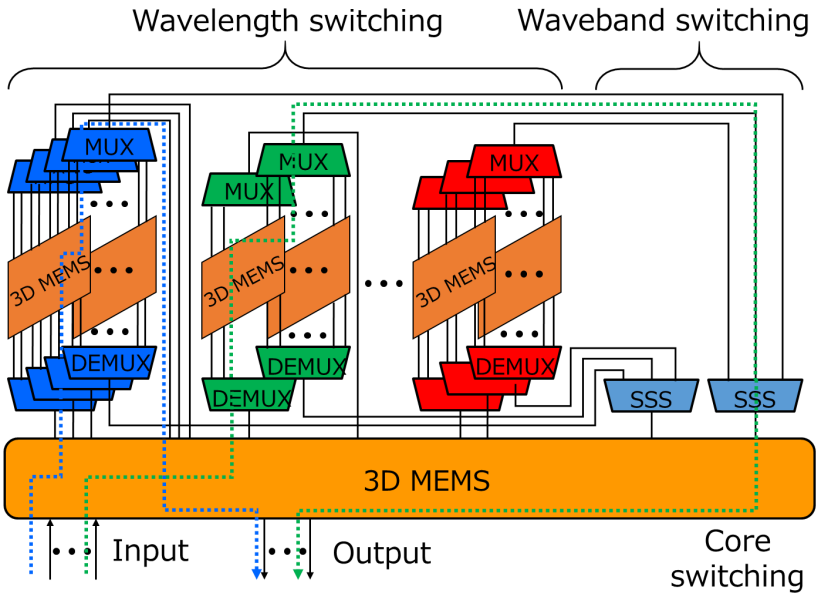

Figure 5.2: Proposed AoD node architecture.

5.3.3 Numerical Analysis and Static Evaluation

In this subsection, the proposed energy-efficient AoD nodes are numerically analyzed, with a focus on the required number of signal processing modules and power consumption. The symbols used in this section are summarized in Table 5.1. Note that the number of DEMUXs is the same as that of MUXs, and this number is determined in advance according to the number of all types of dedicated cores that are connected to the AoD node in order to maintain full flexibility in the spectral width setup for dedicated cores. In this chapter, for simplicity, the power consumption of an optical node is defined as the sum of the power consumption of all SSSs and 3D-MEMSs in operation.

The number of ports of a MUX/DEMUX whose channel spacing is $\Delta\lambda$ FSs is

$$P_{\mathrm{MUX}}^{\Delta\lambda} = \lfloor \frac{F}{\Delta\lambda} \rfloor. \tag{5.4}$$

The value $P_{\mathrm{MUX}}^{\Delta\lambda}$ also represents the number of wavelength channels per core. Then, for wavelength switching of $\Delta\lambda$ FSs, the number of port of the 3D-MEMS per corresponding $\Delta\lambda$-MUX is

$$Ch_{\mathrm{MEMS}}^{\Delta\lambda} = \lfloor \frac{P_{\mathrm{MEMS}}}{N_{\mathrm{MUX}}^{\Delta\lambda}} \rfloor. \tag{5.5}$$

Table 5.1: Symbols used in the numerical analysis of the proposed architecture.

Symbols	Description
F	Number of FSs per core
P	Port count of AoD nodes (supporting $P \times P$ switching)
C	Number of cores of a single installed MCF
$\Delta\lambda$	Channel spacing (number of FSs)
$N_{\mathrm{MUX}}^{\Delta\lambda}$	Number of implemented $\Delta\lambda$-MUXs
P_{MEMS}	Port count of 3D-MEMSs (supporting $P_{\mathrm{MEMS}} \times P_{\mathrm{MEMS}}$ switching)
W_{MEMS}	Power consumption of a 3D-MEMS
W_{SSS}	Power consumption of a SSS
W_{AoD}	Total power consumption of the proposed AoD node

It equals to the maximum number of wavelength channels that are switched in one 3D-MEMS because the same port from each $\Delta\lambda$-MUX/DEMUX has to be connected to the same 3D-MEMS in order to switch the corresponding wavelength channel. The number of 3D-MEMSs used for wavelength switching with a channel spacing of $\Delta\lambda$ FSs is

$$N_{\mathrm{MEMS}}^{\Delta\lambda} = \lceil \frac{P_{\mathrm{MUX}}^{\Delta\lambda}}{Ch_{\mathrm{MEMS}}^{\Delta\lambda}} \rceil = \lceil \frac{\lfloor \frac{F}{\Delta\lambda} \rfloor}{\lfloor \frac{P_{\mathrm{MEMS}}}{N_{\mathrm{MUX}}^{\Delta\lambda}} \rfloor} \rceil. \tag{5.6}$$

Therefore, the total number of 3D-MEMS required in the proposed AoD node is

$$N_{\mathrm{MEMS}} = 1 + \sum_{\Delta\lambda} \lceil \frac{\lfloor \frac{F}{\Delta\lambda} \rfloor}{\lfloor \frac{P_{\mathrm{MEMS}}}{N_{\mathrm{MUX}}^{\Delta\lambda}} \rfloor} \rceil. \tag{5.7}$$

Because the number of MUXs is less than the number of input/output ports of an optical node ($N_{\mathrm{MUX}}^{\Delta\lambda} \leq P$),

$$N_{\mathrm{MEMS}} \leq 1 + \sum_{\Delta\lambda} \lceil \frac{\lfloor \frac{F}{\Delta\lambda} \rfloor}{\lfloor \frac{P_{\mathrm{MEMS}}}{P} \rfloor} \rceil. \tag{5.8}$$

Next, the number of SSSs required in the proposed AoD node N_{SSS} is the same as the number of common cores N_{COM}. The number of common cores is statically determined in advance, and 1 common core is set up for every C cores. The value is determined from preliminary simulation results. When all the input/output ports are connected to the cores of the MCFs,

$$N_{\mathrm{SSS}} = N_{\mathrm{COM}} = \lceil \frac{P}{C} \rceil. \tag{5.9}$$

Therefore, the total power consumption of the proposed AoD node is

$$\begin{aligned} W_{\mathrm{AoD}} &= W_{\mathrm{SSS}} \cdot N_{\mathrm{SSS}} + W_{\mathrm{MEMS}} \cdot N_{\mathrm{MEMS}} \\ &\leq W_{\mathrm{SSS}} \cdot \lceil \frac{P}{C} \rceil \\ &\quad + W_{\mathrm{MEMS}} \cdot \left(1 + \sum_{\Delta\lambda} \lceil \frac{\lfloor \frac{F}{\Delta\lambda} \rfloor}{\lfloor \frac{P_{\mathrm{MEMS}}}{P} \rfloor} \rceil \right). \end{aligned} \tag{5.10}$$

Figure 5.3 shows the numerically analyzed total power consumption of EONs. In this figure, the vertical axis represents the total power consumption of each node, and the horizontal axis represents the port count of each node.

The evaluation is based on formulas (5.10) and (5.3). Static values are defined as follows. The number of spectrum slots F is 320. Because I set the width of FS to 12.5 GHz and the total spectrum resource per core to 4 THz (C band). The port count of the 3D-MEMSs P_{MEMS} is 320. The port count of the SSSs P_{SSS} is 20. The power consumption values W_{SSS} and W_{MEMS} are 40 and 150, respectively. Figure 5.3 shows an explosive increase in the power consumption of the traditional spectrum-routing node architecture (shown in Fig. 1.3(b)) with port count growth. Use of the proposed energy-efficient AoD node can dramatically mitigate the increase, although the larger number of types of required spectral width slightly increases the node's power consumption.

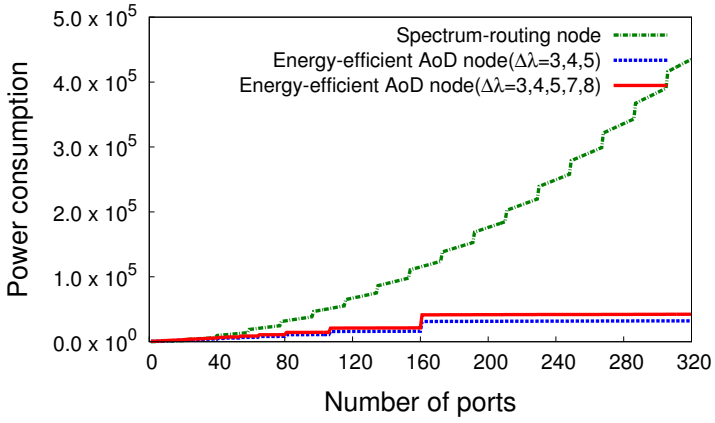

Figure 5.3: Static evaluation of power consumption for EONs.

5.4 On-Demand Routing and Spectrum Allocation for Energy-Efficient Architecture on Demand Nodes

5.4.1 Concept and Definition of Allocation-Cost

In this section, the procedure for the proposed on-demand routing and spectrum allocation method is explained in detail. The proposed allocation method is controlled according to the *allocation cost* of spectra. The allocation cost is defined for each spectrum of all the MCFs according to the status of a core in order to lower the allocation cost of a desirable spectrum. There are three types of allocation costs for a combination of a route and spectrum (k, f), where the selected route is k, and the initial FS of the selected spectrum is f. These three types of allocation costs are defined as follows. The symbols used in the proposed routing and allocation method are summarized in Table 5.2.

Table 5.2: Symbols used in the proposed spectrum and core allocation.

Symbols	Description
f	Index of an initial FS
l	Index of a link
c	Index of a core
k	Index of a route that is one of the precalculated routes
H_k	Number of hops of route k
$\mathcal{L}_k$	Set of links in route k
$\mathcal{C}_l$	Set of cores at link l
u_c	Spectrum utilization of core c

$X_{l,c}^{k,f}$ is the most basic allocation cost and represents the allocation costs of a core c ($c \in \mathcal{C}_l, l \in \mathcal{L}_k$) for (k, f). When the required number of spectrum slots is r,

$$X_{l,c}^{k,f} = \begin{cases} 1 - u_c & \text{if } c \text{ is a core for } r \text{ slots,} \\ 1 & \text{if } c \text{ is an empty dedicated core,} \\ H_k + 1 & \text{if } c \text{ is a common core.} \end{cases} \tag{5.11}$$

Otherwise, the cost $X_{l,c}^{k,f} = \infty$ (that is, the selected spectrum is occupied and cannot be allocated). In my proposed method, the desirable core is the dedicated core for r slots from the perspective of spectrum fragmentation. Moreover, the dedicated core for r slots with the lowest

spectrum utilization is the most desirable in order to maintain a large number of empty dedicated cores.

$X_l^{k,f}$ is the intermediate allocation cost, which represents the allocation costs of a link l ($l \in \mathcal{L}_k$) for (k, f).

$$X_l^{k,f} = \min \left\{ X_{l,c}^{k,f} \middle| \, c \in \mathcal{C}_l \right\}. \tag{5.12}$$

This allocation cost is the cost of a desirable core in link l.

$X^{k,f}$ is the final allocation cost, which represents the allocation costs for (k, f). Its value is the sum of $X_l^{k,f}$ at each link along the route k. Therefore, $X^{k,f}$ is calculated as follows:

$$X^{k,f} = \sum_{l \in \mathcal{R}_k} X_l^{k,f}. \tag{5.13}$$

All these costs are updated when an optical path is set up or released because the actual value of each cost depends only on the state of spectrum utilization. It means that after connection arrival, the spectrum allocation process not calculates but refers the appropriate cost in order to reduce the processing delay.

5.4.2 Flowchart and Example of Allocation-Cost Calculation

Figure 5.4 shows the optical path provisioning flowchart of the proposed routing and spectrum allocation method. When a new connection request arrives, the number of required FSs is calculated for each route k. Next, $X^{k,f}$ is calculated for each (k, f). If the minimum allocation cost $X^{k,f}$ is ∞, there is no available combination of a route and spectrum resources, and the connection request is rejected. Otherwise, the route and spectrum (k, f) are selected to minimize $X^{k,f}$. Then the selected spectrum is allocated to the core c with a minimum $X_{l,c}^{k,f}$ for each link along the route k. Finally, all the $X_{l,c}^{k,f}$ values are updated according to the changed status of the cores, and path provisioning succeeds.

Figure 5.5 shows an example of a cost calculation when the number of required FSs is three and the index of the initial FS is 1. The selected route ($k = 2$) from node A to node D has three links ($l = 1, 2$, and 3). Hence, $H_2 + 1$ is equal to 4. At each link, the minimum value of $X_{l,c}^{2,1}$ is selected as the $X_l^{2,1}$ value ($X_1^{2,1} = 1$, $X_2^{2,1} = 0.5$ and $X_3^{2,1} = 4$). The cost of spectrum $X^{2,1}$ is the sum of these $X_l^{2,1}$ value ($X^{2,1} = X_1^{2,1} + X_2^{2,1} + X_3^{2,1} = 5.5$).

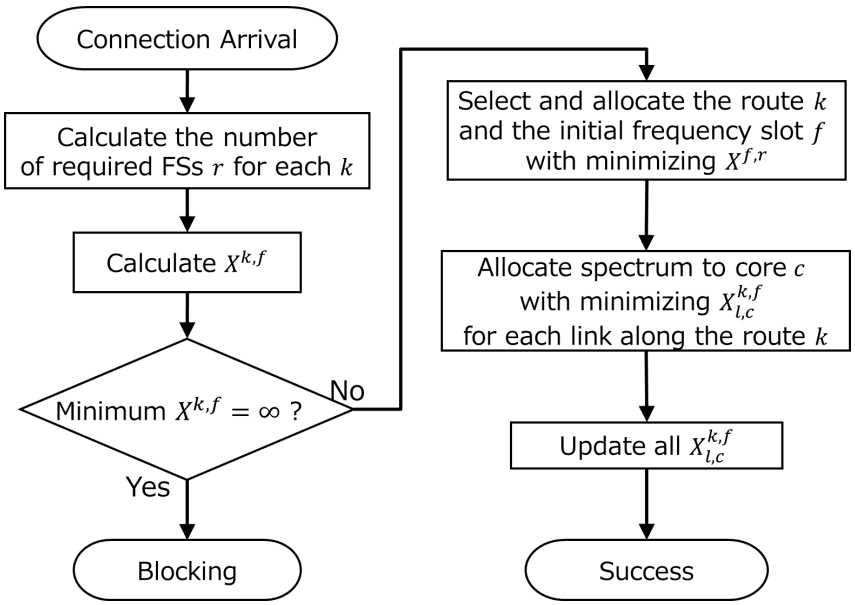

Figure 5.4: Flowchart of the proposed routing and spectrum allocation method.

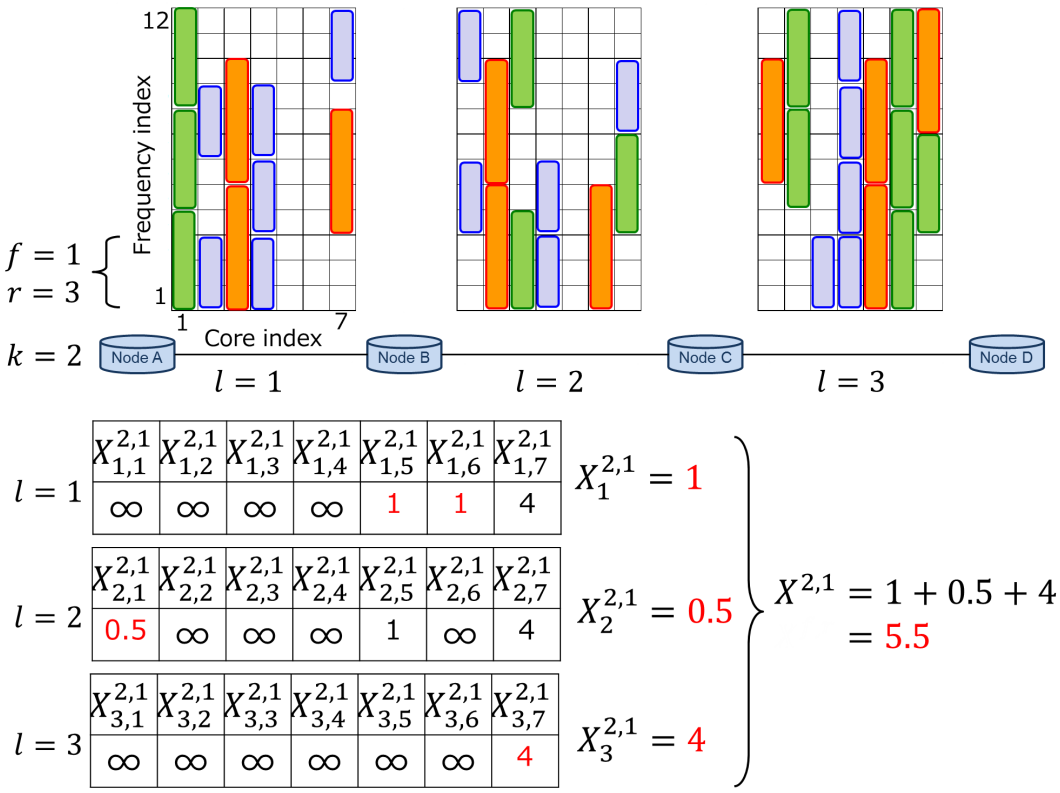

Figure 5.5: Example of an allocation cost calculation.

5.5 Performance Evaluation

5.5.1 Simulation Model

I used my own C++ simulator to evaluate the proposed method. I adopted the JPN-12 topology, USA topology, NSF topology and Deutsche Telekom (DT) topology shown in Figs. 3.4, 3.5, 5.6 and 5.7, respectively. The JPN-12 topology has 12 nodes and 16 links. The USA topology has 28 nodes and 45 links. The NSF topology has 14 nodes and 21 links. The DT topology has 14 nodes and 23 links. Each link has one MCF for each direction. I simply suppose that all links have three MCFs that has 7 cores. I set the width of FS to 12.5 GHz and the total spectrum resource per core to 4 THz (C band). Therefore, the number of FSs per core is $W = 320$. The connection requests were assumed to arrive according to a Poisson process with an average arrival rate λ, and the service time of each connection was assumed to follow a negative exponential distribution with an average $1/\mu$. Thus, overall traffic intensity is represented by λ/μ. The connection requests randomly required one source–destination (SD) pair; the traffic load (Erlang) means traffic intensity per SD pair, and it is represented by $\frac{i}{N\cdot(N-1)} \cdot \frac{\lambda}{\mu}$. Connections require 40, 100, or 400 Gbps transmission randomly. The number of required FSs depends on the bitrate and the hop count of the selected route. Table 5.3 shows the required FS setup for the adopted topology scaled from the setup in Ref. [2]. Note that "short," "intermediate" and "long" are defined as follows when M is the maximum number of hops of all candidate routes.

- short: $0 < h \leq \lceil \frac{M}{3} \rceil$
- intermediate: $\lceil \frac{M}{3} \rceil < h \leq \lceil 2 \cdot \frac{M}{3} \rceil$
- long: $\lceil 2 \cdot \frac{M}{3} \rceil < h \leq M$

Further, $k = 5$ in the k-shortest path algorithm. The number of common cores is one for each MCF. The parameters of the signal processing modules are shown in Table 5.4 [109]. Note that the 3D-MEMS and SSS can be turned off when they are not in use. I introduce "SR with FFS" and "SR with FFC" as comparison methods. Both of these methods suppose that spectrum-routing (SR) node architecture [102] is implemented for EONs. From the k-shortest paths ($k = 5$), both comparison methods select one route that has the least congested bottleneck link.

"SR with FFS" allocates spectra for the first fit of the FS index (FFS). "SR with FFC" allocates spectra for the first fit of the core index (FFC). The combination fo proposed energy-efficient node and resource assignment is denoted "Proposed system" in the evaluations.

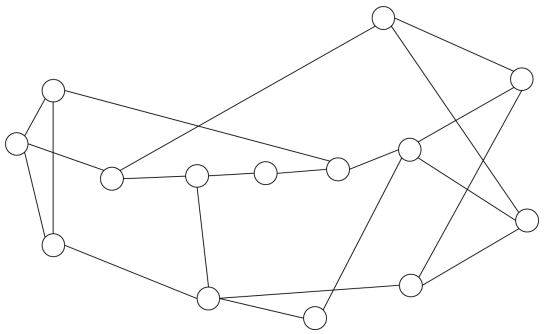

Figure 5.6: NSF topology.

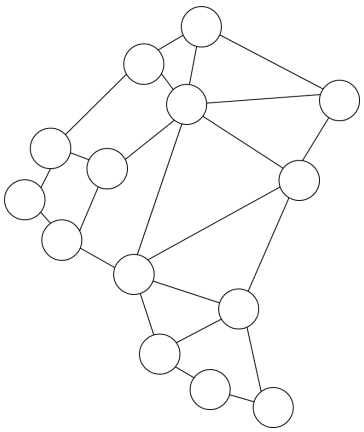

Figure 5.7: DT topology.

Table 5.3: Number of required FSs.

# of Hops	# of required FSs		
	40Gbps	100Gbps	400Gbps
short	3	3	7
intermediate	3	4	7
long	4	5	8

Table 5.4: Parameters of signal processing modules

Module	Port-count	Power consumption [W]
MUX/DEMUX	$\lfloor 320/\Delta\lambda \rfloor$	0
SSS	20	40
3D-MEMS	360	150

5.5.2 Power Consumption

Figures 5.8, 5.9, 5.10, and 5.11 show the total power consumption of optical switching nodes. These figures show that the total power consumption is reduced by 50% at most by utilizing the proposed energy-efficient AoD nodes and cost-aware on-demand routing and spectrum allocation method. By comparing the proposed method with the better comparison method SR with

FFC, the power consumption reduction is high when the traffic load is high, and as the traffic load becomes low, the difference in power consumption becomes small. However, the superiority of the proposed method is lost only under extremely low traffic load conditions in which all connection requests are not blocked, as shown by evaluations of the blocking probability in the next subsection. As a result, the proposed energy-efficient AoD node and resource allocation method can usually reduce the power consumption of optical switching nodes in dynamically operated EONs by arrangement of spectra and simplification of required signal processing modules.

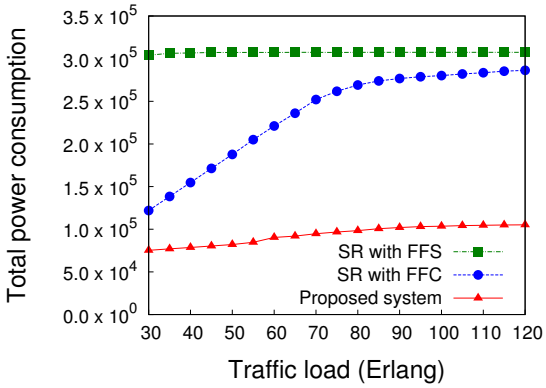

Figure 5.8: Total power consumption (JPN-12).

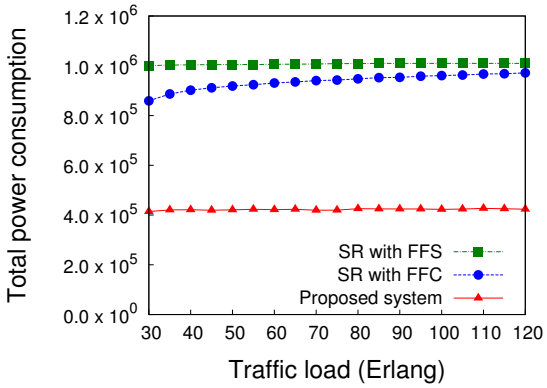

Figure 5.9: Total power consumption (USA).

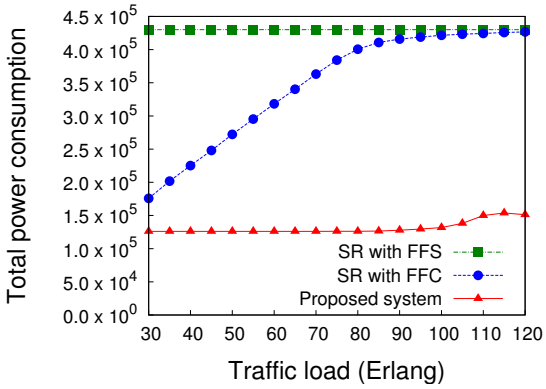

Figure 5.10: Total power consumption (NSF).

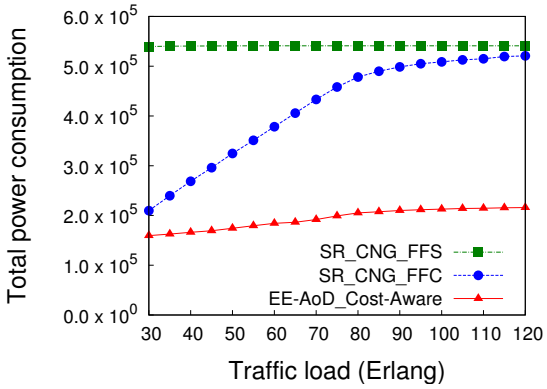

Figure 5.11: Total power consumption (DT).

5.5.3 Blocking Probability

Figures 5.12, 5.13, 5.14, and 5.15 show the blocking probability of the entire network. These figures show that, through the blocking probability performance of the proposed method depends on topology, basically it outperforms that of the comparison methods. Therefore, the proposed resource allocation method reduces the power consumption without degrading the blocking probability.

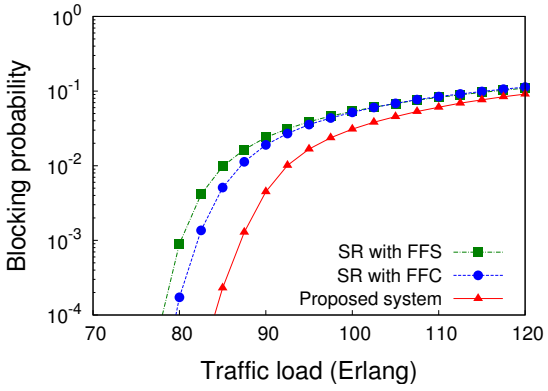

Figure 5.12: Blocking probability (JPN-12).

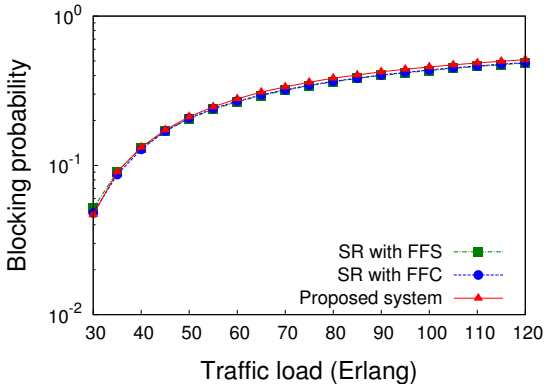

Figure 5.13: Blocking probability (USA).

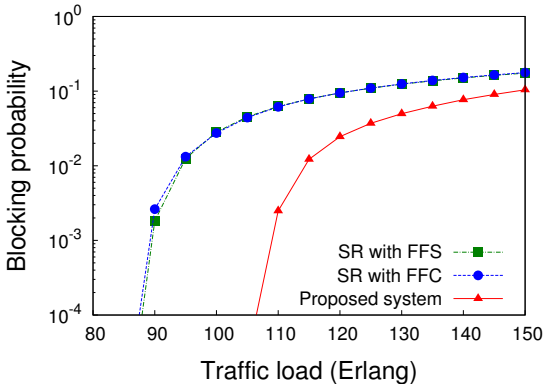

Figure 5.14: Blocking probability (NSF).

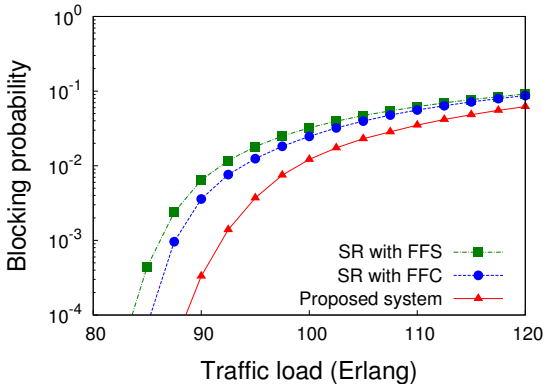

Figure 5.15: Blocking probability (DT).

In terms of the dependence of the blocking probability on the topology, the performance of the proposed method is relatively poor for the topology in which the blocking probability is high at low Erlang. This means that these topologies have many k-shortest paths that include a few

of the same links (these links are particularly congested and obviously bottleneck links) because the traffic volume for each source–destination pair has the same value in these evaluations. This characteristics is analyzed as follows, with a focus on "betweeness centrality" and "betweeness centralization," which are feature values of a topology.

When the number of nodes is V, node betweeness centrality for node v_i is defined as

$$C_B(v_i) = \frac{\sum_{s;s\neq i}^{V} \sum_{t;t\neq i,s}^{V} \frac{g_i(v_s,v_t)}{N_{v_s,v_t}}}{\frac{(V-1)(V-2)}{2}}. \tag{5.14}$$

Note that $g_i(v_s, v_t)$ is the number of shortest paths from v_s to v_t through v_i, and N_{v_s,v_t} is the total number of shortest paths from v_s to v_t.

According to the definition of node betweeness centrality, the link betweeness centrality for link l_i is newly defined as

$$C_B(l_i) = \frac{\sum_{s}^{V} \sum_{t;t\neq s}^{V} \frac{g'_i(v_s,v_t)}{N_{v_s,v_t}}}{V \cdot (V-1)}. \tag{5.15}$$

Note that $g'_i(v_s, v_t)$ is the number of shortest paths from v_s to v_t through l_i.

Betweeness centralization is a feature value that becomes small when the betweeness centralities of a few links or nodes are particularly high. On the basis of the link betweeness centrality, the link betweeness centralization is defined as

$$\frac{\max_i \{C_B(l_i)\}}{\sum_j \{\max_i \{C_B(l_i)\} - C_B(l_j)\}}. \tag{5.16}$$

Table 5.5 shows the link betweeness centralizations of all the topologies that are adopted in the evaluations. From Table 5.5 and Figs. 5.12, 5.13, 5.14, and 5.15, as the performance of the proposed method improves, the link betweeness centralizations increases. Therefore, both the blocking probability and power consumption can be improved dramatically by designing a topology so that its link betweeness centralization becomes high. According to the definition, high link betweenness centralization means each link betweeness centrality tends to take a value close to maximum value. When many links have high link betweeness centrality, these links tend to be congested similarly on the basis of Eq. (5.15). This means that a topology with high link betweeness centralizations does not have a specific bottleneck link, and traffic load of each link is more uniform in such a topology. Therefore, the proposed method is suited for the actual

network topology, in which it is desired that traffic load of each link is as uniform as possible.

Table 5.5: Link betweeness centralizations.

Topology	Link betweeness centralizations
JPN	0.0599$\cdots$
USA	0.0171$\cdots$
NSF	0.0603$\cdots$
DT	0.0422$\cdots$

5.5.4 SDM Scalability

Figures 5.16, 5.17, 5.18, and 5.19 show the scalability of power consumption of optical switching nodes. The vertical axis indicates total power consumption (same as in Sec. 5.5.2), and the horizontal axis indicates the number of cores per link. The values of traffic load are 90, 30, 115, and 100 in Figs. 5.16, 5.17, 5.18, and 5.19, respectively. These figures show that the power consumption of the proposed method is less than that of compared methods, and the difference becomes large as the number of cores becomes large. The shapes of these four figures are similar to that of numerically analyzed Fig. 5.3. Therefore, the proposed method is suited for the future large optical nodes, and it represents superior scalability of power consumption.

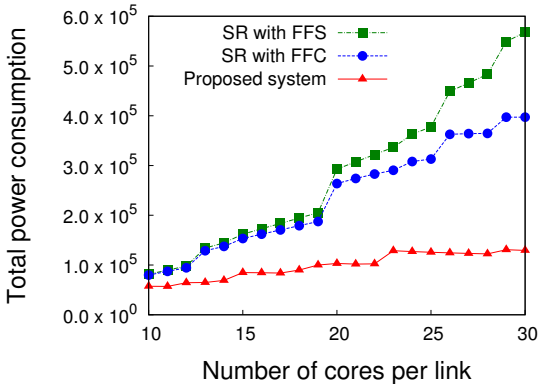

Figure 5.16: Scalability of power consumption (JPN-12).

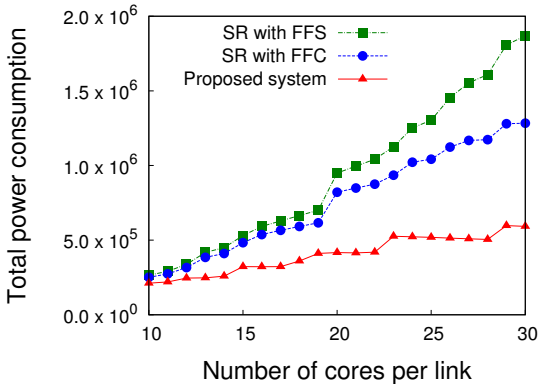

Figure 5.17: Scalability of power consumption (USA).

Figures 5.20, 5.21, 5.22, and 5.23 show the scalability of blocking probability of the entire network. The vertical axis indicates the blocking probability of path set-up requests (same as in

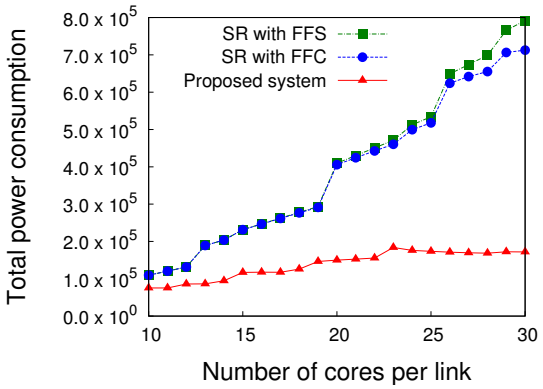

Figure 5.18: Scalability of power consumption (NSF).

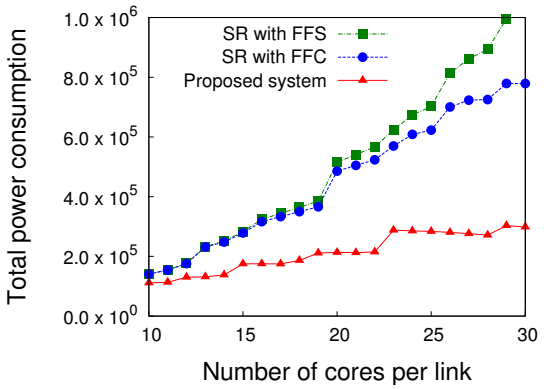

Figure 5.19: Scalability of power consumption (DT).

Sec. 5.5.3), and the horizontal axis indicates the number of cores per link. The values of traffic load are 80, 30, 105, and 90 in Figs. 5.20, 5.21, 5.22, and 5.23, respectively. These figures show that the blocking probability of the proposed method becomes much lower than that of two compared methods as the number of cores becomes large in all topologies except USA topology. This is because there is more flexibility in the setup of dedicated cores for the proposed method when the number of cores is larger, and that effectively reduces the blocking probability. In USA topology, the blocking probability of the proposed method is worse than that of two compared method, however, it is possible to solve the problem of blocking probability by focusing on the link betweeness centralizations (like the discussions in Sec. 5.5.3). Therefore, the proposed method also represents superior scalability of blocking probability.

5.6 Conclusion

An EON with MCFs is expected to exhibit greater transmission capacity. In terms of energy efficiency, however, the power consumption of traditional optical node is expected to increase explosively because of the port-count characteristics of SSSs. In this chapter, I proposed an energy-efficient optical network system. I firstly discussed the proposed energy-efficient optical node architecture based on the AoD concept. My proposed energy-efficient AoD node can reduce its power consumption by using fixed signal processing modules containing MUX/DEMUXs. I also proposed a cost-aware resource allocation method that meets

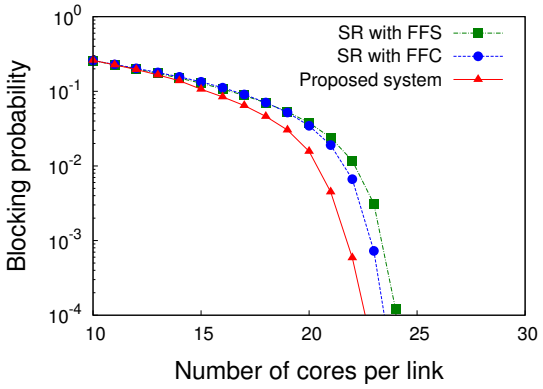

Figure 5.20: Scalability of Blocking probability (JPN-12).

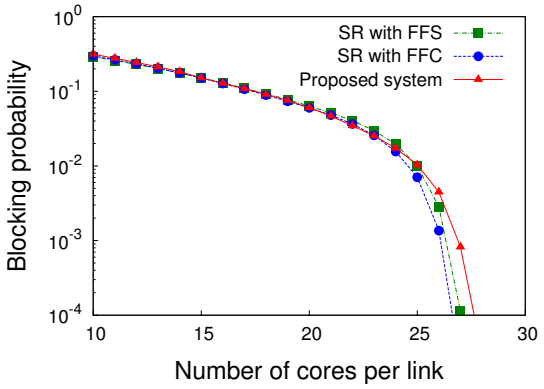

Figure 5.21: Scalability of Blocking probability (USA).

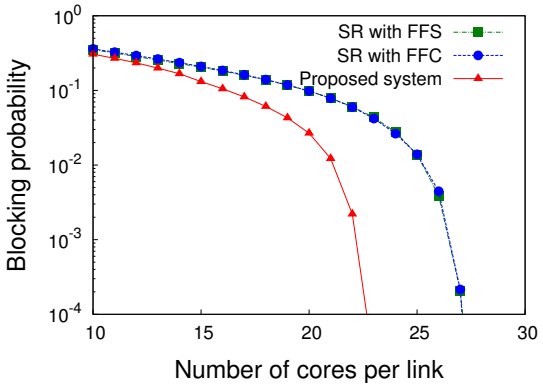

Figure 5.22: Scalability of Blocking probability (NSF).

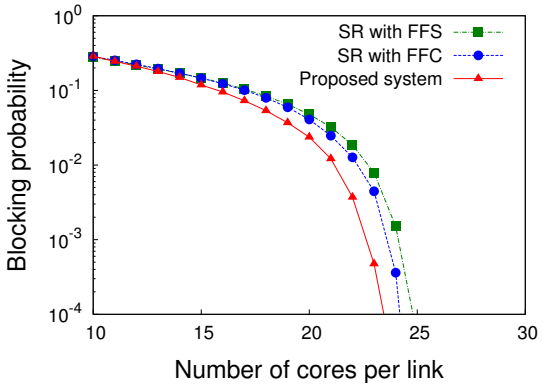

Figure 5.23: Scalability of Blocking probability (DT).

the requirements of the proposed node architecture. I evaluated the proposed method using extensive computer simulations. The proposed method can reduce the power consumption of optical nodes without degrading the blocking probability. Moreover, I showed that the proposed method can dramatically improve both the power consumption and blocking probability if the network topology is appropriately designed, considering an index of link betweenness centralization.

Chapter 6

Conclusions

Chapter 1 summarized background and problem of this dissertation. Elastic optical networks (EONs) have been developed from the traditional wavelength division multiplexing networks to accommodate the future large traffic volume. Moreover, for the further expansion of network capacity beyond the physical limit of existing single-mode single-core optical fibers, space division multiplexing (SDM) technology and novel optical fibers based on the technology is intensively researched; Multicore fibers (MCFs) are the most promising candidate of a future SDM-based optical fiber. From the networking perspective, SDM-EONs need an efficient resource management method to establish appropriate optical paths considering various unique issues, which suppress the capacity improvement of SDM-EONs. Firstly, geographically scalable translucent EONs have to consider placement of signal regeneration. Existing dynamic schemes mainly utilize regeneration to compensate the optical reach of transmission signals; regeneration can be used to improve the spectral efficiency and fairness of EONs. Secondly, inter-core crosstalk (XT) is the most important problem of MCF-implemented SDM-EONs, and there is a requirement of resource management reducing the XT although many contriving structure of MCFs is proposed. Finally, consideration of network equipments, which are suited for spatially multiplexed large optical network, is required. In particular, nodal cost and network performance are in a trade-off relationship. This dissertation propose dynamic path provisioning methods for SDM-EONs. The proposed methods solve these unique problems from the networking perspectives focusing on path segmentation, qualitative characteristics of XT, and parameters of network equipments. Simultaneously, the proposed methods also improve the traffic accommodation rate by contriving arrangement of spectra.

Chapter 2 described the details of proposed spectrum allocation and regeneration placement (SARP) algorithms for provisioning spectrally efficient optical paths in SDM-EONs. I proposed two dynamic SARP algorithms, which divided required optical paths into shorter optical sub-paths by signal regenerations: spectrally efficient SARP (SE-SARP) and blocking aware SARP (BA-SARP). The SE-SARP algorithm divides optical paths into the most spectrally efficient optical sub-paths, which can adopt the highest level modulation format among the selectable ones. The SE-SARP minimizes the allocated bandwidth of all required optical paths although it maximizes the cost of signal regeneration. The BA-SARP algorithm divide optical paths when undivided end-to-end optical paths cannot be provisioned because there are no available resources which satisfies the continuity and contiguity constraints of the routing and spectrum allocation (RSA) problem. The spectral improvement of the BA-SARP is less than that of SE-SARP, however, the BA-SARP suppresses an excessive increase in the cost of signal regeneration. My proposals also improve the fairness issue of EONs by mainly benefiting long-haul transmissions, which are negatively affected by the unfairness of EONs. These proposed algorithms were evaluated by computer simulations. As simulation results, the SE-SARP is superior to the BA-SARP in both spectral efficiency and fairness in throughput of all source-destination pairs. On the other hand, the BA-SARP outperforms the SE-SARP regarding with the spectral improvement per signal regeneration; this chapter concluded that the BA-SARP is more practical algorithm than the SE-SARP.

In Chapter 3, I proposed a novel dynamic RSA method, which is called advance reservation-limited (AR-L), to reduce spectrum fragmentation and to control the service level of immediate reservation (IR) and advance reservation (AR) requests in terms of bandwidth blocking probability (BBP) in SDM-EONs considering multiplexing effect of spatial channels. The proposed RSA method configures prioritized areas based on the required bandwidth to reduce spectrum fragmentation. Each prioritized area is divided into two sub-areas: one is dedicated to IR requests (IR-dedicated sub-area) and another is shareable for both IR and AR requests (shareable sub-area) In addition, the border of the IR-dedicated and shareable sub-areas is moved dynamically to obtain the desired ratio of the BBPs of IR requests to that of AR requests. These

proposed RSA method was evaluated by computer simulations. As simulation results, the proposed RSA method can improve BBP for a overall network by reducing resource fragmentation. Moreover, the proposed RSA method can control a relationship among transmission success ratios of service applications by introducing corresponding parameter.

In Chapter 4, I proposed a spectrum and core allocation method for provisioning crosstalk (XT)-aware optical paths in MCF-implemented SDM-EONs. First of all, I introduced the simple XT model to control the inter-core XT of MCFs from the networking perspective. The model is based on the existing theoretical analyses and focused on the dominant XT, which occurs when the optical signals allocated to the same frequency are transmitted in the nearest cores of a MCF. The proposed allocation method is based on two predefinitions for cores of MCFs: the predefined core prioritization and the predefined core classification. The core prioritization reduces inter-core XT of MCFs by avoiding the spatially close core-selection based on the introduced XT model. Simultaneously, the core classification reduces spectral fragmentation by arranging allocated spectra regarding with the required number of frequency slots. The proposed spectrum and core allocation was evaluated through computer simulations. The simulation results showed that the proposed method is able to reduce both XT and call-blocking probability owing to these two predefinitions. The simulation results also confirmed that the predefinitions are generalized, and they are valid regardless of structure of adopted MCFs.

In Chapter 5, I finally proposed the energy-efficient network system, which consists of novel switching node architecture and path provisioning method organically linked with the architecture. The proposed node architecture reduces the power consumption by replacing power consuming signal processing modules with passive ones based on the architecture on demand (AoD) concept. The proposed AoD node requires mildly restricted arrangement of spectra allocated to optical paths, therefore, the proposed system satisfies the requirement by introducing on-demand spectrum allocation. The introduced spectrum allocation dynamically achieves the required spectrum arrangement by utilizing the spatial channels of SDM-EONs. Moreover, the spectrum allocation method also improves the traffic accommodation rate by reducing spectral fragmentation. I evaluated the proposed network system by computer simulations. The evaluation results showed that the proposed network system achieved a drastic reduction of power

consumption without serious degradation of call-blocking probability. Concerning the blocking probability of the overall network, a discussion in this chapter revealed that the proposed method improves both traffic accommodation rate and power consumption of SDM-EONs when their topologies have no specific bottleneck link. It is also proved that these advantages of the proposed network system has good scalability for spatial enlargement of SDM-EONs.

Through all results, the proposed schemes which provide high spectral efficiency, fairness for throughput, low inter-core XT, low power consumption, and high scalability for spatial expansion are effective to SDM-EONs. Finally, this dissertation discusses the future work. In order to apply the proposed schemes to realistic networks, experimental validation is the most important challenge and the closest future work. In particular, actual amount of XT in MCFs should be controlled by developing the proposed schemes through the experiments. Moreover, I think there are two key issues in the future SDM-EONs; the one is a novel optical fiber based on the multiple SDM technologies, and the other is a SDM amplifier. First, the resent researches said that MCFs are the reliable solution because other SDM fibers, which are multi-mode fibers, few-mode fibers, or vortex fibers for orbital angular momentum multiplexing, have some impossibilities for long-haul backbone transmission. Then, the new SDM fibers which are based on the multiple SDM technologies (e.g. few-mode multicore fibers) attract our attention because such a combination use of SDM technologies can mitigate the difficulty of SDM fibers by reducing the multiplicity of each SDM technology. Therefore, the optical path provisioning scheme should be developed for the future SDM-EONs in which multiple SDM technologies are implemented. Second, SDM amplifiers are also important issue in the future SDM-EONs. This is because SDM-based optical fibers more frequently require SDM amplifiers to compensate the signal degradation due to spatial multiplexing. Moreover, SDM-based new amplification mechanism is recently proposed, and the optical path provisioning scheme should also take these issues into account.

Bibliography

[1] M. Garrich, N. Amaya, G. Zervas, P. Giaccone, and D. Simeonidou, "Architecture on demand: Synthesis and scalability," International Conference on Optical Network Design and Modeling (ONDM), 6 pages, Apr. 2012.

[2] M. Jinno, B. Kozicki, H. Takara, A. Watanabe, Y. Sone, T. Tanaka, and A. Hirano, "Distance-adaptive spectrum resource allocation in spectrum-sliced elastic optical path network," IEEE Communications Magazine, vol. 48, no. 8, pp. 138–145, Aug. 2010.

[3] Ministry of Internal Affairs and Communications, "2016 white paper on information and communications in Japan," July, 2016.

[4] Cisco, "Cisco visual networking index: forecast and methodology, 2015-2020," June, 2016.

[5] B. Mukherjee, "WDM optical communication networks: progress and challenges," IEEE Journal on Selected Areas in Communications, vol. 18, no. 10, pp. 1810–1824, Oct. 2000.

[6] M. Murata, "Challenges for the next-generation internet and the role of IP over photonic networks," IEICE Transactions on Communications, vol. E83.B, no. 10, pp. 2153–2165, 2000.

[7] M. Jinno, H. Takara, B. Kozicki, Y. Tsukishima, Y. Sone, and S. Matsuoka, "Spectrum-efficient and scalable elastic optical path network: architecture, benefits, and enabling technologies," IEEE Communications Magazine, vol. 47, no. 11, pp. 66–73, Nov. 2009.

[8] G. Zhang, M. D. Leenheer, A. Morea, and B. Mukherjee, "A survey on OFDM-based elastic core optical networking," IEEE Communications Surveys and Tutorials, vol. 15,

no. 1, pp. 65–87, Feb. 2012.

[9] O. Gerstel, M. Jinno, A. Lord, and S. J. B. Yoo, "Elastic optical networking: a new dawn for the optical layer?," IEEE Communications Magazine, vol. 50, no. 2, pp. S12–S20, Feb. 2012.

[10] A. Lord, P. Wright, and A. Mitra, "Core networks in the flexgrid era," IEEE Journal of Lightwave Technology, vol. 33, no. 5, pp. 1126–1135, Mar. 2015.

[11] A. Bocoi, M. Schuster, F. Rambach, M. Kiese, C.-A. Bunge, and B. Spinnler, "Reach-dependent capacity in optical networks enabled by OFDM," Optical Fiber Communication Conference/National Fiber Optic Engineers Conference (OFC/NFOEC), OMQ4, Mar. 2009.

[12] K. Christodoulopoulos, I. Tomkos, and E. A. Varvarigos, "Routing and spectrum allocation in OFDM-based optical networks with elastic bandwidth allocation," IEEE Global Telecommunications Conference (GLOBECOM), 6 pages, Dec. 2010.

[13] Y. Wang, X. Cao, and Q. Hu, "Routing and spectrum allocation in spectrum-sliced elastic optical path networks," IEEE International Conference on Communications (ICC), 5 pages, June 2011.

[14] A. Birman and A. Kershenbaum, "Routing and wavelength assignment methods in single-hop all-optical networks with blocking," IEEE International Conference on Computer Communications (INFOCOM), vol. 2, pp. 431–438, Apr. 1995.

[15] D. Banerjee and B. Mukherjee, "A practical approach for routing and wavelength assignment in large wavelength-routed optical networks," IEEE Journal on Selected Areas in Communications, vol. 14, no. 5, pp. 903–908, June 1996.

[16] H. Zang and J. P. Jue, "A review of routing and wavelength assignment approaches for wavelength-routed optical WDM networks," Optical Networks Magazine, vol. 1, pp. 47–60, June 2000.

[17] A. Morea, A. F. Chong, and O. Rival, "Impact of transparent network constraints on capacity gain of elastic channel spacing," Optical Fiber Communication Conference/National Fiber Optic Engineers Conference (OFC/NFOEC), JWA062, Mar. 2011.

[18] G. Zhang, M. D. Leenheer, and B. Mukherjee, "Optical traffic grooming in OFDM-based elastic optical networks [invited]," IEEE/OSA Journal of Optical Communications and Networking, vol. 4, no. 11, pp. B17–B25, Nov. 2012.

[19] A. N. Patel, P. N. Ji, J. P. Jue, and T. Wang, "Defragmentation of transparent flexible optical WDM (FWDM) networks," Optical Fiber Communication Conference/National Fiber Optic Engineers Conference (OFC/NFOEC), OTuI8, Mar. 2011.

[20] K. Wen, Y. Yin, D. J. Geisler, S. Chang, and S. J. B. Yoo, "Dynamic on-demand lightpath provisioning using spectral defragmentation in flexible bandwidth networks," 37th European Conference and Exhibition on Optical Communication (ECOC), Mo.2.K.4, Sep. 2011.

[21] T. Takagi, H. Hasegawa, K. Sato, Y. Sone, A. Hirano, and M. Jinno, "Disruption minimized spectrum defragmentation in elastic optical path networks that adopt distance adaptive modulation," 37th European Conference and Exhibition on Optical Communication (ECOC), Mo.2.K.3, Sep. 2011.

[22] Y. Wang, X. Cao, and Y. Pan, "A study of the routing and spectrum allocation in spectrum-sliced elastic optical path networks," IEEE International Conference on Computer Communications (INFOCOM), pp. 1503–1511, Apr. 2011.

[23] Y. Wang, X. Cao, Q. Hu, and Y. Pan, "Towards elastic and fine-granular bandwidth allocation in spectrum-sliced optical networks," IEEE/OSA Journal of Optical Communications and Networking, vol. 4, no. 11, pp. 906–917, Nov. 2012.

[24] K. Christodoulopoulos, I. Tomkos, and E. Varvarigos, "Time-varying spectrum allocation policies and blocking analysis in flexible optical networks," IEEE Journal on Selected Areas in Communications, vol. 31, no. 1, pp. 13–25, Jan. 2013.

[25] R. Muñoz, R. Casellas, R. Martínez, L. Liu, T. Tsuritani, and I. Morita, "Experimental evaluation of efficient routing and distributed spectrum allocation algorithms for GMPLS elastic networks," Optics Express, vol. 20, no. 27, pp. 28532–28537, Dec. 2012.

[26] L. Liu, R. Muñoz, R. Casellas, T. Tsuritani, R. Martínez, and I. Morita, "OpenSlice: an OpenFlow-based control plane for spectrum sliced elastic optical path networks," Optics Express, vol. 21, no. 4, pp. 4194–4204, Feb. 2013.

[27] L. Velasco, M. Klinkowski, M. Ruiz, V. López, and G. Junyent, "Elastic spectrum allocation for variable traffic in flexible-grid optical networks," Optical Fiber Communication Conference/National Fiber Optic Engineers Conference (OFC/NFOEC), JTh2A.39, Mar. 2012.

[28] K. Christodoulopoulos, I. Tomkos, and E. A. Varvarigos, "Elastic bandwidth allocation in flexible OFDM-based optical networks," IEEE Journal of Lightwave Technology, vol. 29, no. 9, pp. 1354–1366, May 2011.

[29] Z. Zhu, W. Lu, L. Zhang, and N. Ansari, "Dynamic service provisioning in elastic optical networks with hybrid single-/multi-path routing," IEEE Journal of Lightwave Technology, vol. 31, no. 1, pp. 15–22, Jan. 2013.

[30] M. Jinno, K. Yonenaga, H. Takara, K. Shibahara, S. Yamanaka, T. Ono, T. Kawai, M. Tomizawa, and Y. Miyamoto, "Demonstration of translucent elastic optical network based on virtualized elastic regenerator," Optical Fiber Communication Conference/National Fiber Optic Engineers Conference (OFC/NFOEC), PDP5B.6, Mar. 2012.

[31] X. Wang, M. Brandt-Pearce, and S. Subramaniam, "Impact of wavelength and modulation conversion on translucent elastic optical networks using MILP," IEEE/OSA Journal of Optical Communications and Networking, vol. 7, no. 7, pp. 644–655, July 2015.

[32] F. M. Madani, "Scalable framework for translucent elastic optical network planning," IEEE Journal of Lightwave Technology, vol. 34, no. 4, pp. 1086–1097, Feb. 2016.

[33] M. Klinkowski and K. Walkowiak, "On performance gains of flexible regeneration and modulation conversion in translucent elastic optical networks with superchannel transmission," IEEE Journal of Lightwave Technology, vol. 34, no. 23, pp. 5485–5495, Dec. 2016.

[34] J. Zhu, X. Chen, D. Chen, S. Zhu, and Z. Zhu, "Service provisioning with energy-aware regenerator allocation in multi-domain eons," IEEE Global Communications Conference (GLOBECOM), 6 pages, Dec. 2015.

[35] M. Aibin and K. Walkowiak, "Adaptive modulation and regenerator-aware dynamic routing algorithm in elastic optical networks," IEEE International Conference on Communications (ICC), pp. 5138–5143, June 2015.

[36] A. Fallahpour, H. Beyranvand, S. A. Nezamalhosseini, and J. A. Salehi, "Energy efficient routing and spectrum assignment with regenerator placement in elastic optical networks," IEEE Journal of Lightwave Technology, vol. 32, no. 10, pp. 2019–2027, May 2014.

[37] N. Wang, J. P. Jue, X. Wang, Q. Zhang, H. C. Cankaya, and M. Sekiya, "Holding-time-aware scheduling for immediate and advance reservation in elastic optical networks," IEEE International Conference on Communications (ICC), pp. 5180–5185, June 2015.

[38] W. Lu, Z. Zhu, and B. Mukherjee, "On hybrid IR and AR service provisioning in elastic optical networks," IEEE Journal of Lightwave Technology, vol. 33, no. 22, pp. 4659–4670, Nov. 2015.

[39] D. P. Hand and P. S. J. Russell, "Solitary thermal shock waves and optical damage in optical fibers: the fiber fuse," OSA Optics Letters, vol. 13, no. 9, pp. 767–769, Sep. 1988.

[40] P. P. Mitra and J. B. Stack, "Nonlinear limits to the information capacity of optical fibre communications," Nature, vol. 441, pp. 1027–1030, June 2001.

[41] E. B. Desurvire, "Capacity demand and technology challenges for lightwave systems in

the next two decades," IEEE Journal of Lightwave Technology, vol. 24, no. 12, pp. 4697–4710, Dec. 2006.

[42] T. Morioka, "New generation optical infrastructure technologies: "EXAT Initiative" towards 2020 and beyond," 14th OptoElectronics and Communications Conference (OECC), FT.4, July 2009.

[43] M. Koshiba, K. Saitoh, and Y. Kokubun, "Heterogeneous multi-core fibers: proposal and design principle," IEICE Electronics Express, vol. 6, no. 2, pp. 98–103, Jan. 2009.

[44] K. Takenaga, S. Tanigawa, N. Guan, S. Matsuo, K. Saitoh, and M. Koshiba, "Reduction of crosstalk by quasi-homogeneous solid multi-core fiber," Optical Fiber Communication Conference/National Fiber Optic Engineers Conference (OFC/NFOEC), OWK7, Mar. 2010.

[45] K. Imamura, Y. Tsuchida, K. Mukasa, R. Sugizaki, K. Saitoh, and M. Koshiba, "Investigation on multi-core fibers with large Aeff and low micro bending loss," Optics Express, vol. 19, no. 11, pp. 10595–10603, May 2011.

[46] J. Tu, K. Saitoh, M. Koshiba, K. Takenaga, and S. Matsuo, "Design and analysis of large-effective-area heterogeneous trench-assisted multi-core fiber," Optics Express, vol. 20, no. 14, pp. 15157–15170, July 2012.

[47] B. Kozicki, H. Takara, Y. Tsukishima, T. Yoshimatsu, K. Yonenaga, and M. Jinno, "Experimental demonstration of spectrum-sliced elastic optical path network (SLICE)," Optics Express, vol. 18, no. 21, pp. 22105–22118, Oct. 2010.

[48] B. Collings, "The next generation of ROADM devices for evolving network applications," 37th European Conference and Exhibition on Optical Communication (ECOC) Market Focus, Sep. 2011.

[49] B. Collings, "New devices enabling software-defined optical networks," IEEE Communications Magazine, vol. 51, no. 3, pp. 66–71, Mar. 2013.

[50] H. Ishida, H. Hasegawa, and K. Sato, "Hardware scale and performance evaluation of a compact subsystem modular optical cross connect that adopts tailored add/drop architecture," IEEE/OSA Journal of Optical Communications and Networking, vol. 7, no. 6, pp. 586–595, June 2015.

[51] A. J. Lowery, L. B. Du, and J. Armstrong, "Performance of optical OFDM in ultralong-haul wdm lightwave systems," IEEE Journal of Lightwave Technology, vol. 25, no. 1, pp. 131–138, Jan. 2007.

[52] B. Kozicki, H. Takara, T. Tanaka, Y. Sone, A. Hirano, K. Yonenaga, and M. Jinno, "Distance-adaptive path allocation in elastic optical path networks," IEICE Transactions on Communications, vol. E94.B, no. 7, pp. 1823–1830, 2011.

[53] H. Takara, B. Kozicki, Y. Sone, and M. Jinno, "Spectrally-efficient elastic optical path networks," 15th OptoElectronics and Communications Conference (OECC), pp. 116–117, July 2010.

[54] Y. Sone, A. Watanabe, W. Imajuku, Y. Tsukishima, B. Kozicki, H. Takara, and M. Jinno, "Bandwidth squeezed restoration in spectrum-sliced elastic optical path networks (SLICE)," IEEE/OSA Journal of Optical Communications and Networking, vol. 3, no. 3, pp. 223–233, March 2011.

[55] Z. Shen, H. Hasegawa, K. Sato, T. Tanaka, and A. Hirano, "A novel elastic optical path network that utilizes bitrate-specific anchored frequency slot arrangement," Optics Express, vol. 22, no. 3, pp. 3169–3179, Feb. 2014.

[56] R. A. Scaraficci and N. L. S. Fonseca, "Alternative routing and zone-based spectrum assignment algorithm for flexgrid optical networks," IEEE International Conference on Communications (ICC), pp. 3295–3300, June 2014.

[57] H. Beyranvand and J. A. Salehi, "A quality-of-transmission aware dynamic routing and spectrum assignment scheme for future elastic optical networks," IEEE Journal of Lightwave Technology, vol. 31, no. 18, pp. 3043–3054, Sep. 2013.

[58] Y. Wang, J. Zhang, Y. Zhao, J. Zhang, J. Zhao, X. Wang, and W. Gu, "Path connectivity based spectral defragmentation in flexible bandwidth networks," Optics Express, vol. 21, no. 2, pp. 1353–1363, Jan. 2013.

[59] X. Chen, A. Jukan, and A. Gumaste, "Multipath de-fragmentation: Achieving better spectral efficiency in elastic optical path networks," IEEE International Conference on Computer Communications (INFOCOM), pp. 390–394, Apr. 2013.

[60] L. Liu, Y. Yin, M. Xia, M. Shirazipour, Z. Zhu, R. Proietti, Q. Xu, S. Dahlfort, and S. J. B. Yoo, "Software-defined fragmentation-aware elastic optical networks enabled by openflow," 39th European Conference and Exhibition on Optical Communication (ECOC), We.3.E.2, Sep. 2013.

[61] M. Zhang, C. You, H. Jiang, and Z. Zhu, "Dynamic and adaptive bandwidth defragmentation in spectrum-sliced elastic optical networks with time-varying traffic," IEEE Journal of Lightwave Technology, vol. 32, no. 5, pp. 1014–1023, Mar. 2014.

[62] G. Shen and R. S. Tucker, "Translucent optical networks: the way forward," IEEE Communications Magazine, vol. 45, no. 2, pp. 48–54, Feb. 2007.

[63] JPN-Model [Online]. Available: `http://www.ieice.org/~pn/jpn/jpnm.html`.

[64] J. Sangiamwong, K. Tsukamoto, and S. Komaki, "Frequency channel blocking scheme in mesh-topology millimeter-wave broad-band entrance networks," IEEE Transactions on Microwave Theory and Techniques, vol. 53, no. 12, pp. 3723–3730, Dec. 2005.

[65] R. Jain, D. Chiu, and W. Hawe, "Quantitative measure of fairness and discrimination for resource allocation in shared computer systems," DEC Research Report TR-301, Sep. 1984.

[66] G. Roberts, T. Kudoh, I. Monga, J. Sobieski, J. MacAuley, and C. Guok, "NSI connection services v2.0," Grid Forum Document-Proposed Recommendation, vol. 212, pp. 1–119, May 2014.

[67] C. Wang, G. Shen, and S. K. Bose, "Distance adaptive dynamic routing and spectrum allocation in elastic optical networks with shared backup path protection," IEEE Journal of Lightwave Technology, vol. 33, no. 14, pp. 2955–2964, July 2015.

[68] J. Zheng and H. T. Mouftah, "Supporting advance reservations in wavelength-routed WDM networks," IEEE Tenth International Conference on Computer Communications and Networks (ICCCN), pp. 594–597, Oct. 2001.

[69] N. Charbonneau and V. M. Vokkarane, "A survey of advance reservation routing and wavelength assignment in wavelength-routed WDM networks," IEEE Communications Surveys Tutorials, vol. 14, no. 4, pp. 1037–1064, Fourth 2012.

[70] N. Charbonneau and V. M. Vokkarane, "Static routing and wavelength assignment for multicast advance reservation in all-optical wavelength-routed WDM networks," IEEE/ACM Transactions on Networking, vol. 20, no. 1, pp. 1–14, Feb. 2012.

[71] A. Gadkar, T. Entel, J. M. Plante, and V. M. Vokkarane, "Slotted advance reservation for multicast-incapable optical wavelength division multiplexing networks," IEEE/OSA Journal of Optical Communications and Networking, vol. 6, no. 3, pp. 340–354, Mar. 2014.

[72] T. Entel, A. Gadkar, and V. M. Vokkarane, "Dynamic advance reservation multicast overlay for slotted optical WDM networks," IEEE Global Communications Conference (GLOBECOM), pp. 3007–3012, Dec. 2012.

[73] W. Lu and Z. Zhu, "Dynamic service provisioning of advance reservation requests in elastic optical networks," IEEE Journal of Lightwave Technology, vol. 31, no. 10, pp. 1621–1627, May 2013.

[74] H. Chen, Y. Zhao, J. Zhang, R. He, W. Wang, J. Wu, Y. Wang, Y. Ji, H. Zheng, Y. Lin, and B. Hou, "Time-spectrum consecutiveness based scheduling with advance reservation in elastic optical networks," IEEE Communications Letters, vol. 19, no. 1, pp. 70–73, Jan. 2015.

[75] I. T. Okumus and F. U. Dizdar, "Advance and immediate request admission: a preemptable service definition for bandwidth brokers," International Journal of Computers Communications and Control, vol. 7, no. 2, pp. 353–364, June 2012.

[76] Y. Hirota, Y. Hatada, T. Watanabe, and H. Tode, "Dynamic spectrum allocation based on connection alignment for elastic optical networks," 10th Asia-Pacific Symposium on Information and Telecommunication Technologies (APSITT), pp. 34–36, Aug. 2015.

[77] P. Wright, M. C. Parker, and A. Lord, "Minimum- and maximum-entropy routing and spectrum assignment for flexgrid elastic optical networking [invited]," IEEE/OSA Journal of Optical Communications and Networking, vol. 7, no. 1, pp. A66–A72, Jan. 2015.

[78] X. Wang, Q. Zhang, I. Kim, P. Palacharla, and M. Sekiya, "Utilization entropy for assessing resource fragmentation in optical networks," Optical Fiber Communication Conference/National Fiber Optic Engineers Conference (OFC/NFOEC), OTh1A.2, Mar. 2012.

[79] K. Igarashi, K. Takeshima, T. Tsuritani, H. Takahashi, S. Sumita, I. Morita, Y. Tsuchida, M. Tadakuma, K. Maeda, T. Saito, K. Watanabe, K. Imamura, R. Sugizaki, and M. Suzuki, "110.9-Tbit/s SDM transmission over 6,370 km using a full C-band seven-core EDFA," Optics Express, vol. 21, no. 15, pp. 18053–18060, July 2013.

[80] S. Fujii, Y. Hirota, H. Tode, and K. Murakami, "On-demand spectrum and core allocation for multi-core fibers in elastic optical network," Optical Fiber Communication Conference/National Fiber Optic Engineers Conference (OFC/NFOEC), OTh4B.4, Mar. 2013.

[81] S. Fujii, Y. Hirota, and H. Tode, "Dynamic resource allocation with virtual grid for space division multiplexed elastic optical network," 39th European Conference and Exhibition on Optical Communication (ECOC), P.5.15, Sep. 2013.

[82] H. Takara, K. Yonenaga, and M. Jinno, "Spectrally-efficient elastic optical path networks toward 1 Tbps era," Optical Fiber Communication Conference/National Fiber Optic Engineers Conference (OFC/NFOEC), OTh3B.3, Mar. 2012.

[83] H. Takara, A. Sano, T. Kobayashi, H. Kubota, H. Kawakami, A. Matsuura, Y. Miyamoto, Y. Abe, H. Ono, K. Shikama, Y. Goto, K. Tsujikawa, Y. Sasaki, I. Ishida, K. Takenaga, S. Matsuo, K. Saitoh, M. Koshiba, and T. Morioka, "1.01-Pb/s (12 SDM/222 WDM/456 Gb/s) crosstalk-managed transmission with 91.4-b/s/Hz aggregate spectral efficiency," 38th European Conference and Exhibition on Optical Communication (ECOC), Th.3.C.1, Sep. 2012.

[84] A. Turukhin, O. V. Sinkin, H. G. Batshon, H. Zhang, Y. Sun, M. Mazurczyk, C. R. Davidson, J. X. Cai, M. A. Bolshtyansky, D. G. Foursa, and A. Pilipetskii, "105.1 Tb/s power-efficient transmission over 14,350 km using a 12-core fiber," Optical Fiber Communications Conference (OFC), Th4C.1, Mar. 2016.

[85] J. M. Fini, B. Zhu, T. F. Taunay, and M. F. Yan, "Statistics of crosstalk in bent multicore fibers," Optics Express, vol. 18, no. 14, pp. 15122–15129, July 2010.

[86] T. Hayashi, T. Nagashima, O. Shimakawa, T. Sasaki, and E. Sasaoka, "Crosstalk variation of multi-core fibre due to fibre bend," 36th European Conference and Exhibition on Optical Communication (ECOC), We.8.F.6., Sep. 2010.

[87] M. Koshiba, K. Saitoh, K. Takenaga, and S. Matsuo, "Multi-core fiber design and analysis: coupled-mode theory and coupled-power theory," Optics Express, vol. 19, no. 26, pp. B102–B111, Dec. 2011.

[88] K. Takenaga, Y. Arakawa, S. Tanigawa, N. Guan, S. Matsuo, K. Saitoh, and M. Koshiba, "An investigation on crosstalk in multi-core fibers by introducing random fluctuation along longitudinal direction," IEICE Transactions on Communications, vol. E94.B, no. 2, pp. 409–416, 2011.

[89] T. Hayashi, T. Taru, O. Shimakawa, T. Sasaki, and E. Sasaoka, "Characterization of crosstalk in ultra-low-crosstalk multi-core fiber," IEEE Journal of Lightwave Technology, vol. 30, no. 4, pp. 583–589, Feb. 2012.

[90] M. Cvijetic, I. B. Djordjevic, and N. Cvijetic, "Dynamic multidimensional optical networking based on spatial and spectral processing," Optics Express, vol. 20, no. 8, pp. 9144–9150, Apr. 2012.

[91] N. Amaya, M. Irfan, G. Zervas, R. Nejabati, D. Simeonidou, J. Sakaguchi, W. Klaus, B. Puttnam, T. Miyazawa, Y. Awaji, N. Wada, and I. Henning, "Fully-elastic multi-granular network with space/frequency/time switching using multi-core fibres and programmable optical nodes," Optics Express, vol. 21, no. 7, pp. 8865–8872, Apr. 2013.

[92] N. Amaya, S. Yan, M. Channegowda, B. R. Rofoee, Y. Shu, M. Rashidi, Y. Ou, E. Hugues-Salas, G. Zervas, R. Nejabati, D. Simeonidou, B. Puttnam, W. Klaus, J. Sakaguchi, T. Miyazawa, Y. Awaji, H. Harai, and N. Wada, "Software defined networking (SDN) over space division multiplexing (SDM) optical networks: features, benefits and experimental demonstration," Optics Express, vol. 22, no. 3, pp. 3638–3647, Feb. 2014.

[93] A. Sano, H. Takara, T. Kobayashi, and Y. Miyamoto, "Crosstalk-managed high capacity long haul multicore fiber transmission with propagation-direction interleaving," IEEE Journal of Lightwave Technology, vol. 32, no. 16, pp. 2771–2779, Aug. 2014.

[94] B. Li, Z. Feng, M. Tang, Z. Xu, S. Fu, Q. Wu, L. Deng, W. Tong, S. Liu, and P. P. Shum, "Experimental demonstration of large capacity WSDM optical access network with multicore fibers and advanced modulation formats," Optics Express, vol. 23, no. 9, pp. 10997–11006, May 2015.

[95] A. Muhammad, G. Zervas, and R. Forchheimer, "Resource allocation for space-division multiplexing: Optical white box versus optical black box networking," IEEE Journal of Lightwave Technology, vol. 33, no. 23, pp. 4928–4941, Dec. 2015.

[96] K. Hashino, Y. Hirota, Y. Tanigawa, and H. Tode, "Crosstalk-aware spectrum and core allocation with crosstalk-prohibited frequency slot in space-division multiplexing elastic optical networks," OSA Advanced Photonics Congress on Photonics in Switching (PS), 3 pages, july 2017.

[97] J. Sakaguchi, B. J. Puttnam, W. Klaus, Y. Awaji, N. Wada, A. Kanno, T. Kawanishi, K. Imamura, H. Inaba, K. Mukasa, R. Sugizaki, T. Kobayashi, and M. Watanabe, "19-core fiber transmission of 19x100x172-Gb/s SDM-WDM-PDM-QPSK signals at 305Tb/s," Optical Fiber Communication Conference/National Fiber Optic Engineers Conference (OFC/NFOEC), PDP5C.1, Mar. 2012.

[98] S. Matsuo, K. Takenaga, Y. Sasaki, Y. Amma, S. Saito, K. Saitoh, T. Matsui, K. Nakajima, T. Mizuno, H. Takara, Y. Miyamoto, and T. Morioka, "High-spatial-multiplicity multicore fibers for future dense space-division-multiplexing systems," IEEE/OSA Journal of Lightwave Technology, vol. 34, no. 6, pp. 1464–1475, Mar. 2016.

[99] T. Hayashi, Y. Tamura, T. Hasegawa, and T. Taru, "125-μm-cladding coupled multi-core fiber with ultra-low loss of 0.158 dB/km and record-low spatial mode dispersion of 6.1 ps/km$^{1/2}$," Optical Fiber Communication Conference (OFC/NFOEC), Th5A.1, Sep. 2016.

[100] R. Younce, J. Larikova, and Y. Wang, "Engineering 400G for colorless-directionless-contentionless architecture in metro/regional networks [invited]," IEEE/OSA Journal of Optical Communications and Networking, vol. 5, no. 10, pp. A267–A273, Oct. 2013.

[101] A. Morea, J. Renaudier, T. Zami, A. Ghazisaeidi, and O. Bertran-Pardo, "Throughput comparison between 50-GHz and 37.5-GHz grid transparent networks [invited]," IEEE/OSA Journal of Optical Communications and Networking, vol. 7, no. 2, pp. A293–A300, Feb. 2015.

[102] N. Amaya, G. Zervas, and D. Simeonidou, "Introducing node architecture flexibility for elastic optical networks," IEEE/OSA Journal of Optical Communications and Networking, vol. 5, no. 6, pp. 593–608, June 2013.

[103] S. Yan, E. Hugues-Salas, V. J. F. R. no, Y. Shu, G. Saridis, B. R. Rofoee, Y. Yan, A. Peters, S. Jain, T. C. May-Smith, P. Petropoulos, D. J. Richardson, G. Zervas, and D. Simeonidou, "First demonstration of all-optical programmable SDM/TDM intra data centre

and WDM inter-DCN communication," 40th European Conference and Exhibition on Optical Communication (ECOC), PD.1.2, Sep. 2014.

[104] A. Muhammad, G. Zervas, N. Amaya, D. Simeonidou, and R. Forchheimer, "Introducing flexible and synthetic optical networking: Planning and operation based on network function programmable ROADMs," IEEE/OSA Journal of Optical Communications and Networking, vol. 6, no. 7, pp. 635–648, July 2014.

[105] M. Garrich, N. Amaya, G. S. Zervas, J. R. F. Oliveira, P. Giaccone, A. Bianco, D. Simeonidou, and J. C. R. F. Oliveira, "Architecture on demand design for high-capacity optical SDM/TDM/FDM switching," IEEE/OSA Journal of Optical Communications and Networking, vol. 7, no. 1, pp. 21–35, Jan. 2015.

[106] M. Dzanko, M. Furdek, G. Zervas, and D. Simeonidou, "Evaluating availability of optical networks based on self-healing network function programmable ROADMs," IEEE/OSA Journal of Optical Communications and Networking, vol. 6, no. 11, pp. 974–987, Nov. 2014.

[107] S. Fujii, Y. Hirota, H. Tode, and T. Watanabe, "Dynamic spectrum and core allocation reducing costs of architecture on demand nodes," 40th European Conference and Exhibition on Optical Communication (ECOC), P.6.23, Sep. 2014.

[108] S. Fujii, Y. Hirota, T. Watanabe, and H. Tode, "Dynamic spectrum and core allocation with spectrum region reducing costs of building modules in AoD nodes," IEEE 16th International Telecommunications Network Strategy and Planning Symposium (Networks), wed.s2.3, Sep. 2014.

[109] M. Garrich, N. Amaya, G. S. Zervas, P. Giaccone, and D. Simeonidou, "Power consumption analysis of architecture on demand," 38th European Conference and Exhibition on Optical Communication (ECOC), P5.06, Sep. 2012.